Chapter 1

Introduction

The difference between inorganic light emitting diode (LED) and organic light emitting diode (OLED), the two most common emissive materials, is that the materials in OLED can be easily designed and synthesized. The improvements of chemical and physical properties (i.e. color, solubility, electro-affinity, and lifetime) in OLED can be effectively adjusted by varying functional groups. OLED have engrossed much attention as a result of their possible applications in full-colored, high-luminescent, low driving-voltage, and hefty area displays.[1] Organic electroluminescent (EL) materials used for the LED devices are typically alienated into two types, i.e. low molecular weight organic molecules and high molecular weight polymers. The vacuum deposition method is generally used in the low molecular weight organic LED materials. Nevertheless, heat-induced crystallization and aggregation are injurious to the evaporated films of low-molecular compounds and cause failures in most organic LED devices.[2] Despite the fact that LED polymers are not essentially better than organic LED materials in all portions, LED polymers possess admirable film formability and mechanical properties, which are compatible with wet processing capability of polymer solutions, such as dip-coating and spin-coating methods. Semiconducting and luminescent p-conjugated polymers are of

interest in LED materials since 1990.[1] However, soluble p-conjugated LED polymer systems with high EL efficiency are limited. Approaches are strenuous to the adjustment of poly(p-phenylene vinylene) with improved solubility.[2] Recent reports were demonstrated that molecularly doped LED polymers,[3-5] where EL dopants were blended with soluble polymer matrices, such as poly(*N*-vinylcarbazole) (PVK) (also as a hole-transporting material)[4-10] or poly(methyl methacrylate),[5,11] are a much more flexible material design than intrinsically conductive polymers. Hence, even low molecular weight organic LED compounds, which may show poor film processability by the vacuum deposition method, can be doped into polymer matrices to form LED polymer blends. Therefore, a single-layer doped polymer film combining carriers (holes and/or electrons) transport and light emission functions is adopted in the study of our LED moieties. A series of novel electroluminescent compounds, which cannot be vacuum-deposited, were doped into PVK to investigate the structural influence of the electroluminescence on the LED properties. These compounds and complexes includes several series of alkoxy substituted oligo(*p*-phenylene-vinylene)s and poly(*p*-phenylene-vinylene)s containing different side groups (on the central phenyl rings) and alkoxy end groups (on both of the end phenyl rings),[12,13] liquid crystalline supramolecules containing acceptor emitters,[14] and carbazole doped into fluorescent fluorene derivatives.[15,16] In devices based on these complexes, it is expected that both

singlet and triplet excitons generated by electrical injection and charge recombination can be utilized for EL emission through Förster-type singlet–singlet exciton transfer or Dexter-type triplet-triplet exciton transfer.[17,18]

From these researches, we are able to list out some of the most important results as following:

A. aggregation, excimer, and exciplex

In consideration of absorption and excitation spectra, the ‘‘site-selectivity’’ of the PL, and the concentration dependence of the PL spectrum, we demonstrate that the red-shifted film spectra are a result of the formation of low-energy aggregate sites due to strong interchain interactions. Time-resolved measurements from literature suggest a longer radiative lifetime for the aggregate vs solution, leading to the lower efficiency. Aggregation formation is found to be morphologically dependent, and is minimal in ‘‘powder’’ samples. If the excited state delocalization is accompanied by charge separation, where the electron resides on one chain and the hole on an adjacent chain, the species is referred to as a “spatially indirect exciton” or “polaron pair”. On the other hand, if the excited state has no significant degree of charge separation and is equally shared between multiple chains, the species is referred to as an “excimer”. A neutral excited state shared between unequal chains (or unequally between similar chains) is sometimes called an “exciplex”.[19, 20]

B. electroplex and electromer

The diodes emitted light in the green-blue range; the electroluminescence spectra varied between diodes with different thicknesses of the polymer and molecular layers. The optical phenomena (electroplex) were simulated with a model accounting for interference effects; simulated results showed that the electroluminescence from the organic diode can be attributed neither to luminescence of the polymer nor of the molecular layer. On the other hand, the emission spectrum is composed of a red component originating from the new excited dimer in addition to the blue-green component from an individual lumophore and excimer. This excited dimer is formed under a strong electric field inside the diode and cannot be produced by photoexcitation, which is different from the excimer or exciplex that is often found both in photoluminescence and electroluminescence, and it is termed the ‘‘electromer’’.[21,22]

Chapter 2

Characterization of Light-Emitting Oligo(*p*-phenylene-vinylene)s and Polymeric Derivatives Containing Three- and Five-Conjugated Phenylene Rings

2.1 Abstract

Several series of light-emitting oligo(*p*-phenylene-vinylene)s (BIII and BV series containing three- and five-conjugated phenylene rings) with various side groups and end groups attached to the cores were characterized. The analogous PBV polymers derived from BV series were also investigated. Blue and greenish light emissions were observed in the photoluminescence (PL) and electroluminescence (EL) spectra of blend and pure films utilizing these π-conjugated structures. In contrast to three-conjugated ring oligomers, five-conjugated ring derivatives (oligomers and polymers) have larger λmax values of PL and EL emissions. The mesomorphism is introduced to BV series by the replacement of 3-conjugated rings (BIII series) with 5-conjugated phenyl cores (BV series). The liquid crystalline (LC) properties of BV series with end groups (on both end rings) are better than those of analogous BV-OC_8 without end groups. Polarized PL emissions were obtained by the alignment of liquid crystalline phase in rubbing cells. Upon heating, different PL emission wavelengths

and intensities were observed in various phases. Not only the solubility and thermal properties but also the PL and EL properties can be effectively adjusted by the attachment of flexible alkoxy groups either on the central rings or on both end rings of the conjugated cores.

2.2 Introduction

Luminescent polymers with highly extended π-conjugated systems have attracted considerable attention from both fundamental and practical points of view, because various novel physical properties have been observed and also various applications have been proposed widely. Polymers with an extended π-conjugation hold promise for electronic and photonic applications, such as light emitting diodes, photovoltaics, sensors, thin film transistors.[23] Most of liquid-crystalline materials carried out on photoluminescence (PL) and electroluminescence (EL) have involved different polarized light emission. For instance, cyanobiphenyl liquid crystals can be aligned by rubbed polyimide and thus to have dichroic ratios in absorption spectra.[24] The frequently used materials were polyacrylate[25-28], polyfluorene[29-40] and their oligomer derivatives.[41,42] Additionally, liquid crystals with a hexagonal mesophase to solubilize the monomer and direct its electropolymerization, leads to PEDOT films that replicate the texture and birefringence of the LC template.[43] In particular, liquid crystalline conducting polymers possessing mesogenic parts in their side chains[44-47] or dyes

doped in liquid crystalline structure[48,49] have attracted much interest in their molecular alignment, which is anticipated for use in polarized emission. Besides, mesogenic structures containing electron-transporting 1,3,4-oxadiazole units have also been utilized to emit polarized light.[50,51] Moreover, polarized OLEDs were constructed using heptafluorene lightly doped with monodisperse conjugated oligomers for an efficient emission of green, red, and white light, and a high polarization ratio up to 26 was obtained.[52]

Several highly extended π-conjugated systems containing oligo(*p*-phenylene vinylene)s (OPV) units are utilized in polymeric light-emitting diode (PLED) and organic LED (OLED) applications. For instance, polymerizable hexacatenar mesogens[53] containing a photo-active OPV core were thermally initiated and polymerized in the absence of light to afford effective crosslinking with retention of both LC order and the desired emission properties. Different generations of poly(propylene imine) dendrimers modified peripherically with urea OPV having a 3,4,5-tri(dodecyloxy)phenyl mesogenic unit (OPV-dendrimers) will lead to liquid crystalline behavior resulting in order on a supramolecular level.[54] Besides, covalently linked dyads of OPV with [60]fullerene (C60)[55-57], amphiphilic diblock co-poly(ester oxide),[58] ferrocencethiol,[59] and bis(thioacetyl)[60] structures exhibit interesting photophysical properties, among which energy and electron transfer reactions have

been used to make photovoltaic devices. Oligomers with defined chain length can be considered as model compounds of their regarding polymers. Therefore, the oligomeric OPV systems gained considerable interest because of their reproducible properties and their well-defined structure, which are prerequisites for the exploration of the physical properties of corresponding polymeric materials.[61-65] In comparison to the extensive attention that has been devoted to PLED systems, there are limited studies about structure-property relationships, for example, the correlation between the conjugation length and the LED performance, in oligomeric systems.[66-75]

Chart 2.1

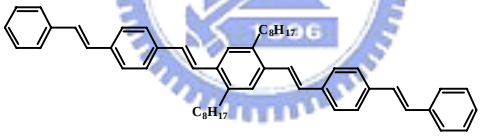

BV-C_8

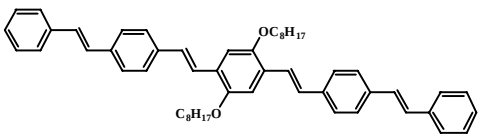

BV-OC_8

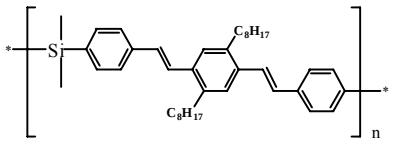

Si-PPV

In some reported literature results, a series of substituted oligo(*p*-phenylene-vinylene)s (BV-OC_8 and BV-C_8 in Chart 2.1) with a liquid crystalline (nematic) phase were synthesized and emission properties were

surveyed.[76,77] In addition, a PPV polymer derivative (Si-PPV in Chart 2.1), which has a well-defined backbone consisting of regularly alternating distyrylbenzene and dimethylsilylene units, was also investigated.[78] In this report, several series of alkoxy substituted oligo(*p*-phenylene-vinylene)s and poly(*p*-phenylene-vinylene)s containing different side groups (on the central phenyl rings) and alkoxy end groups (on both of the end phenyl rings) are explored. Various side groups, including methoxy (-OMe), butoxy (-OC_4), octoxy (-OC_8), decoxy (-OC_{12}), and ethylhexoxy (branched –OC_8) side chains, are introduced to the central phenyl rings to enhance the solubility of these conjugated molecules. Oligo(*p*-phenylene-vinylene)s and analogous polymers containing three- and five-conjugated phenylene rings are synthesized to inspect the structural effects on the thermal and electro-optical properties. The rubbing effects on the photoluminescent (PL) properties, i.e. polarized emission properties, of some mesogenic compounds are also studied.

2.3 Experimental

2.3.1 General Information

NMR measurements were carried out on a Bruker AC 300 spectrometer. Absorption spectra were acquired on a HP 8453 spectrometer. PL and EL emission spectra were obtained on a Hitachi 8453 spectrometer. The textures of mesophases were studied using a polarizing optical microscope (Leica DMLP) equipped with a hot stage. Transition temperatures were determined by differential scanning calorimetry (Perkin Elmer DSC-7 and Pyris 7) with a heating and cooling rate of 10 °C/min under nitrogen. Thermogravimetric analysis (TGA) was conducted on a Du Pont Thermal Analyst 2100 system with a TGA 2950 thermogravimetric analyzer under a heating rate of 20 ˚C/min under nitrogen. The highest occupied molecular orbital (HOMO) energy levels were estimated from the optical response on a Riken Photoelectron Spectrometer AC-2. The work function and ionization potential can be measured by the photoelectron spectrometer for the OLED materials in air. These materials were sealed in anti-parallel rubbing cells with a 9 μm cell gap, and the polarized PL emission spectra and PL dichroic ratios were measured at corresponding mesophasic temperatures. The textures of all mesogenic products were chacterized by a Leitz Laborlux S polarizing optical microscope (POM) equipped with a THMS-600 heating stage. The heating and cooling rates were 10 °C min^{-1} for all measurements in

N_2 unless mentioned. Powder X-ray diffraction (XRD) patterns were obtained from a Siemens D-5000 X-ray diffractometer (40 kV, 30 mA) fitted with a TTK450 temperature controller. Nickel-filtered CuKα radiation was used as the incident X-ray beam. The values of number-average molecular weight (Mn), weight-average molecular weight (Mw), and polydispersity index (PDI) were determined by gel permeation chromatography (GPC). GPC analysis was conducted on a Water 1515 separation module using polystyrene as a standard and THF as an eluant. Fluorescence quantum yields of solutions and films (ca. 50 nm) were determined by comparing a reference quinine sulfate in 0.1 M H_2SO_4 solution with a known quantum yield of 0.54 (concentration = 1x 10^{-5} M) and comparing MEHPPV films (by spin-coating of chloroform solutions with concentration = 1x 10^{-5} M) with a known quantum yield of 0.22, respectively.[29]

2.3.2 Device Fabrication

Pre-patterned ITO substrates with an effective individual device area of 3.14 mm^2 were cleaned by ultrasonic machine in various detergent solution and D. I. water. After that the ITO substrates were treated with oxygen plasma for 2 min before spin coating. Polymer thin films were spin-coated on ITO substrates from dichloroethane solution with a concentration of 1.65 wt% (the thickness is about 60 nm), whereas the

molecular emitters were doped into poly(9-vinylcarbozol) (PVK) matrix with a concentration of 1:100 wt%. The metal calcium was deposited as the cathode by thermal evaporation, consecutively capped with aluminum serving as a protecting layer. The current-voltage-luminescence response behavior was measured on ambient conditions by Keithley 2400 Source meter and Newport 1835C Optical meter equipped with 818ST silicon photodiode.

2.3.3 Materials

2.3.3.1 Oligo(*p*-phenylene-vinylene)s (1-14)

The structures of Oligo(*p*-phenylene-vinylene)s (1-14) were according to Chart 2.1 (BIII series containing three-conjugated rings, 1-6) Chart 2.2 (BV series containing five-conjugated rings, 7-14) and Chart 2.3 (PBV series containing five-conjugated rings, 7-14).

BIII-OMe (1) Anal Calcd for $C_{24}H_{22}O_2$: C, 84.18; H, 6.48. Found: C, 83.80; H, 7.00.

BIIIMe-OMe (2) Anal Calcd for $C_{26}H_{26}O_2$: C, 84.29; H, 7.07. Found: C, 84.53; H, 7.13.

BIIIOMe-OMe (3) Anal Calcd for $C_{26}H_{26}O_4$: C, 77.59; H, 6.51. Found: C, 77.57; H, 6.49.

BIIIOC$_8$-OMe (4) Anal Calcd for $C_{40}H_{54}O_4$: C, 80.22; H, 9.09. Found: C, 79.96; H,

8.98.

BIIIOC$_{12}$-OMe (5) Anal Calcd for $C_{48}H_{70}O_4$: C, 81.08; H, 9.92. Found: C, 81.3; H, 9.64.

BIIIOC$_8$-OC$_8$ (6) Anal Calcd for $C_{54}H_{82}O_4$: C, 81.56; H, 10.39. Found: C, 82.51; H, 10.92.

Chart 2.1 Oligo(*p*-phenylene-vinylene)s Containing 3-Conjugated Rings (BIII Series)

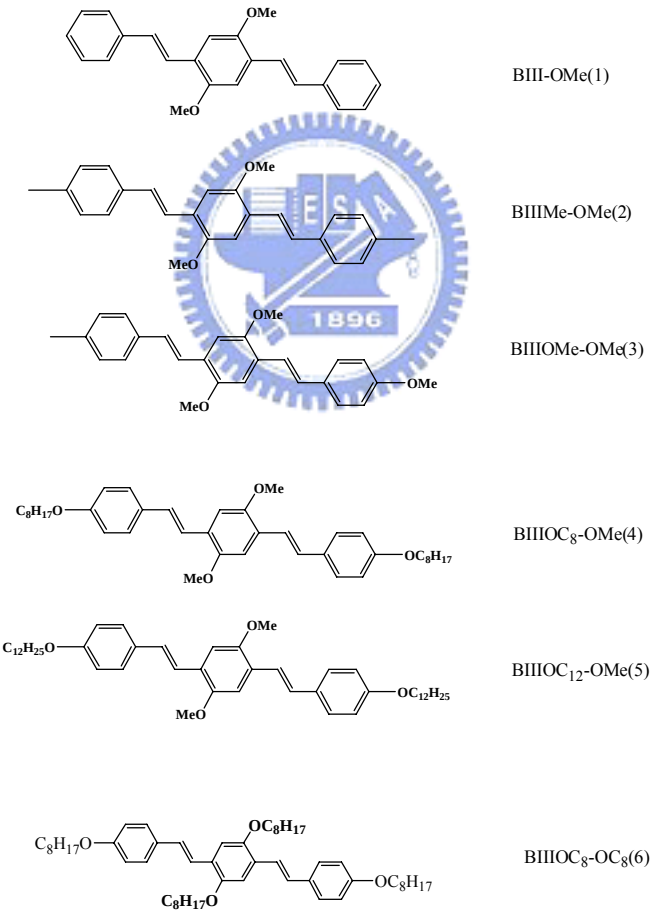

BVOC$_4$-OEh (7) Anal Calcd for $C_{62}H_{78}O_4$: C, 83.93; H, 8.86. Found: C, 82.48; H, 8.52.

$BVOC_4$-OC_8 (8) Anal Calcd for $C_{62}H_{78}O_4$: C, 83.93; H, 8.86. Found: C, 83.88; H, 8.87.

Chart 2.2 Oligo(*p*-phenylene-vinylene)s Containing 5-Conjugated Rings (BV Series)

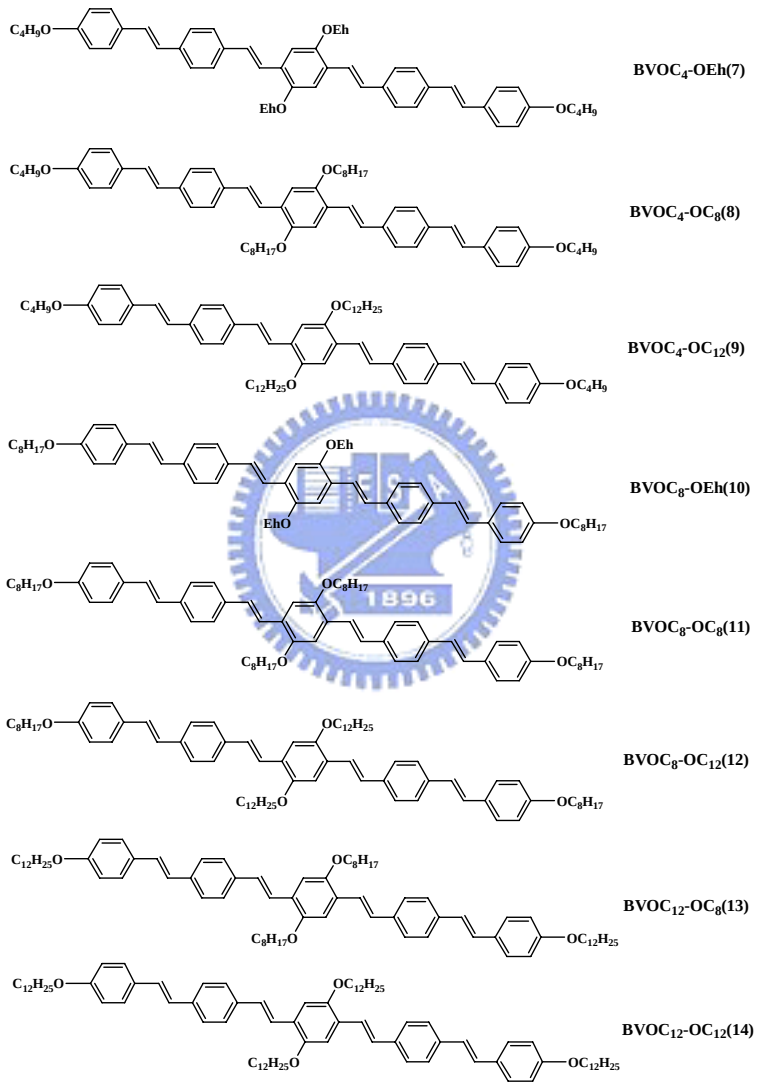

$BVOC_4$-OC_{12} (9) Anal Calcd for $C_{70}H_{94}O_4$: C, 84.12; H, 9.48. Found: C, 83.59; H, 9.31.

$BVOC_8$-OEh (10) Anal Calcd for $C_{70}H_{94}O_4$: C, 84.12; H, 9.48. Found: C, 83.76; H,

9.07.

$BVOC_8$-OC_8 (11) Anal Calcd for $C_{70}H_{94}O_4$: C, 84.12; H, 9.48. Found: C, 84.07; H, 9.26.

$BVOC_8$-OC_{12} (12) Anal Calcd for $C_{78}H_{110}O_4$: C, 84.27; H, 9.97. Found: C, 84.48; H, 9.71.

$BVOC_{12}$-OC_8 (13) Anal Calcd for $C_{78}H_{110}O_4$: C, 84.27; H, 9.97. Found: C, 84.02; H, 9.51.

$BVOC_{12}$-OC_{12} (14) Anal Calcd for $C_{86}H_{126}O_4$: C, 84.39; H, 10.38. Found: C, 83.87; H, 10.10.

2.3.3.2 (15-18) Polymers

$PBVOC_8$-OC_4 **(15)**

$PBVOC_8$-OC_8 **(16)**

$PBVOC_8$-OC_{12} **(17)**

$PBVOC_8$-OEh **(18)**

Chart 2.3 the structures of Poly(*p*-phenylene-vinylene)s (PBV Series)

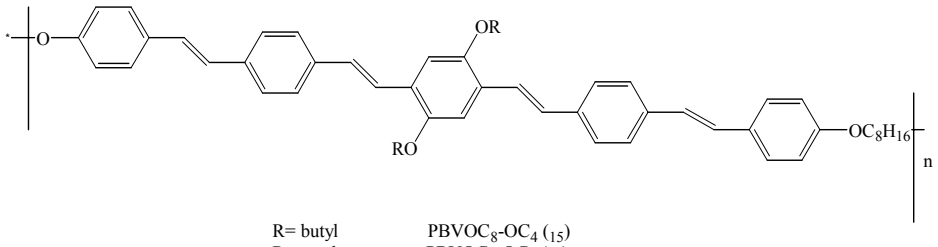

R= butyl PBVOC$_8$-OC$_4$ ($_{15}$)
R= octyl PBVOC$_8$-OC$_8$ ($_{16}$)
R= dodecyl PBVOC$_8$-OC$_{12}$ ($_{17}$)
R= $_2$-ethylhexyl PBVOC$_8$-OEh ($_{18}$)

2.4 Results and Discussion

2.4.1 Thermal Properties

The thermal behavior and phase transition temperatures of alkoxy-substituted oligo(*p*-phenylene-vinylene)s (1-14) and poly(*p*-phenylene-vinylene)s (15-18), which were characterized by differential scanning calorimetry (DSC) and polarizing optical microscopy (POM) measurements, are listed in Tables 2.1-2.3. For 3-conjugated phenyl oligomers (i.e. BIII series), the melting and crystallization temperatures (Tm and Tcr) are demonstrated in the following order: BIIIOMe-OMe (3) > BIIIMe-OMe (2) > BIII-OMe (1) > BIIIOC$_8$-OMe (4) > BIIIOC$_{12}$-OMe (5) > BIIIOC$_8$-OC$_8$ (6) (shown in Table 2.1). In general, owing to the weaker intermolecular interaction induced by the longer flexible chains, the longer alkoxy groups either on the central rings or on both end rings of the conjugated cores cause the reduction of the phase transition temperatures (i.e. the melting temperature, Tm, and the crystallization temperature, Tcr) in BIII series of 3-conjugated ring oligomers (1-6). For instance, their phase transition temperatures (i.e. Tm and Tcr) are in the order of BIIIOMe-OMe (3) > BIIIOC$_8$-OMe (4) > BIIIOC$_{12}$-OMe (5) by increasing the length of alkoxy terminal chains (on both end rings) and keeping the same length of lateral alkoxy chains -OMe (on the central ring), or in the order of BIIIOC$_8$-OMe (4) > BIIIOC$_8$-OC$_8$ (6) by enlarging the length of alkoxy side chains (on the central ring)

but keeping the same length of alkoxy terminal chains -OC_8 (on both end rings). As for BIIIOMe-OMe (3) > BIIIMe-OMe (2) > BIII-OMe (1) in Tm and Tcr, it can be explained by the short terminal groups of -OMe and -Me groups in BIIIOMe-OMe (3) and BIIIMe-OMe (2) generate larger molecular weights than that of BIII-OMe (1) without terminal groups, which accounts for the lowest transition temperature in BIII-OMe (1). In addition, comparing BIIIOMe-OMe (3) with BIIIMe-OMe (2), methoxy groups containing oxygens have higher polarity and electronic density than methyl group, which produce the highest Tm and Tcr in BIIIOMe-OMe (3).

Table 2.1 Thermal Properties of BIII Derivatives

Compd	Phase Transition Temperature[a] (°C)
BIII-OMe (1)	K $\underset{156.3(-75.2)}{\overset{177.7(68.2)}{\rightleftharpoons}}$ I
BIIIMe-OMe (2)	K $\underset{174.7(-86.5)}{\overset{190.3(85.4)}{\rightleftharpoons}}$ I
BIIIOMe-OMe (3)	K $\underset{204.8(-118.6)}{\overset{219.2(118.2)}{\rightleftharpoons}}$ I
$BIIIOC_8$-OMe (4)	K $\underset{118.4(-112)}{\overset{137.4(107.8)}{\rightleftharpoons}}$ I
$BIIIOC_{12}$-OMe (5)	K $\underset{104.0(-90.6)}{\overset{123.1(98.1)}{\rightleftharpoons}}$ I
$BIIIOC_8$-OC_8 (6)	K $\underset{73.0(-43.4)}{\overset{86.2(41.4)}{\rightleftharpoons}}$ I

[a] the corresponding enthalpy (J/g) is shown in the parentheses, and K: Crystalline phase; I: Isotropic liquid.

Table 2.2 Thermal Properties of BV Derivatives

Compd	Phase Transition Temperature[a] (°C)
$BVOC_4$-OEh(7)	K $\underset{168.5\ (-40.1)}{\overset{185.6\ (40.1)}{\rightleftharpoons}}$ N $\underset{242.0\ (-1.9)}{\overset{253.9\ (0.9)}{\rightleftharpoons}}$ I
$BVOC_4$-OC_8(8)	K $\underset{156.8\ (-41.2)}{\overset{184.2\ (43.0)}{\rightleftharpoons}}$ N $\underset{266.6\ (-1.9)}{\overset{274.7\ (2.2)}{\rightleftharpoons}}$ I
$BVOC_4$-OC_{12}(9)	K $\underset{74.7\ (-11.9)}{\overset{79.1\ (11.6)}{\rightleftharpoons}}$ K' $\underset{164.8\ (-43.2)}{\overset{185.6\ (43.2)}{\rightleftharpoons}}$ N $\underset{220.0\ (-1.4)}{\overset{222.5\ (1.7)}{\rightleftharpoons}}$ I
$BVOC_8$-OEh(10)	K $\underset{139.2\ (-43.0)}{\overset{165.3\ (64.9)}{\rightleftharpoons}}$ N $\underset{219.8\ (-5.6)}{\overset{255.2\ (3.4)}{\rightleftharpoons}}$ I
$BVOC_8$-OC_8(11)	K $\underset{121.5\ (-44.9)}{\overset{145.8\ (49.6)}{\rightleftharpoons}}$ N $\underset{248.5\ (-2.1)}{\overset{250.9\ (2.3)}{\rightleftharpoons}}$ I
$BVOC_8$-OC_{12}(12)	K $\underset{132.6\ (-52.7)}{\overset{155.2\ (51.6)}{\rightleftharpoons}}$ N $\underset{201.0\ (-1.3)}{\overset{203.7\ (1.1)}{\rightleftharpoons}}$ I
$BVOC_{12}$-OC_8(13)	K $\underset{107.0\ (-38.0)}{\overset{117.8\ (2.9)}{\rightleftharpoons}}$ K' $\underset{187.0\ (-0.5)}{\overset{141.3\ (36.2)}{\rightleftharpoons}}$ N $\underset{}{\overset{189.5\ (0.4)}{\rightleftharpoons}}$ I
$BVOC_{12}$-OC_{12}(14)	K $\underset{142.6\ (-51.4)}{\overset{157.3\ (49.4)}{\rightleftharpoons}}$ N $\underset{186.6\ (-1.1)}{\overset{188.3\ (1.0)}{\rightleftharpoons}}$ I
BV-OC_8[b]	K $\underset{172.0\ (--)}{\overset{183.0\ (77.0)}{\rightleftharpoons}}$ N $\underset{202.0\ (--)}{\overset{204.0\ (1.0)}{\rightleftharpoons}}$ I

[a] the corresponding enthalpy (J/g) is shown in the parentheses, and K: crystalline phase; N: nematic phase; I: isotropic liquid.

[b] as a comparison from ref. 76,77.

Table 2.3 Thermal Properties of PBV Polymers

Compd	Phase Transition Temperature[a] (°C)	Td[b] (°C)
$PBVOC_8$-OC_4 (15)	G $\overset{75}{\rightleftharpoons}$ K $\underset{112}{\overset{130}{\rightleftharpoons}}$ N $\underset{260}{\overset{280}{\rightleftharpoons}}$ I	411
$PBVOC_8$-OC_8 (16)	G $\overset{54}{\rightleftharpoons}$ K $\underset{104}{\overset{117}{\rightleftharpoons}}$ N $\underset{220}{\overset{230}{\rightleftharpoons}}$ I	409
$PBVOC_8$-OC_{12} (17)	G $\overset{85}{\rightleftharpoons}$ K $\underset{100}{\overset{110}{\rightleftharpoons}}$ N $\underset{235}{\overset{245}{\rightleftharpoons}}$ I	393
$PBVOC_8$-OEh (18)	G $\overset{85}{\rightleftharpoons}$ K $\underset{115}{\overset{125}{\rightleftharpoons}}$ N $\underset{245}{\overset{255}{\rightleftharpoons}}$ I	400

[a] the phase transition temperatures are obtained from POM, and G: glassy state; K: crystalline phase; N: nematic phase; I: isotropic liquid.

[b] Td (thermal decomposition temperature): temperature of 5 % weight loss measured by TGA under nitrogen.

Similar effects in the melting and isotropization temperatures (Tm and Ti) are also observed in 5-conjugated ring series (i.e. BV series), besides that the mesomorphism is introduced in BV series (shown in Table 2.2) by the replacement of 3-conjugated rings with 5-conjugated phenyl cores. Compared with $BVOC_4$-OC_8 (8) , $BVOC_8$-OC_8 (11), and $BVOC_{12}$-OC_8 (13), compound BV-OC_8 without terminal groups on both end rings of the cores, which was synthesized and reported by Hadziioannou et al.,[76,77] possesses the narrowest mesophasic range (21 °C on heating) among BV series with the same 5-conjugated phenyl cores and lateral -OC_8 alkoxy substituents in Table 2.2. Hence, the introduction of alkoxy terminal chains on both end rings of the conjugated cores may enhance the stability of the mesophase (the nematic phase). However, comparing $BVOC_{12}$-OC_8 (13) with $BVOC_8$-OC_8 (11), elongating the alkoxy terminal chains on both end rings of the cores from -OC_8 to -OC_{12} would weaken the longitudinal force, which makes the nematic (N) phase become more unfavorable in $BVOC_{12}$-OC_8 (13). Similar results, i.e. the most proper alkoxy terminal chains (on both end rings) of $BVOC_8$, also occur in analogous $BVOC_n$-OC_{12} and $BVOC_n$-OEh systems containing lateral -OC_{12} and -OEh groups as side chains (on the central ring). Once the most suitable terminal chains -OC_8 (on both end rings) of $BVOC_8$ is chosen, $BVOC_8$-OEh (10), $BVOC_8$-OC_8 (11), and $BVOC_8$-OC_{12} (12) analogues can be compared to justify the most favorable side-chain

length on the central ring. Again, elongating or branching the alkoxy side chains (on the central ring) from -OC_8 to -OC_{12} or from -OC_8 to -OEh would weaken the favorable force to form the nematic (N) phase. Therefore, $BVOC_8$-OC_8 (11) has the most appropriate chain length on both ends (on both end rings) and sides (on the central ring) of the conjugated core and thus to have the widest mesophasic range (105 °C on heating) among BV series (7-14) in Table 2.2.

Based on the same consideration of the widest mesophasic ranges in $BVOC_8$ derivatives, analogous polymers, i.e. PBV series (15-18), containing various side groups on the central rings are synthesized in this study. Their thermal properties are shown in Table 2.3; and their molecular weights and polydispersity indexes (PDI) are listed in Table 2.4. Similar phase behavior, i.e. possessing Tg and the nematic phase, of these PBV derivatives are observed (see Table 2.3). Due to the variation of molecular weights and broaden transition temperatures (determined by POM) of the polymers, the alkoxy side-group effect on the polymers is not as obvious as that on their oligo-analogues. The temperature ranges of the liquid crystalline phase (i.e. the nematic phase) of polymers are wider than those of analogous oligomers, because the rigid cores of the polymer backbones are connected end-to-end by the flexible alkoxy spacers, which enhance the mesogenic longitudinal interaction in the nematic phase. Accordingly, owing to the introduction of flexible alkoxy groups either on the central

rings or on both end rings of the conjugated cores, not only the solubility but also the thermal properties (including the phase behavior and phase transition temperatures, i.e. Tm and Ti) of both 3-conjugated and 5-conjugated ring derivatives can be adjusted.

Table 2.4 Molecular Weights and Polydispersity Indexes (PDI) of PBV Polymers

Compd	*M*w	*PDI* (*M*w/*M*n)
PBVOC$_8$-OC$_4$(15)	11778	1.7
PBVOC$_8$-OC$_8$(16)	7240	1.3
PBVOC$_8$-OC$_{12}$(17)	10193	1.4
PBVOC$_8$-OEh(18)	15166	1.8

2.4.2 Optical Properties

The UV-Vis absorption spectra of these compounds in solution states (dichloroethane as the solvent) were measured and their λmax values are listed in Table 2.5. The peaks of UV-Vis spectra are near 393~398 nm for three-conjugated ring oligomers (1-5), 423~431 nm for five-conjugated ring oligomers (7-14), and 422~423 nm for five-conjugated ring polymers (15-18), correspondingly. In comparison with three-conjugated ring oligomers, five-conjugated ring derivatives have larger λmax values, i.e. red-shifted absorption, due to the smaller energy gaps of longer conjugations in five-conjugated ring derivatives. Similar absorption λmax values are observed in both oligomers and polymers of five-conjugated ring derivatives due to their alike conjugation lengths in solutions.

Table 2.5 The UV-Vis, Photoluminescent,[a] and Electroluminescent Properties of BIII, BV, and PBV Derivatives

Compd	λ_{max} (nm)				
	UV-vis (abs)[a]	PL (soln)[b]	PL (pure film)	PL (blend film)[c]	EL (blend film)[d]
BIII-OMe(1)	393	442	474	444	449
BIIIMe-OMe(2)	394	441(461)[e]	477	444	449
BIIIOMe-OMe(3)	397	444(465)	495	448	447
BIIIOC_8-OMe(4)	398	445(467)	501(527)	453	450
BIIIOC_{12}-OMe(5)	397	445(466)	501(529)	447	456
BIIIOC_8-OC_8(6)	398	447(470)	503(538)	448	459
BVOC_4-OEh(7)	426	483(513)	530	508	504
BVOC_4-OC_8(8)	424	483(512)	528	503	501
BVOC_4-OC_{12}(9)	423	486(514)	528	510	503
BVOC_8-OEh(10)	431	486(513)	526	525	510
BVOC_8-OC_8(11)	431	487(512)	532(567)	498	504
BVOC_8-OC_{12}(12)	431	487(514)	537	492	504
BVOC_{12}-OC_8(13)	430	487(512)	529	497	493
BVOC_{12}-OC_{12}(14)	431	487(514)	542	486	489
PBVOC_8-OC_4(15)	423	491(510)	543	492	495
PBVOC_8-OC_8(16)	422	486(511)	545	496	497
PBVOC_8-OC_{12}(17)	422	493(512)	544	492	499
PBVOC_8-OEh(18)	423	490(511)	531	495	498
BV-OC_8[c]	422	483	529	---	---

[a] PL measurements are excited at wavelength of 285 nm.

[b] dichloroethane as the solvent.

[c] PVK as the matrix (dopant:PVK =1:100 wt%).

[d] as a comparison from ref. 76,77.

[e] second peaks are shown in the parentheses.

The PL and EL spectra of these compounds in solutions (dichloroethane as the solvent) and films were measured and their λmax values are also listed in Table 2.5, and the PL measurements are excited at wavelength of 285 nm. The maximum emission wavelength (λmax) values of PL and EL spectra of analogous derivatives BIIIOC$_8$-OC$_8$ (6), BVOC$_8$-OC$_8$ (11), and PBVOC$_8$-OC$_8$ (16) (shown in Table 2.5) are as follows: for three-conjugated ring oligomer BIIIOC$_8$-OC$_8$ (6), λmax (PL) = 447, 503, and 448 nm in solutions, pure films, and blend films, respectively, and λmax (EL) = 459 nm in blend films; for five-conjugated ring oligomer BVOC$_8$-OC$_8$ (11), λmax (PL) = 487, 532, and 498 nm, respectively, and λmax (EL) = 504 nm in blend films; for five-conjugated ring polymer PBVOC$_8$-OC$_8$ (16), λmax (PL) = 486, 545, and 496 nm in solutions, pure films, and blend films, respectively, and λmax (EL) = 497 nm in blend films. All above blend films are solid solutions of PVK as the solvent in the ratio of dopant:PVK=1:100 wt%. Because the role of PVK matrix in the blend films is similar to that of the solvent in the solution, the blend films are solid solutions which show the same effect as the solutions with high concentrations of chromophores. Comparing λmax (PL) in solutions, pure films, and blend films of analogous derivatives BIIIOC$_8$-OC$_8$ (6), BVOC$_8$-OC$_8$ (11), and PBVOC$_8$-OC$_8$ (16), respectively, their λmax (PL) values are all in the order of: pure films > blend films > solutions. This can be reasoned by that higher degrees of aggregation take place in solid

solutions of pure and blend films which contain higher concentrations of chromophores. Compared with pure films, solid solutions of blend films lead to declined intermolecular interaction, and less aggregate states of blend films will occur, thus to produce less red-shifted emissions. The red shifts of λmax (PL) values in pure and blend films of analogous derivatives BIIIOC$_8$-OC$_8$ (6), BVOC$_8$-OC$_8$ (11), and PBVOC$_8$-OC$_8$ (16), are comparable, so their extents of aggregation in pure and blend films are similar. Besides, their λmax (EL) values are correspondent to their λmax (PL) values in blend films, since the aggregation levels in blend films are roughly equivalent in both EL and PL measurements. Therefore, the π-π stacking effect appears in solid-state films to form excimers, so the red-shifted phenomena were observed. The λmax values of PL and EL spectra in pure PVK films are usually found around 400 nm and this emission wavelength is not so obvious in the PL and EL spectra of PVK doped systems. Therefore, the PVK matrix might act as an energy-transfer component in the blend film systems.

As for three-conjugated ring oligomers in pure films, we can not observe a second peak in the PL spectra of BIII-OMe (1) (see Table 2.5). The second PL (pure film) peaks of BIIIMe-OMe (2) and BIIIOMe-OMe (3) are also not obvious, but those of BIIIOC$_8$-OMe (4), BIIIOC$_{12}$-OMe (5), and BIIIOC$_8$-OC$_8$ (6) are easier to be detected. Besides, the latter compounds with longer alkoxy terminal chains (on both

end rings), i.e. BIIIOC$_8$-OMe (4), BIIIOC$_{12}$-OMe (5), and BIIIOC$_8$-OC$_8$ (6), also have larger red shifts of λmax values in PL (pure film) emissions compared with their corresponding PL (solution) emissions. Probably the longer and polar end alkoxy chains stack each other to cause red shifts on the major PL peaks (i.e. λmax). The reason to cause stronger second peaks in these compounds possibly originats from the excimers, which is confirmed by the concentration study of the solution samples, i.e. gradual appearance of second peaks in higher concentrations. Additionally, compared with BIII-OMe (1) and BIIIMe-OMe (2), BIIIOMe-OMe (3) possessing the same core and lateral OMe groups has a stronger red-shifted PL emission in pure films, though all of them have similar λmax values in PL (solution) emissions. This can be explained by the extra polar interaction of alkoxy chains on both ends of BIIIOMe-OMe (3) to cause more aggregation. Similar aggreration and red shifts of λmax values in PL emissions occur in pure films compared with the corresponding solutions of BV and PBV series. Consequently, blend films of three-conjugated ring oligomers show blue PL and EL emissions (λmax = 444-459 nm), and those of five-conjugated ring derivatives (oligomers and polymers) illustrate blue-greenish PL and EL emissions (λmax = 486-525 nm).

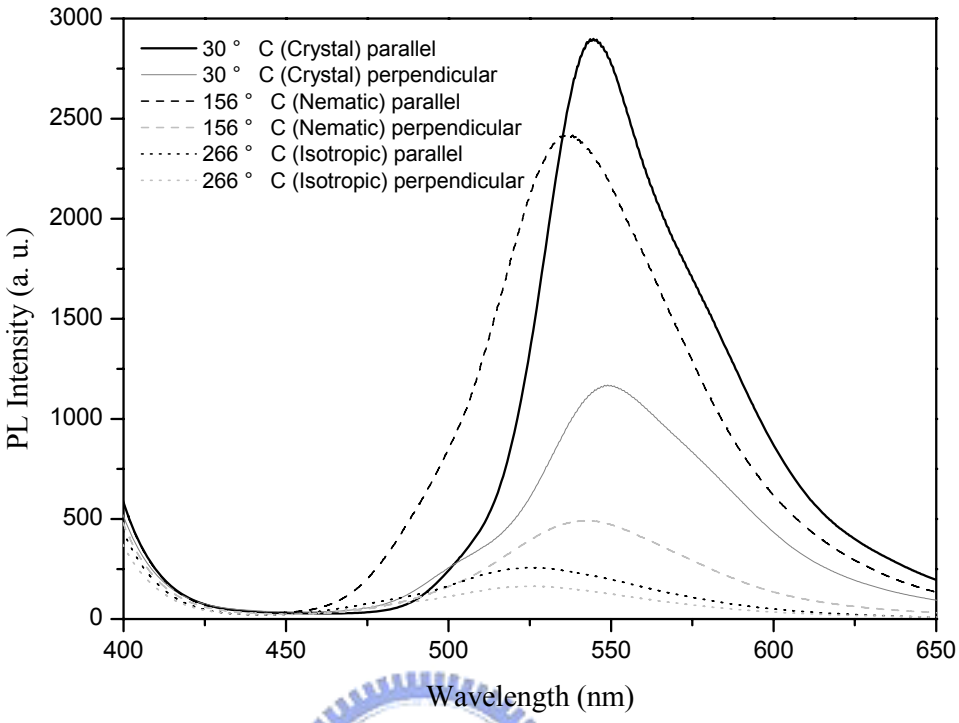

Figure 2.1 The photoluminescence spectra of $BVOC_8$-OC_8 (11) in various phases while the polarizer is to feed the rubbing direction (parallel and perpendicular).

Interestingly, the PL emissions of five-conjugated ring oligomers show different colors in different phases. Figure 2.1 shows the PL spectra of $BVOC_8$-OC_8 (11) by heating from the crystalline state (λmax of PL = 545 nm) to the liquid crystalline (LC) state (λmax of PL = 535 nm), and sequentially to the isotropic phase (λmax of PL = 525 nm). Due to larger aggregation caused by parallel alignment and larger film thickness inside the rubbing cell (with 9 μm cell gap) of Figure 2.1, λmax (PL) = 545 nm of $BVOC_8$-OC_8 (11) in the aligned crystalline state (Figure 2.1) is larger than λmax (PL) = 532 nm in the film state (ca. 40 nm by spin-coating on glass substrate) of $BVOC_8$-OC_8 (11) in Table 2.5. When $BVOC_8$-OC_8 (11) is heated serially from the

crystalline phase to the isotropic phase, blue shifts in PL spectra are observed in Figure 2.1. One of the possible reason for the blue shift of λmax (PL) upon heating is that increasing temperature may eliminate the coplanar configuration of the molecular structure and reduce its conjugation length (thus to increase the energy gap), so it shows blue shifts due to non-coplanar structures at higher temperatures. It is also possible that the aggregation level of molecular stacking decreases to cause the blue shift as the temperature increases. However, less aggregation levels should have higher PL intensities, which do not agree with the lowest PL emission possessed by the isotropic state in Figure 2.1. Hence, the order of the PL emission intensity (revealed in Figure 2.1), i.e. (crystalline state) > (LC state) > (isotropic state), rules out the possibility of the blue shift of the isotropic state (with much lower PL intensity) caused by the less aggregation level. In addition, comparing the full width half maximum (FWHM) values of various phases, they are as follows: FWHM (crystalline state) = 56 nm < FWHM (LC state) = 70 nm < FWHM (isotropic state) = 76 nm. It is conceived that broaden electron transition state distributions in various states of molecular architecture will have larger FWHM values which indicates molecules possess more types of twisted conformations at higher temperatures. Since the blue shift of the isotropic state having the lowest PL intensity can not be explained by the least aggregation of the isotropic phase, therefore, the least coplanar configuration

with wide distribution of conformation (as well as conjugation) in the isotropic phase may be more favorable to explain the blue shift and the reduction of PL intensity with the broadest FWHM value in the isotropic state. When the polarizer is perpendicular to the rubbing direction, these tendencies (e.g. FWHM values, PL emission intensities and wavelengths) are similar to those parallel to the rubbing direction.

As we know if the sample possesses a LC phase, the LC phase can be aligned in a rubbing cell. When the rubbing cell is parallel to the polarizer, the conjugated core, which is aligned in the rubbing direction, will be also parallel to the polarizer at the same time. Therefore, a maximum PL emission is observed as the polarizer is in the parallel direction of rubbing, and a minimum PL emission will be observed as the polarizer is in the perpendicular direction of rubbing. The polarized PL of $BVOC_8$-OC_8 (11) in the LC phase is shown in Figure 2.2. The polarization ratio is defined by $(PL_{//})/(PL_{\perp})$, where $PL_{//}$ and $PL_{\perp}$ are the maximum PL emission intensities as the polarizer is parallel and perpendicular to the rubbing direction, respectively. Figure 2.3 shows the polarization ratio and λmax (PL) values of $BVOC_8$-OC_8 (11) in rubbing cells at various temperatures. The polarization ratio reaches a maximum value at the transition of the crystalline phase to the mesophase upon heating, and the polarization ratio decreases as the temperature increases, which is similar to the behavior of the order parameter of LC materials upon heating.

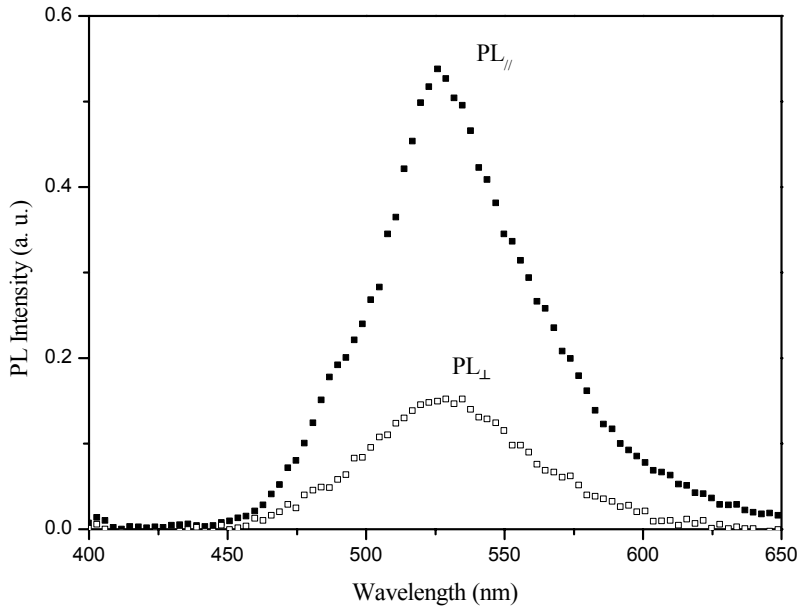

Figure 2.2 The photoluminescence spectra of $BVOC_8$-OC_8 (11) at 156 °C (in the nematic phase), where $PL_{//}$ and $PL_{\perp}$ are the maximum PL emission intensities as the polarizer is parallel and perpendicular to the rubbing direction, respectively.

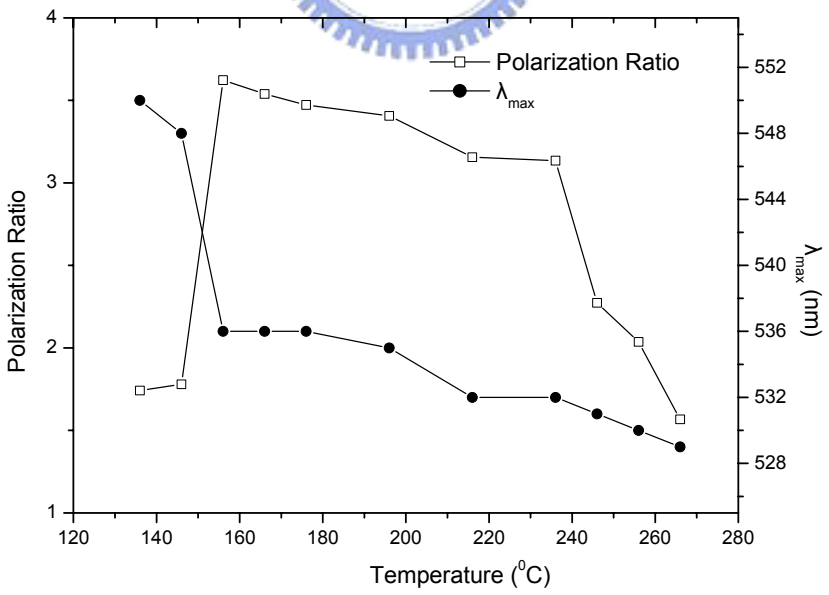

Figure 2.3 The polarization ratio and λmax (PL) values of $BVOC_8$-OC_8 (11) in rubbing cells at various temperatures.

As mentioned previously, blue shifts in PL spectra are observed upon heating, which is due to the reduction of coplanar configurations and conjugation lengths and thus to have larger energy gaps at higher temperatures. Interestingly, the largest reduction of λmax value and the largest increasement of polarization ratio both have occurred at the transition temperatures around heating into the mesophase, which illustrates the alignment of the mesogenic cores by surface may cause twisted configurations and non-coplanar conformations. The maximum polarization ratio and related optical properties (including HOMO/LUMO energy levels, optical band gaps, and PL quantum yield Φ) of all compounds are shown in Table 2.6. The maximum polarization ratio of $BVOC_8$-OC_8 (11) is 3.6 (also shown in Figure 2.3) and the highest value of polarization ratio is 6.2 found in $BVOC_{12}$-OC_8 (13). These values of oligomers are generally higher (except for $BVOC_{12}$-OC_{12} (14) polarization ratio = 2.5, which may be due to the symmetrical long flexible chains on both sides and ends of conjugated cores) than those of polymers (polarization ratio = 1.6 ~ 3.1 for PBV series), because polymer chains cannot be aligned completely in the rubbing direction (due to higher viscosity and entanglement of polymer chains), which induces the reduction of polarization ratios in the polymers. Overall, the maximum polarization ratios of PL emissions are not correlated to the lengths of side groups and end groups attached to the cores.

Table 2.6 The Optical Properties of BIII, BV, and PBV Derivatives

Compd	HOMO/LUMO (eV)	Band Gap[a] (eV)	Φ (PL)[b]	Φ (PL)[c]	Maximum Polarization Ratio
BIII-OMe(1)	5.63/2.92	2.71	0.30	0.34	NA[d]
BIIIMe-OMe(2)	5.62/2.93	2.69	0.30	0.34	NA
BIIIOMe-OMe(3)	5.76/3.01	2.75	0.27	0.33	NA
$BIIIOC_8$-OMe(4)	5.87/3.15	2.72	0.33	0.36	NA
$BIIIOC_{12}$-OMe(5)	5.70/2.95	2.75	0.26	0.31	NA
$BIIIOC_8$-OC_8(6)	5.61/2.86	2.74	0.30	0.33	NA
$BVOC_4$-OEh(7)	5.62/3.06	2.56	0.51	0.52	4.4
$BVOC_4$-OC_8(8)	5.45/2.89	2.56	0.50	0.52	3.9
$BVOC_4$-OC_{12}(9)	5.61/3.05	2.56	0.48	0.50	5.0
$BVOC_8$-OEh(10)	5.69/3.14	2.55	0.45	0.49	4.5
$BVOC_8$-OC_8(11)	5.58/3.07	2.51	0.52	0.52	3.6
$BVOC_8$-OC_{12}(12)	5.74/3.23	2.51	0.49	0.52	4.8
$BVOC_{12}$-OC_8(13)	5.64/3.13	2.51	0.51	0.52	6.2
$BVOC_{12}$-OC_{12}(14)	5.69/3.18	2.51	0.47	0.50	2.5
$PBVOC_8$-OC_4(15)	5.98/3.42	2.56	0.40	0.46	1.6
$PBVOC_8$-OC_8(16)	5.60/3.05	2.55	0.35	0.44	1.7
$PBVOC_8$-OC_{12}(17)	5.59/3.03	2.56	0.43	0.46	2.1
$PBVOC_8$-OEh(18)	5.68/3.11	2.57	0.53	0.48	3.1

[a] optical band gap obtained by UV-Vis.

[b] in solutions with a concentration of 10^{-5} M in dichloroethane and quinine sulfate as the reference with a quantum yield of 0.54.

[c] in films with a weight ratio of 1:100 (PVK as the matrix) and MEHPPV as the reference with a quantum yield of 0.22.

[d] data not available due to no LC phase.

The lowest occupied molecular orbital (LUMO) values, which are calculated by the highest occupied molecular orbital (HOMO) values (by AC-2) minus the optical band gap values (by UV-Vis), are also listed in Table 2.6. The band gap values of three-conjugated ring oligomers (BIII series) are between 2.67 to 2.75 eV. Compared with three-conjugated ring oligomers, five-conjugated ring derivatives (BV oligomers and PBV polymers) possess smaller band gaps between 2.51 and 2.57 eV, due to the longer conjugated length of five-conjugated ring derivatives, and thus to generate longer wavelengths of PL and EL emissions. Whereas, the band gaps of five-conjugated ring oligomers and analogous polymers are too indistinct to have divergent PL and EL emissions. The PL quantum yields (in solutions) of BIII oligomers, BV oligomers, and PBV polymers (shown in Table 2.6) are 0.48~0.56, 0.84~0.95, and 0.65~0.99, respectively. Oligomers and polymers of five-conjugated ring derivatives have similar PL quantum yields. Accordingly, five-conjugated ring derivatives (BV oligomers and PBV polymers) have larger PL quantum yields than three-conjugated ring BIII oligomers, which may be due to the longer conjugation lengths in five-conjugated ring systems. The PL and EL spectra of analogous derivatives BIIIOC_8-OC_8 (6), BVOC_8-OC_8 (11), and PBVOC_8-OC_8 (16) containing the same length of alkoxy groups (-OC_8) on both of the sides and ends are compared in Figures 2.4-2.6, respectively. For these analogous derivatives BIIIOC_8-OC_8 (6),

$BVOC_8$-OC_8 (11), and $PBVOC_8$-OC_8 (16), they induce variations of energy gaps and luminescence behavior. In their solution and pure film states, two peaks were found in the PL spectra (shown in Figures 2.4 and 2.5) of oligomers $BIIIOC_8$-OC_8 (6) and $BVOC_8$-OC_8 (11) and a single peak was found in the PL spectra (demonstrated in Figure 2.6) of polymer $PBVOC_8$-OC_8 (16). Thus, more types of twisted conformations and conjugations, or more aggregation, including vibronic motion, occur in oligomers than in polymers. As shown in Table 2.3, the glassy state of reduced crystallinity in PBV polymers have been observed in their thermal properties (all possess Tg between 54 and 85 °C) and have also been confirmed by XRD measurements (as glassy states with broaden peaks at ca. 21°), so polymers have less crystallinity (i.e. less aggregation) than oligomers.

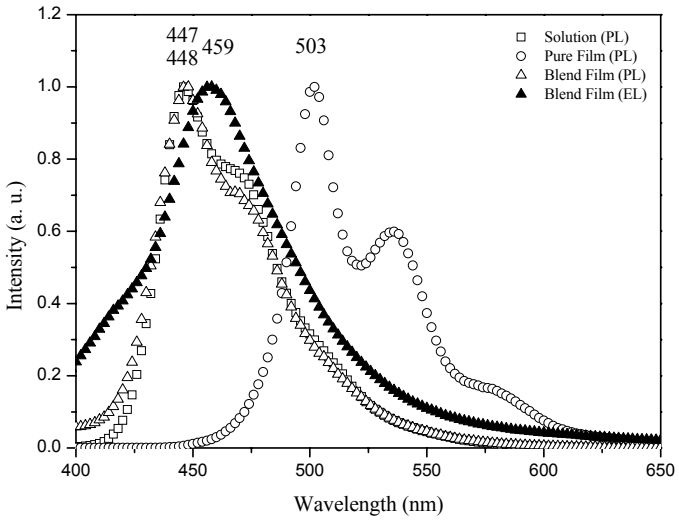

Figure 2.4 The photoluminescence and electroluminescence spectra of $BIIIOC_8$-OC_8 (6). (PVK matrix is used in blend films; chromophore: PVK = 1: 100 wt%.)

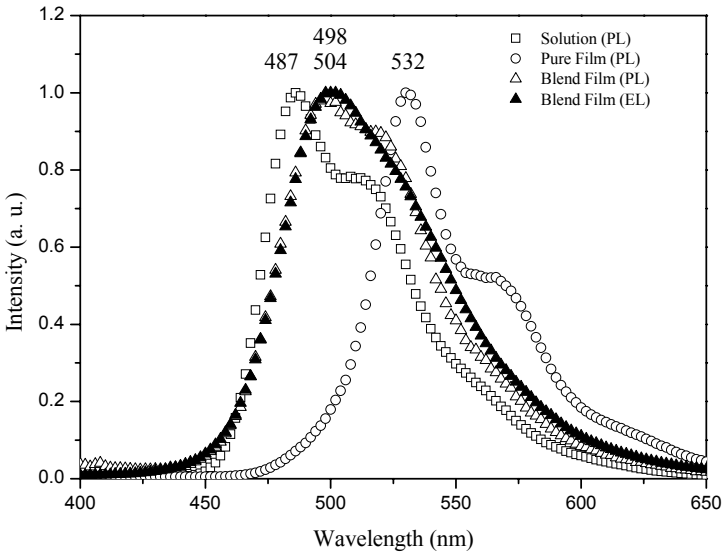

Figure 2.5 The photoluminescence and electroluminescence spectra of $BVOC_8$-OC_8 (11). (PVK matrix is used in blend films; chromophore: PVK = 1: 100 wt%.)

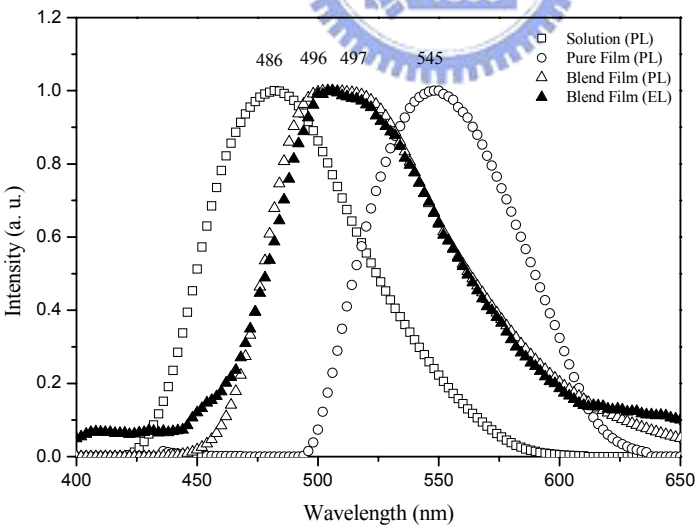

Figure 2.6 The photoluminescence and electroluminescence spectra of $PBVOC_8$-OC_8 (16). (PVK matrix is used in blend films; chromophore: PVK = 1: 100 wt%.)

Due to the poor film quality of these chromophores, oligo(*p*-phenylene-vinylene)s (1-14) and poly(*p*-phenylene-vinylene)s (15-18) are doped into PVK to form various blend films in PVK matrix (chromophore:PVK = 1:100 wt%). The EL spectra and λmax values of EL are also demonstrated in Table 2.5 and Figures 2.4-2.6. The I-V-L curves of blend films containing $BIIIOC_8$-OC_8 (6), $BVOC_8$-OC_8 (11), and $PBVOC_8$-OC_8 (16) are shown in Figure 2.7. Similar turn-on voltages around 9-12 volts are obtained, and the blend film containing 3-conjugated ring oligomer $BIIIOC_8$-OC_8 (6) has the highest brightness of 120 cd/m^2. Though the highest brightness is only around 120 cd/m^2 among these blend films, they can be further improved to have the brightness over 50000 cd/m^2 by the introduction of hole and electron transporting layers in the multilayer design. Related results of various device configurations and characteristics of the multilayer devices will be deliberated in another report.

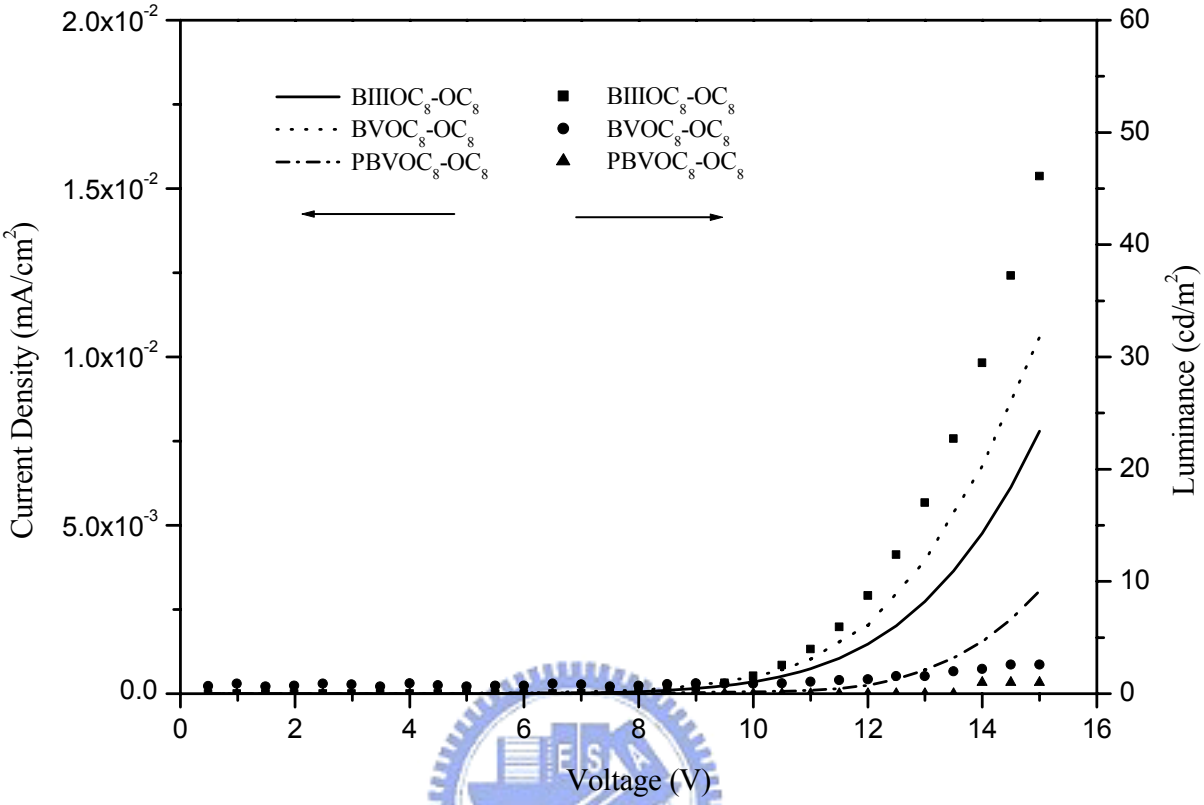

Figure 2.7 The I-V-L curves of blend films containing $BIIIOC_8$-OC_8 (6), $BVOC_8$-OC_8 (11), and $PBVOC_8$-OC_8 (16) in PVK matrix (chromophore: PVK = 1: 100 wt%). The void symbols are I-V curves, and the solid symbols are L-V curves.

2.5 Conclusions

The mesomorphism is introduced to BV series by the replacement of 3-conjugated rings with 5-conjugated phenyl cores, and $BVOC_8$-OC_8 (11) has the most appropriate chain length on both terminals (on both end rings) and sides (on the central ring) of the conjugated core and thus to have the widest mesophasic range (105 °C on heating) in BV series. In comparison with three-conjugated ring BIII oligomers,

five-conjugated ring derivatives (BV oligomers and PBV polymers) have larger λmax values, i.e. red-shifted absorption, due to the smaller energy gaps of longer conjugations in five-conjugated ring systems. Analogous polymers, i.e. PBV series, containing various side groups have wider mesophasic temperature ranges than those of analogous oligomers, because the rigid cores of the polymer backbones are connected by the flexible alkoxy spacers which enhance the mesogenic longitudinal interaction in the nematic phase. According to the λmax values of PL emissions in various phases (i.e. λmax in crystalline state > λmax in LC state > λmax in isotropic state), the blue shifts of PL emissions may be due to the reduction of coplanar configurations and conjugation lengths by heating to the less ordered phases. In addition, the polarization ratios of PL emissions in various phases reach the maximum values at temperatures just entering the nematic phase, and the PL polarization ratios reduced upon heating, which is similar to the reduction of the order parameter upon heating of the LC phase. By adjusting of flexible alkoxy groups either on the central rings or on both end rings of the conjugated cores, not only the solubility and thermal properties (including phase behavior and phase transition temperatures, i.e. Tm and Ti) but also the PL and EL properties, including λmax (LUMO, HOMO, FWHM, and energy gap) values, turn-on voltage, brightness, and quantum yield, of both 3-conjugated and 5-conjugated ring derivatives can be modified easily.

Chapter 3

Characterization of Light-Emitting Oligo(*p*-phenylene-vinylene)s and Polymeric Derivatives Containing Three- and Five-Conjugated Phenylene Rings. II. Electro-Optical Properties and Optimization of PLED Performances

3.1 Abstract

A series of multilayer polymeric light-emitting-diodes (PLEDs) containing an electron-transporting layer (ETL), i.e. tris(8-quinolinolato)-aluminum(III) (Alq) and 2,2',2"-(1,3,5-phenylene)-tris[1-phenyl-1H-benzimidazole] (TPBI), were fabricated by doping fluorescent oligo(*p*-phenylene-vinylene)s (BIII and BV) and polymer derivatives (PBV) into poly(*N*-vinyl carbazole) (PVK). These PLEDs can be optimized by the design of multilayer device configurations (brightness increased 8~15 times by adding an ETL) and possess greenish electroluminescent (EL) spectra peaked around 500-540 nm. A remarkably high brightness of 56935 cd/m^2 with a power efficiency of 3.25 lm/W was obtained in the device of PVK:BVOC$_8$-OC$_8$ (100:20)/Alq (60 nm/60 nm). It suggests that the emission mechanism (including the conjugated and excimer emissions of BVOC$_8$-OC$_8$ emitters) originates from both of

$BVOC_8$-OC_8 and ETL (Alq and TPBI) by varying the concentration of chromophores and adjusting the thickness of ETL. The concentration effect of the emitters in PVK (i.e. PVK:$BVOC_8$-OC_8 = 100:5, 100:20, and 100:100 wt%) and the influence of the ETL (including its thickness) on the EL characteristics are also reported.

3.2 Introduction

During the last few years the studies of the emission properties of molecular electroluminescent diodes have gained much attention.[23, 79-81] Polymer LEDs (PLEDs) and organic LEDs (OLEDs) can be modified and applied to LED technologies. In PLED[82-84] devices, electrons and holes are injected from opposite electrodes and combined to form either singlet or triplet excitons.[85] Because triplet radiative decay is typically forbidden in organic materials[86] and spin statistics implies that the ratio of triplets to singlets is 3:1, even 100% photoluminescence (PL) efficiency from the singlet excitations can only result in a maximum internal quantum efficiency of 25% for electroluminescence (EL). Transition metal complexes have attracted interest in fabrication of OLEDs, originally from the expectation that they could overcome the maximum 25% theoretical efficiency by singlet-triplet mixing.[87-89] As a result, EL quantum efficiencies as high as 50% have been reported.[90]

For pure polymeric LED systems, a maximum luminescence of 100,000 cd/m^2

was found in poly(phenylene vinylene)s (PPV).[91] However, polymer blend systems are easy to adjust their EL characteristics and doped PLED devices with efficient brightness are described in the following examples. For instance, in polymer blend systems containing poly(*N*-vinyl carbazole) (PVK) (Mw = 1,000,000) as the matrix, poly[4,4'-biphenylene-α-(9",9"-dihexyl-3-fluorenyl)vinylene] (PBPHFV) doping device (PBPHFV:PVK=1:5)[92,93] can reach up to a brightness of 9,342 cd/m^2 and poly[9,9-biscoctyl]-fluorene-2,7-diyl] (PF) doping device (PF:PVK=1:100) can attain a brightness around 8,300 cd/m^2.[94] Besides, green light emission for electrophosphorescent OLEDs with an external quantum (Qext.) efficiency of 19.2% and a luminescence efficiency of 73 cd/A at a current density (*j*) of 0.55 mA/cm^2 were reported in the device containing perfluorinated phenylene as a both hole- and exciton-blocking layer, and a hole-transporting host 4,4',4"-tri(*N*-carbazolyl)triphenylamine doped with a phosphorescent dye [Ir(ppy)$_3$] as an emitting layer.[95] Furtheremore, if [Ir(ppy)$_3$] dyes are doped into PVK in a triple-layer device configuration, Qext. efficiency = 7.5% is reported.[96] Moreover, phosphorescent tris(4,7-diphenyl-1,10-phenanthroline)rhenium complexed with various doping ratios of phosphorescent [Ir(ppy)$_3$] in doubly doped PVK systems can modify the driving voltage.[97-99] In addition, for green light emission, the full width at half maximum (FWHM) and lifetime of an efficient OLED device, which contains

TPBI as an electron-transporting material and a fluorescent {6-*N*,*N*-diethylamino-1-methyl-3-phenyl-1*H*-pyrazolo[3,4-*b*]quinoline} as a dopant in the hole-transporting layer of NPB, are measured to be 60 nm and 10,000 h, respectively.[100] Another electrophosphorescent device with *fac*-tris(2-phenylpyridine)iridium as a green dopant emitter and aluminum(III)bis(2-methyl-8-quinolinato)4-phenylphenolate (BAlq) as a hole-blocking material demonstrates an efficiency of 19 cd/A with a projected operational lifetime of 10,000 h, or 50,000 h normalized to 100 cd/m^2.[101] In the meanwhile, doping devices of red and white electroluminescence with high brightness were developed, e.g. 6,800 cd/m^2 in Ir complexes-based OLED[102] and 20,000 cd/m^2 in (ITO/PEDOT/PF:TBH/LiF/Ca) PLED[103] devices.

Previously, a series of light-emitting oligo(*p*-phenylene-vinylene)s (BIII and BV) and polymer derivatives (PBV) have been reported.[12] Due to the poor film quality of these chromophores, OPVs and poly(p-phenylenevinylene)s were doped into PVK to form various blend films in a PVK matrix (chromophore/PVK = 1:100 wt %), which were applied to PLED devices. Though the blend films containing three-conjugated ring oligomers can only have the highest brightness of 120 cd/m^2 or so, they can be further improved to have a brightness greater than 50,000 cd/m^2 by the optimization of electro-optical properties. Related results by introduction of hole- and

electron-transporting layers in the multilayer design of PLED devices will be reported in this article, where Alq and TPBI are utilized as electron-transporting layers (ETLs) to obtain high brightness and efficiencies. The characteristics of PLED devices are explored by changing the concentration of dopants in PVK and by adjusting various thicknesses of electron-transporting layers. The PLED devices are also investigated by blending NPB hole-transporting dopants into the emitting layer or by inserting a hole-blocking layer of bathocuproine (BCP) between the emitting layer and the ETL (Alq). The result shows that mesogenic BV derivatives with proper alkoxy groups possess excellent hole-transporting property and high brightness in PLED devices, which contain an electron-transporting Alq layer (or Alq as an emitting layer simultaneously). In general, the photophysical characteristics, including brightness and efficiency, of these PLEDs can be much improved by the multilayer design of device configurations.

3.3 Experimental

The solutions (30 mg/ml) of light-emitting materials in 1,2-dichloroethane were spin-coated on glass slides precoated with indium tin oxide (ITO) with sheet resistances of ~20 Ω/square and with an effective individual device area of 3.14 mm^2. The ITO glasses were routinely cleaned by ultrasonic treatment in detergent solutions

and diluted water, followed by through rinsing in acetone and then ethanol. After drying, the ITO glasses were kept in oxygen plasma for 3 min before being loaded into the vacuum chamber. The doping concentrations of emitters in PVK were 5:100, 20:100, and 100:100 (emitter:PVK) wt%. The spin coating rate was 3000 rpm for 40 s, and the thickness of the emitting layer was about 60 nm (with a total thickness of 100 nm, including 40 nm of TPBI or Alq). The organic layers of small molecules were deposited thermally at a rate of 0.1-0.3 Å/s under a pressure of ~$2x10^{-5}$ torr in an Ulvac Cryogenic deposition system. One layer of magnesium and silver alloy (ca. 10:1, 50 nm) was deposited as a cathode, which was capped with 100 nm of silver. The current-voltage-luminescence properties were measured in ambient conditions with a Keithley 2400 Source meter and a Newport 1835C Optical meter equipped with an 818ST silicon photodiode. The optical band gap (Eg) and HOMO values were measured by UV-Vis (solution) and AC2 (powder), respectively. Then, the LUMO values can be calculated from the HOMO and Eg values. The synthetic procedures of TPBI and Alq were reported in the literature.[100]

3.4 Results and Discussion

The device configuration and molecular structures of emitters and materials used in the PLED devices are shown in Figures 3.1 and 3.2. The synthesis and physical

characterization of light-emitting oligo(*p*-phenylene-vinylene)s (BIII and BV) and polymer derivatives (PBV) have been reported previously.[12]

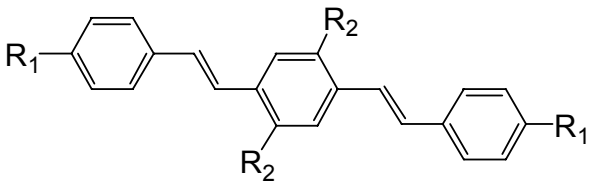

R_1 = H, CH_3, OMe, OC_8H_{17}, or $OC_{12}H_{25}$ R_2 = OMe, or OC_8H_{17}

BIIIR_1-R_2

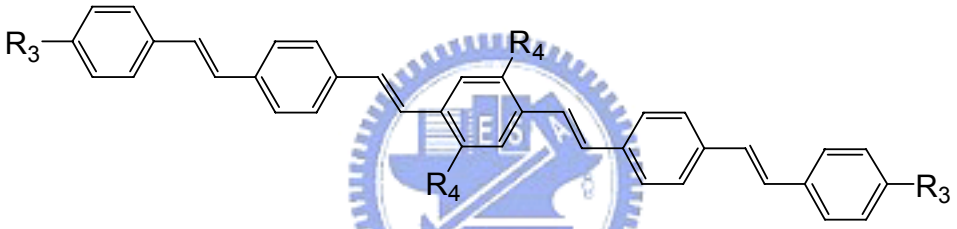

R_3 = OC_4H_9, OC_8H_{17}, or $OC_{12}H_{25}$ R_4 = OC_4H_9, OC_8H_{17}, $OC_{12}H_{25}$, or OEh (ethyl-hexyl)

BVR_3-R_4

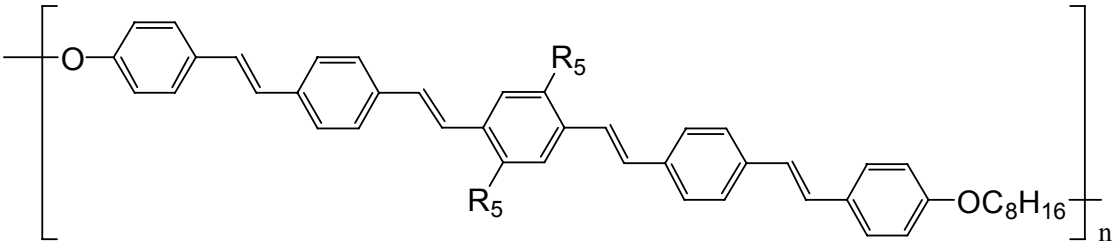

R_5 = OC_4H_9, OC_8H_{17}, $OC_{12}H_{25}$, or OEh (ethyl-hexyl)

PBVOC_8-R_5

Figure 3.1 Molecular structures of fluorescent oligo(*p*-phenylene-vinylene)s (BIII and BV) and polymer derivatives (PBV).

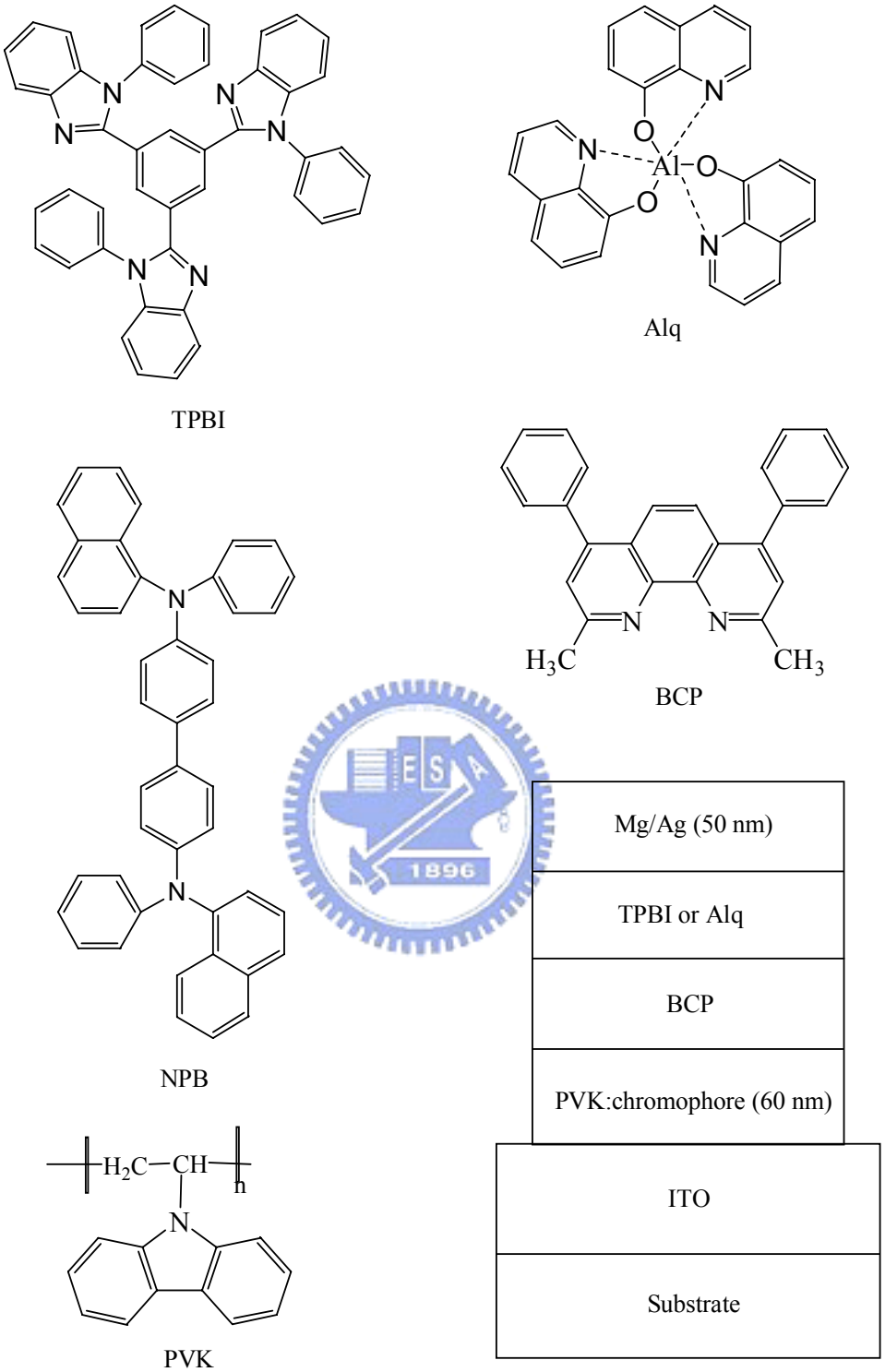

Figure 3.2 Architecture of PLED device and molecular structures of materials used in this study.

Table 3.1 EL Characteristics of Various PLED Devices Containing BV Derivatives and ETL (40 nm) of Alq or TPBI

	$BVOC_4$-OC_4[a]	$BVOC_4$-OC_8[a]	$BVOC_4$-OEh[a]	$BVOC_4$-OC_{12}[a]	$BVOC_8$-OC_8[a]	$BVOC_8$-OEh[a]	$BVOC_8$-OC_{12}[a]	$BVOC_{12}$-OC_8[a]	$BVOC_{12}$-OC_{12}[a]	$BVOC_8$-OC_8[a]	$BVOC_8$-OC_8[b]	$BVOC_8$-OC_8[c]
ETL	Alq/TPBI	Alq /TPBI	Alq /TPBI	Alq /TPBI	Alq /TPBI	Alq /TPBI	Alq /TPBI	Alq /TPBI	Alq /TPBI		Alq /TPBI	Alq /TPBI
Turn-on voltage, V	2.4/3.5	3.1/3.8	2.3/3.0	2.2/3.3	2.9/3.0	3.1/3.1	3.1/3.2	3.0/3.0	3.0/3.3	6.0	3.5/3.2	2.2/2.9
Max. brightness,	15935/	32592/	22495/	18551/	50144/	26855/	15569/	46633/	24291/	3319	17334/	25280/
cd/m^2	7362	12306	8096	8790	27328	9494	10679	16710	12093		22578	28868
Max. external quantum effic., %	1.7/2.0	1.4/0.5	1.4/1.1	1.6/1.9	2.0/1.6	1.0/1.1	0.9/1.9	0.8/0.7	1.4/3.0	0.06	0.5/1.8	3.1/2.9
Max. power effic., lm/W	1.2/1.4	1.6/0.4	1.5/0.7	1.8/1.4	2.9/2.5	0.9/1.1	1.0/1.1	0.9/0.7	1.4/1.6	0.05	1.0/1.4	4.0/3.7
λ_{em} (FWHM), nm	524 (86)/	528 (80)/	520 (86)/	516 (86)/	534 (84)/	512 (80)/	512 (88)/	538(72)/	518 (88)	508(74)	518(88)	538(68)/
(EL)	504 (78)	512 (84)	512(76)	500 (76)	534 (66)	506 (68)	494 (94)	538(70)	486 (122)		504(70)	538(68)
CIE,	0.29, 0.55/	0.30, 0.61/	0.29, 0.59/	0.27, 0.57/	0.33, 0.61/	0.28, 0.58/	0.26, 0.54/	0.35, 0.60/	0.28, 0.54/	0.25, 0.58	0.28, 0.56/	0.36, 0.62
x,y	0.21, 0.44	0.31, 0.60	0.26, 0.61	0.21, 0.47	0.30, 0.62	0.24, 0.55	0.18, 0.33	0.36, 0.60	0.17, 0.25		0.23, 0.54	0.36, 0.60
Voltage at 100 mA/cm^2, V	12.4/14.1	13.9/18.3	14.2/22.0	12.7/16.0	11.6/9.6	12.2/13.4	11.7/14.2	13.6/13.2	12.3/11.9	13.4	12.4/12.5	14.1/12.8
Brightness at 100 mA/cm^2, cd/m^2	4710/2721	5059/1573	4656/2618	5045/2602	6867/5619	3475/2466	2908/2615	2695/2776	4595/3329	198	3097/5340	11545/10937
external quantum effic. at 100 mA/cm^2, %	1.7/1.2	1.4/0.4	1.3/0.7	1.5/1.0	1.8/1.6	1.0/0.8	0.9/1.3	0.7/0.7	1.4/2.2	0.06	0.5/1.8	2.7/2.8
power effic. At 100 mA/cm^2, lm/W	1.2/0.6	1.1/0.3	1.0/0.4	1.3/0.5	1.9/1.9	0.9/0.6	0.8/0.6	0.6/0.7	1.2/0.9	0.05	0.8/1.4	2.6/2.7

[a] The thickness of Alq or TPBI is 40 nm and PVK: chromophore =100: 20.
[b] The thickness of Alq or TPBI is 40 nm and PVK: chromophore =100: 5.
[c] The thickness of Alq or TPBI is 40 nm and PVK: chromophore =100: 100

The EL characteristics of PLED devices containing BV derivatives with five-conjugated rings are shown in Table 3.1. Among all the fluorescent oligo(p-phenylene-vinylene)s (BIII and BV) and polymer derivatives (PBV), $BVOC_8$-OC_8 is the brightest (EL) compound in this study. With regard to the PLED device of PVK: $BVOC_8$-OC_8 (100:20)/Alq (60 nm), the maximum luminescence (EL) = 56935 cd/m^2 and the full width at half maximum (FWHM) = 92 nm, C.I.E. (x, y) = (0.34, 0.59), and the wavelength of maximum emission = 536 nm are obtained. Since light-emitting $BVOC_8$-OC_8 is the brightest EL compound, related EL properties of various PLED device configurations regarding $BVOC_8$-OC_8 emitters are surveyed.

The concentration effects of $BVOC_8$-OC_8 emitters on PL spectra in solution and blend film states are demonstrated in Figures 3.3 and 3.4, respectively. In addition to pure films, the PL spectra of $BVOC_8$-OC_8 blended in PVK with various concentrations, i.e. PVK:$BVOC_8$-OC_8 = 100:5, 100:20, and 100:100 wt%, are measured in the film states (see Figure 3.4). Owing to the aggregation of chromophores, the λmax values of PL emission peaks are all red-shifted at higher concentrations in solution and film states, which are also observed in the EL spectra of Figure 3.5. None the less, the PL emission of PVK (c.a. 400 nm) in Figure 3.4 is more obvious (i.e. the lower concentration of the chromophore, the higher the PL emission peak of PVK relative to the maximum PL emission peak of $BVOC_8$-OC_8) than the EL emission of PVK in Figure 3.5. As described in the literature, $Ir(DPPF)_3$ emitters doped in PVK matrix,[104] the absence of PVK EL emission from devices of $BVOC_8$-OC_8 (doped in PVK matrix with various concentrations) may be due to the charge trapping of $BVOC_8$-OC_8 emitters, rather than Förster transfer, as the dominant mechanism in these PLED Devices. If energy transfer were the dominant EL mechanism, the EL emission of PVK would be expected to appear when $BVOC_8$-OC_8

emitters become saturated. As revealed by Figure 3.3, the red-shifted PL emissions originated from the aggregation of chromophores at higher concentrations are verified by the PL emission of $BVOC_8$-OC_8 solution with various concentrations in dichloroethane. Hence, the excimers are formed as the concentration of light-emitting materials (i.e. $BVOC_8$-OC_8) increases, and additional red shifts of λmax values in $BVOC_8$-OC_8 PL emissions are further confirmed by increasing the concentration of $BVOC_8$-OC_8 in PVK (see Figure 3.4). The PL spectrum of the pure film has the longest λmax value (along with an obvious shoulder around 570 nm) due to the largest aggregation of emitters in the film state, and the PL spectrum (excluding the PVK emission) in the blend film of PVK:$BVOC_8$-OC_8 = 100:5 wt% is similar to those of dilute solutions at 10^{-5}~10^{-6} M. Therefore, most $BVOC_8$-OC_8 molecules in PVK matrix could be dispersed well in the blend film of PVK:$BVOC_8$-OC_8 = 100:5 wt%, so the charge hopping would occur mainly between the molecules. However, in PLED devices of PVK: $BVOC_8$-OC_8 = 100:20 and 100:100 wt%, higher concentrations would cause larger electronic interaction[105] among most $BVOC_8$-OC_8 molecules due to the decreased separation between them. As a result, the charges injected from two opposite electrodes would transport and recombine mainly on these sites.

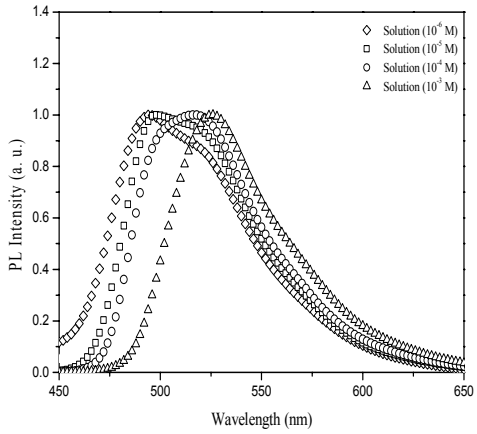

Figure 3.3 PL spectra of $BVOC_8$-OC_8 in solutions (dichloroethane as solvent) with various concentrations.

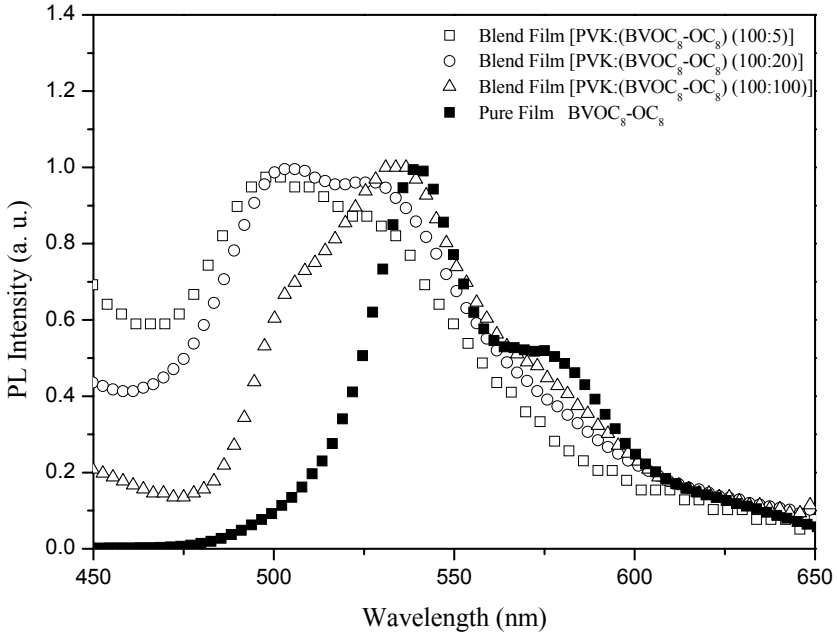

Figure 3.4 PL spectra of $BVOC_8$-OC_8 in pure and blend films.

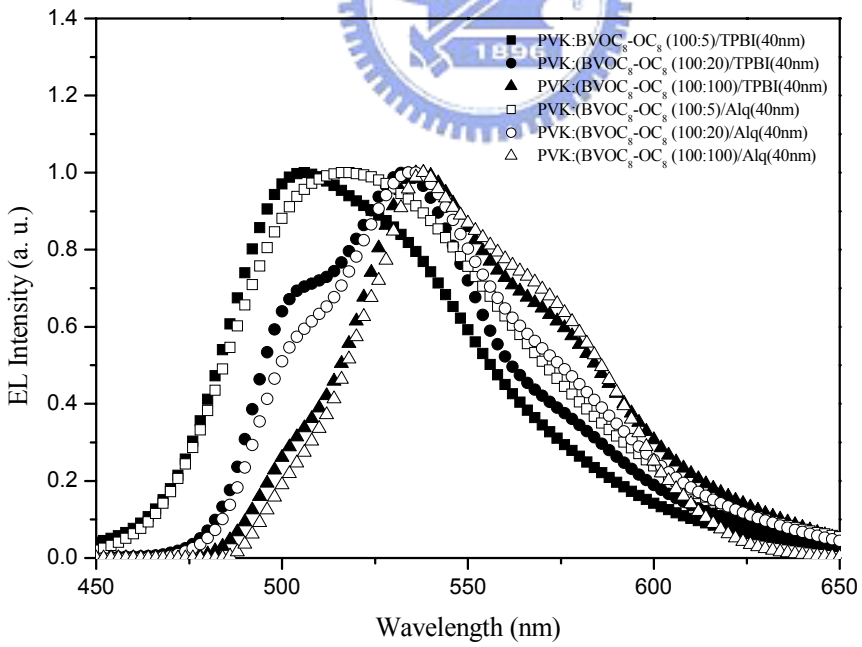

Figure 3.5 EL spectera of PLED devices containing Alq or TPBI (with a thickness of 40 nm) as the ETL and various concentrations of $BVOC_8$-OC_8 blended in PVK (with a thickness of 60 nm) as the light-emitting layer.

Since, using PVK as matrixes in this study, the PVK EL emission is not observed in the EL spectra of blend film devices, and the PVK PL emission is not overlapped with the major emission peaks in the PL spectra of blend films (see Figure 3.4). Thus, it is adequate to judge the emission phenomena of these blend films and PLED devices. In order to improve the PLED performance, all polymer blend (with different wt.% concentrations of emitters in PVK matrix) devices incorporate a layer of Alq or TPBI as the electron transporter. The EL spectra of PLED devices containing Alq or TPBI (with a thickness of 40 nm) as the electron transporting layer (ETL) and various concentrations of light-emitting $BVOC_8$-OC_8 blended in PVK (with a thickness of 60 nm) as the light-emitting layers are depicted in Figure 3.5. In devices with TPBI as ETL, at lower concentrations of $BVOC_8$-OC_8, i.e. PVK:$BVOC_8$-OC_8 = 100:5 wt%, the λmax values of EL emission peaks around 500 nm and weaker shoulders (ca. 540 nm) originated from the excimers of molecular aggregation are observed. For PLED devices with higher concentrations of $BVOC_8$-OC_8, i.e. PVK:$BVOC_8$-OC_8 = 100:20 wt% and 100:100 wt%, the λmax values of EL emission peaks have shifted to ca. 540 nm due to the aggregation of chromophores at higher concentrations. The original EL emission peaks (ca. 500 nm) in the lowest concentration (i.e. PVK:$BVOC_8$-OC_8 = 100:5 wt%) devices becomes weak shoulders in the medium concentration (i.e. PVK:$BVOC_8$-OC_8 = 100:20 wt%) devices, which even diminish at the highest concentration (i.e. PVK:$BVOC_8$-OC_8 = 100:100 wt%) devices. Similar trend of EL spectra is observed in devices using either Alq or TPBI as the ETL (see Figure 3.5). In addition, shoulders around 570 nm originated from different degrees of aggregation become more detectable in the EL spectra of higher concentrations of $BVOC_8$-OC_8 blended devices, which are also observable in the PL spectra of $BVOC_8$-OC_8 blend films in Figure 3.4 (especially an obvious shoulder at 567 nm observed in the pure

film of $BVOC_8$-OC_8 due to the aggregation of the pure film state). To test the possible origin of electroplex formation in the shoulder of EL spectra in Figure 3.5, voltage-dependent EL spectra were measured. As the relative intensity of the main peak and the shoulder of EL spectra do not change with voltages, one can exclude the possibility of electroplex formation in these devices.

Because the blend films are solid solutions having various doping ratios of emitters in PVK, they have similar results as normal solutions. The π-π stacking effect appears in solid films to form excimers, so, compared with solution forms, red shifts of λmax values were observed. In order to realize the difference among the devices of $BVOC_8$-OC_8, PL spectra of solutions, thin films, and blend films (emitters doped in PVK) are analyzed to confirm this assumption. The maximum emission peaks of PL spectra in pure films are seriously red-shifted due to the aggregation of π-π stacking among these three conditions (i.e. solutions, pure films, and blend films), so it shows the largest red shift in pure films (see Figure 3.4). Interestingly, as shown in Figures 3.3-3.5, the λmax values of PL spectra in blend films (PVK:$BVOC_8$-OC_8=100:5 wt%) and solution (10^{-5}~10^{-6} M) are similar to that of EL spectra (TPBI as an ETL) with the same doping concentration of $BVOC_8$-OC_8 (PVK:$BVOC_8$-OC_8=100:5 wt%), though the concentration of $BVOC_8$-OC_8 in PVK (PVK:$BVOC_8$-OC_8 = 100:5 wt%) is much larger than that of the solution (10^{-5}~10^{-6} M). In general, the concentration effects of emitters on the λmax values of EL devices are similar to those of PL spectra with various concentrations.

The electroluminescent properties of various PLED devices containing BV derivatives and ETL (40 nm) of Alq or TPBI are shown in Table 3.1. Among these PLED (PVK: BV derivatives = 100:20) devices, the device containing $BVOC_8$-OC_8 emitters blended in PVK has the highest brightness. By adding an ETL (with a

thickness of 40 nm) of Alq or TPBI, the EL properties of PVK:$BVOC_8$-OC_8 = 100:20 device are much enhanced and the maximum brightness has increased 8~15 times (from 3319 cd/m^2 without an ETL to 50144 cd/m^2 by adding Alq and to 27328 cd/m^2 by adding TPBI) due to the improved device configuration with an ETL. In order to evaluate the concentration effect of the emitters, the EL properties of PLED devices containing $BVOC_8$-OC_8 emitters blended in PVK with various concentrations, i.e. PVK:$BVOC_8$-OC_8 = 100:5, 100:20, and 100:100 wt%, are also compared in Table 3.1. Their properties of the maximum luminescence, along with the turn-on voltage and Qext. efficiency, while using TPBI as an ETL (shown in Table 3.1) are listed according to the luminescence order: (28868 cd/m^2, 2.9 V, and 2.9%) for (PVK:$BVOC_8$-OC_8 = 100:100 wt%), (27328 cd/m^2, 3.0 V, and 1.6%) for (PVK:$BVOC_8$-OC_8 = 100:20 wt%), and (22578 cd/m^2, 3.2 V, and 1.8%) for (PVK:$BVOC_8$-OC_8 = 100:5 wt%), respectively. Similar to the luminescence result, it shows the best value of Qext. efficiency (2.9%) in the PLED device of (PVK:$BVOC_8$-OC_8 = 100:100 wt%) where TPBI may supply a proper electron transporting speed to match the hole transporting speed. Whereas replacing TPBI with Alq as an ETL, the concentration effect of $BVOC_8$-OC_8 on EL peaks of Alq devices are similar to that of TPBI devices. Nevertheless, comparing the efficiency and brightness of PLED systems using either Alq or TPBI as an ETL, Alq is better than TPBI since Alq seems to provide multiple properties (including both roles of ETL and luminescent layer) in PVK: $BVOC_8$-OC_8/Alq devices. The multiple properties in luminescence will be discussed later.

As shown in Tables 3.2-3.5, to evaluate the hole-transporting capability and the emitting mechanism of the multilayer PLED devices, the EL characteristics of the doped PLED devices containing $BVOC_8$-OC_8 emitters are affected by adding

hole-transporting NPB dopants in PVK and by the thickness of ETL (TPBI or Alq) and BCP (hole-blocking layer). The device characteristics (the maximum electroluminescence, turn-on voltage, and Qext. efficiency) of PLEDs doped with hole-transporting NPB are as follows (see Table 3.2): (24012 cd/m^2, 5.3 V, 1.71%) for device PVK: NPB (100:5)/Alq (60 nm/40 nm); (9877 cd/m^2, 4.2 V, 2.3%) for device PVK:NPB:BVOC$_8$-OC$_8$ (100:5:20)/Alq (60 nm/40 nm). It is not clear why the complexity of the components in NPB doped (PVK:NPB:BVOC$_8$-OC$_8$ = 100:5:20) devices may cause the falling off in above EL properties, which may be due to the mismatch of the LUMO and HOMO energy levels in NPB and BVOC$_8$-OC$_8$. However, though the maximum electroluminescence of device PVK: NPB: BVOC$_8$-OC$_8$ (100:5:20)/Alq (60 nm/40 nm) is not as good as that of a standard device NPB/Alq (60 nm/40 nm) (41378 cd/m^2, 3.2 V, 2.56%), BVOC$_8$-OC$_8$ (without NPB) can improve the luminescent properties in PLED devices. Despite the fact that PVK is a hole-transporting material, the maximum electroluminescence and Qext. efficiency of PVK/Alq (60 nm/40 nm) are 10033 cd/m^2 and 0.72% shown in Table 3.4, which are not as good as NPB/Alq (60 nm/40 nm). Furthermore, the turn-on voltage and luminescence (at 20 V) of the device without NPB, i.e. PVK: BVOC$_8$-OC$_8$ (100:20)/Alq (60 nm/40 nm) with (50144 cd/m^2, 2.9 V, 2.02%) revealed in Table 3.3, are better than those of NPB doped devices. Therefore, it is verified that BVOC$_8$-OC$_8$ is a good hole-transporting material in the previous comparison.

Table 3.2 EL Characteristics of PLED Devices Containing NPB and ETL (40 nm) of Alq

	NPB/Alq 60 nm/40 nm	PVK:NPB/Alq (100:5) 60 nm/40 nm	PVK:NPB:$BVOC_8$-OC_8/Alq (100:5:20) 60 nm/40 nm
Turn-on voltage, V	3.2	5.3	4.2
Max. brightness, cd/m^2	41378	24012	9877
Max. external quantum effic., %	2.56	1.71	2.3
Max. power effic., lm/W	2.67	1.32	1.66
λmax (FWHM), nm (EL)	525(66)	526(66)	528(68)

Table 3.3 EL Characteristics of PVK: $BVOC_8$-OC_8 (100:20)/TPBI (X nm) Devices [a] with Different Thicknesses of ETL (TPBI)

	PVK:$BVOC_8$-OC_8/ TPBI (20 nm)	PVK:$BVOC_8$-OC_8/ TPBI (40 nm)	PVK:$BVOC_8$-OC_8/ TPBI (60 nm)
Turn-on voltage, V	3.5	2.7	2.4
Max. brightness, cd/m^2	18034	26199	27437
Max. external quantum effic., %	1.13	1.55	1.71
Max. power effic., lm/W	1.83	2.41	2.49
λmax (FWHM), nm (EL)	538(60)	534(66)	504(80)

[a] The thickness of the emitting layer is 60 nm and PVK: chromophore =100: 20.

Table 3.4 EL Characteristics of PVK: $BVOC_8$-OC_8 (100:20)/Alq (X nm) Devices with Different Thicknesses of ETL (Alq)

	PVK:$BVOC_8$-OC_8/ Alq (20 nm)	PVK:$BVOC_8$-OC_8/ Alq (40 nm)	PVK:$BVOC_8$-OC_8/ Alq (60 nm)	PVK/Alq 60 nm/20 nm	PVK/Alq 60 nm/40 nm	PVK/Alq 60 nm/60 nm
Turn-on voltage, V	2.8	2.9	3.1	4.1	3.9	3.6
Max. brightness, cd/m^2	39584	50144	56935	10067	10033	9605
Max. external quantum effic., %	0.91	2.02	2.44	0.20	0.72	1.14
Max. power effic., lm/W	1.02	2.93	3.25	0.43	1.51	2.43
λmax (FWHM), nm (EL)	506(78)	534(84)	536(92)	518(90)	521(90)	526(90)

[a] The thickness of the emitting layer is 60 nm and PVK: chromophore =100: 20.

Table 3.5 EL Characteristics of PVK: $BVOC_8$-OC_8 (100:20)/BCP (X nm)/Alq(Y nm) Devices with Different Thicknesses of Hole-blocking BCP Layer and ETL (Alq)

	PVK:$BVOC_8$-OC_8/ BCP/Alq (5 nm/20 nm)	PVK:$BVOC_8$-OC_8/ BCP/Alq (5 nm/40 nm)	PVK:$BVOC_8$-OC_8/ BCP/Alq (5 nm/60 nm)	PVK:$BVOC_8$-OC_8/ BCP/Alq (10 nm/20 nm)	PVK:$BVOC_8$-OC_8/ BCP/Alq (10 nm/40 nm)	PVK:$BVOC_8$-OC_8/ BCP/Alq (10 nm/60 nm)
Turn-on voltage, V	3.5	3.2	3.2	4.3	3.5	3.5
Max. brightness, cd/m^2	9304	9978	9932	4978	6943	7653
Max. external quantum effic., %	0.32	0.34	0.48	0.29	0.35	0.48
Max. power effic., lm/W	0.44	0.53	0.61	0.49	0.55	0.64
λmax (FWHM), nm (EL)	506(76)	506(86)	534(92)	504(78)	508(84)	530(86)

[a] The thickness of the emitting layer is 60 nm and PVK:$BVOC_8$-OC_8 =100: 20.

In order to evaluate the electron-transporting behavior of TPBI and Alq, the EL characteristics of PVK: $BVOC_8$-OC_8 (100:20)/TPBI (X nm) and PVK: $BVOC_8$-OC_8 (100:20)/Alq (X nm) devices with different thicknesses of ETL (TPBI or Alq), i.e. X = 20, 40, and 60 nm, are shown in Figures 3.6-3.7 and Tables 3.3-3.4. By decreasing the thickness of TPBI (ETL), the emission λmax values in EL spectra are red-shifted from 504 nm (as TPBI = 60 nm) to 538-534 nm (as TPBI = 20 and 40 nm), and stronger excimer emissions occur as TPBI = 20 and 40 nm. Since the EL emission peaks of PVK and TPBI are around 400 nm, the EL spectra and characteristics of PVK: $BVOC_8$-OC_8 (100:20)/TPBI (X nm) illustrated in Figure 3.6 and Table 3.3 are mainly from $BVOC_8$-OC_8 emitters. The excimer emission has more contribution by the device configuration of thinner ETL of TPBI (as TPBI = 20 and 40 nm); whereas, the major EL emission peak (λmax = 504 nm) in the device with thicker ETL of TPBI (as TPBI = 60 nm) is similar to that without TPBI (λmax = 508 nm shown in Table 3.1 and Figure 3.8b), where the excimer emission is suppressed. On the other hand, by increasing the thickness of Alq (ETL), the EL emission λmax values are red-shifted from 506 nm (Alq = 20 nm) to 534-536 nm (Alq = 40 and 60 nm) shown in Figure 3.7 and Table 3.4. Since the EL emission peak of Alq is around 518-526 nm (see the device of PVK/Alq in Table 3.4), the red-shift of EL emission peak (from 506 nm to 534-536 nm) in the device of PVK: $BVOC_8$-OC_8 (100:20)/Alq (X nm) may be enhanced by increasing the thickness of Alq, which may be due to stronger EL emissions of thicker Alq and/or excimer emissions of $BVOC_8$-OC_8 emitters. Besides, higher maximum brightnesses and Qext. efficiencies of PLEDs are obtained by increasing the thickness (i.e. from 20 nm to 40 and 60 nm) of ETL (either Alq or TPBI) in Tables 3.3 and 3.4.

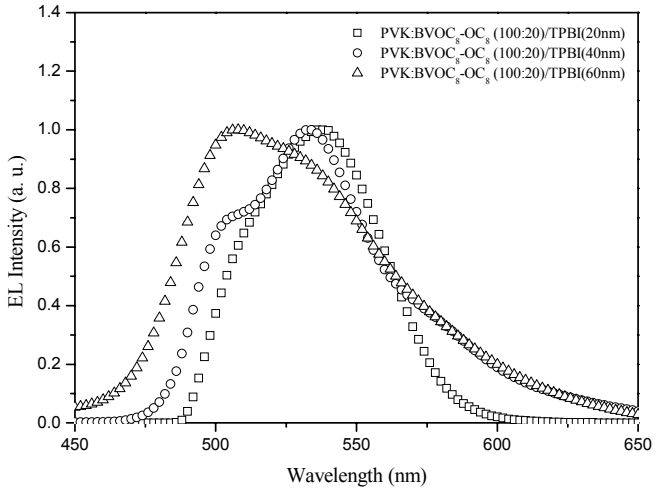

Figure 3.6 The EL characteristics of PVK: $BVOC_8$-OC_8 (100:20)/TPBI (X nm) devices with different thicknesses of ETL (TPBI), i.e. X = 20, 40, and 60 nm.

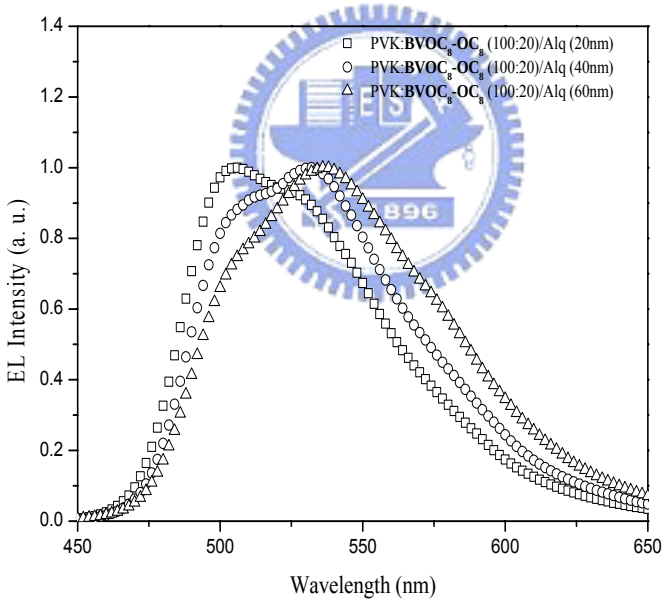

Figure 3.7 The EL characteristics of PVK: $BVOC_8$-OC_8 (100:20)/Alq (X nm) devices with different thicknesses of ETL (Alq), i.e. X = 20, 40, and 60 nm.

Since Alq provides multiple properties (including both roles of ETL and luminescent layer) in PVK: $BVOC_8$-OC_8/Alq devices, the emission ratios between $BVOC_8$-OC_8 and Alq are analyzed. The theoretical EL spectrum of PVK: $BVOC_8$-OC_8 (100:20) device is shown in Figure 3.8(a) by the subtraction of the EL

spectrum of PVK/Alq (60 nm) from that of PVK: $BVOC_8$-OC_8 (100:20)/Alq (60 nm). The ratio of emission by $BVOC_8$-OC_8 vs. Alq can be obtained from the integration areas of EL spectra, so the EL emission ratio of $BVOC_8$-OC_8 and Alq is 5:1 for theoretical EL emission of PVK: $BVOC_8$-OC_8 (100:20) vs. PVK/Alq (60 nm) by their integration areas in Figure 3.8(a). According to above evidence, $BVOC_8$-OC_8 is confirmed to play a major role of emitting light in most of our devices. In addition, similar theoretical EL emission curves of PVK: $BVOC_8$-OC_8 as Alq = 20 and 40 nm shown in Figure 3.8(b) are acquired from the EL spectrum of PVK:$BVOC_8$-OC_8 (100:20)/Alq (20 nm) minus that of PVK/Alq (20 nm), and the EL spectrum of PVK:$BVOC_8$-OC_8 (100:20)/Alq (40 nm) minus that of PVK/Alq (40 nm), respectively. In comparison with previous results, a real EL emission curve of PVK: $BVOC_8$-OC_8 device without Alq is also measured and demonstrated in Figure 3.8(b). Interestingly, the theoretical EL emission curve of PVK: $BVOC_8$-OC_8 as Alq = 20 nm is most matched with the real EL emission curve of PVK: $BVOC_8$-OC_8 device without Alq. Thus, the mismatch of theoretical EL emission curves of PVK: $BVOC_8$-OC_8 as Alq = 40 and 60 nm may be due to the excimer emissions of $BVOC_8$-OC_8 emitters and/or the enhanced Alq emission by the hole transporting effect of $BVOC_8$-OC_8 in devices of PVK:$BVOC_8$-OC_8 (100:20)/Alq (40 nm) and /Alq (60 nm). Conclusively, the EL spectra of PVK: $BVOC_8$-OC_8 (100:20)/TPBI (60 nm) (in Figure 3.6) and PVK: $BVOC_8$-OC_8 (100:20)/Alq (20 nm) (in Figure 3.7) are quite similar to that of PVK: $BVOC_8$-OC_8 (100:20) without ETL (shown in Figure 3.8b), so the EL emissions of these results are originated from the conjugated emissions of $BVOC_8$-OC_8 emitters.

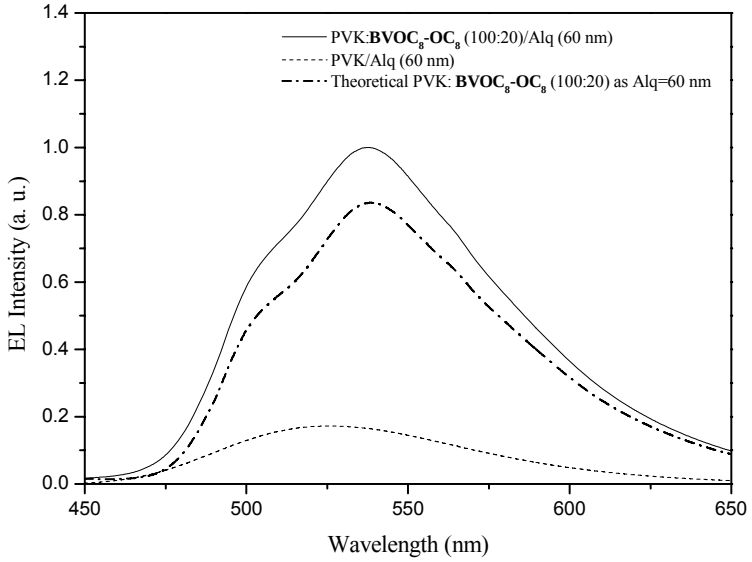

(a)

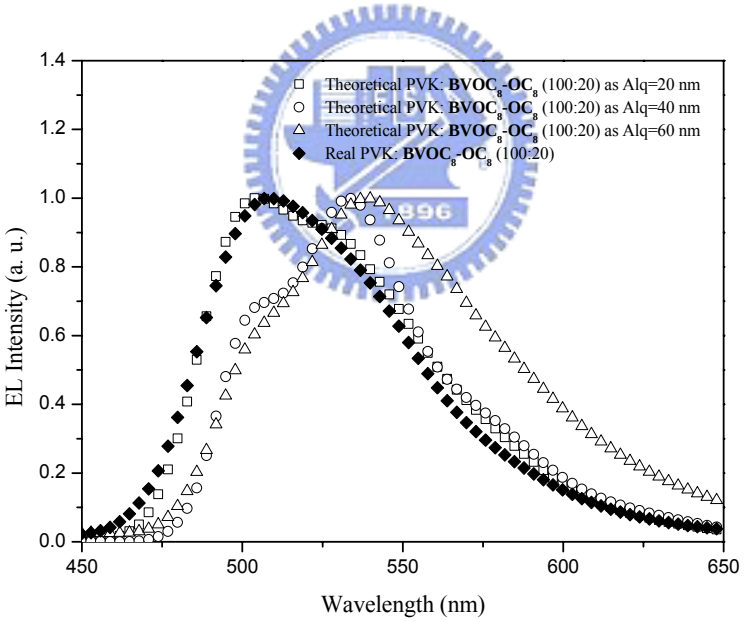

(b)

Figure 3.8 (a) The theoretical EL spectrum of PVK: $BVOC_8$-OC_8 (100:20) is obtained from the EL spectra of PVK: $BVOC_8$-OC_8 (100:20)/Alq (60 nm) minus that of PVK/Alq (60 nm). (b) The theoretical EL spectra of PVK: $BVOC_8$-OC_8 (100:20) obtained from devices of PVK: $BVOC_8$-OC_8 (100:20)/Alq (X nm), where the thicknesses of Alq (X nm) is 20, 40, and 60 nm, respectively, and the real EL spectrum of PVK: $BVOC_8$-OC_8 (100:20) are compared.

Since Alq is proved not to be a main luminescent ingredient, $BVOC_8$-OC_8 plays a more important role in electroluminescence. Thus, one layer of hole-blocking BCP is added between the emitting layer and Alq (ETL) to evaluate the role of ETL and the emission mechanism. In principle, Alq emits partial light in the device without hole-blocking layer of BCP (or with 5 nm of BCP), the main light-emission may come from the layer of PVK: $BVOC_8$-OC_8 (100:20). By increasing the thickness of BCP (from 0 and 5 nm to 10 nm) in [PVK: $BVOC_8$-OC_8 (100:20)/BCP/Alq] devices, the EL emission intensity of Alq relative to that of the chromophore should decrease. The decrease in the relative Alq emission (10 nm of BCP) originates from the reduction of electron and hole recombination in Alq and the emitting light may be confined within the emitting layer of PVK:$BVOC_8$-OC_8. To confirm and eliminate the light emission of Alq, different thicknesses (5 and 10 nm) of BCP (hole-blocking layer) are added between an emitting layer (60 nm) of PVK: $BVOC_8$-OC_8 (100:20) and an ETL of Alq (20, 40 and 60 nm), which will result in less green emission of Alq. Usually, adding a BCP layer causes a higher Qext. efficiency but a higher turn-on voltage. However, hole-blocking BCP attached to PVK layer in this case induces a serious decay in electroluminescence and Qext. efficiency, which may be due to the large variations of HOMO and LUMO energy levels between BCP and PVK. By increasing the thicknesses (from 5 to 10 nm) of BCP (hole-blocking layer) the turn-on voltage is increased and the maximum brightness is reduced, but the Qext. efficiency is about the same. For instance, the turn-on voltage, the maximum luminescence (EL), and efficiency of previous devices are 3.2 V, 9978 cd/m^2, 0.34% for PVK: $BVOC_8$-OC_8 (100:20)/BCP (5 nm)/Alq (40 nm) and 3.5 V, 6943 cd/m^2, 0.35% for PVK: $BVOC_8$-OC_8 (100:20)/BCP (10 nm)/Alq (40 nm). No matter what thickness of BCP, the EL emission λmax values (shown in Figure 3.9) are red-shifted from 506 nm (as

Alq = 20 and 40 nm) to 534 nm (as Alq = 60 nm) in the devices of PVK: $BVOC_8$-OC_8 (100:20)/BCP (5 nm)/Alq (X nm), which is similar to those devices without BCP, i.e. PVK: $BVOC_8$-OC_8 (100:20)/Alq (X nm). If the hole-blocking layer of BCP does work, the EL emission λmax values should not shift by increasing the thickness of ETL (Alq), or the EL emission λmax values should shift by increasing the thickness of BCP. Therefore, it is cionfirmed that the hole-blocking layer of BCP did not function well in these devices.

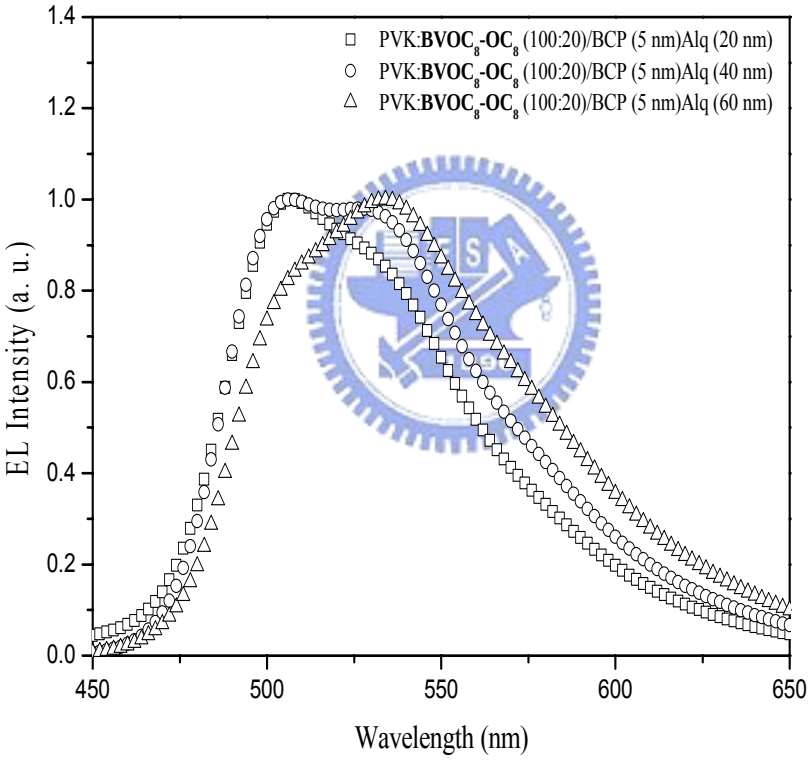

Figure 3.9 The EL characteristics of PVK: $BVOC_8$-OC_8 (100:20)/ BCP (5 nm)/ Alq (X nm) devices with different thicknesses of ETL (Alq), i.e. X = 20, 40, and 60 nm.

As for devices without hole-blocking layer of BCP, the thicknesses of Alq are adjusted to be 20, 40, and 60 nm (see Table 3.4). When the thickness of Alq is 20 nm, the maximum luminescence (EL), turn-on voltage, and efficiency of the device are (39584 cd/m^2, 2.8 V, and 0.91%), where the electrons can go through Alq and reach PVK layer completely. When the thickness of Alq is 60 nm, the corresponding EL properties of the device are (56935 cd/m^2, 3.1 V, and 2.44%). The brightness of the latter device (60 nm Alq) is comparably larger than that of the former device (20 nm Alq), which is due to the light emission of the latter device (60 nm Alq) originated from both of the Alq layer and the interface between PVK:$BVOC_8$-OC_8 (100:20) and Alq. This can be explained by the LUMO (Lowest Unoccupied Molecular Orbital) and HOMO (Highest Occupied Molecular Orbital) energy levels of device materials which are shown in Figure 3.10. For example, (2.3, 5.6 eV) for PVK, (3.1, 5.6 eV) for $BVOC_8$-OC_8, (3.0, 6.0 eV) for Alq, and (3.2, 6.7 eV) for BCP, respectively. The LUMO values of $BVOC_8$-OC_8 (3.1 eV) and Alq (3.0 eV) are almost the same to make the electrons have equivalent possibility to stay at Alq and $BVOC_8$-OC_8 layers.

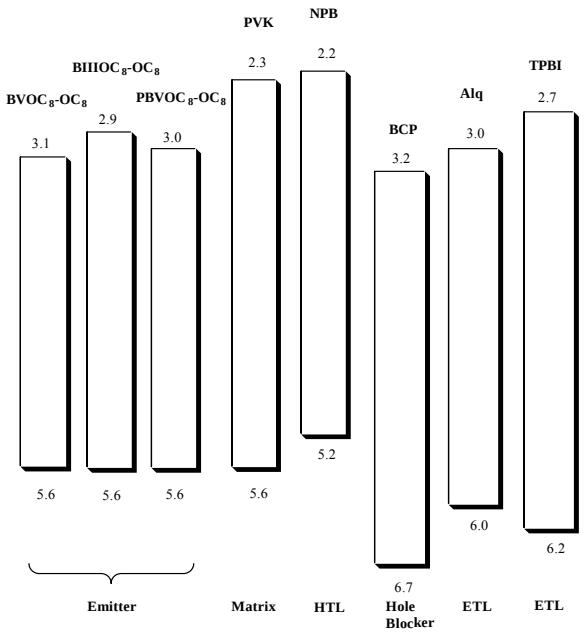

Figure 3.10 LUMO and HOMO energy values of various materials used in the PLED devices.

The EL characteristics of PVK:chromophore (100:5)/TPBI devices with emitting three-conjugated ring (BIII) and polymer ($PBVOC_8$) derivatives are shown in Tables 3.6-3.7, where the best ratio of PVK:chromophore possessing the brightest EL is 100:5 along with an ETL (40 nm) of TPBI. Compared with five-conjugated ring derivatives, three-conjugated ring derivatives possess lower densities of electron and larger energy gaps, thus to have blue shift of λmax values in PL and EL spectra (see Table 3.6). The band gaps of three-conjugated ring derivatives are around 2.7 eV and their PL and EL spectra all show blue light emissions. The smaller band gaps are due to the longer conjugation lengths of five-conjugated rings and their band gaps are around 2.5 eV to show greenish-blue light. Because an ETL of Alq will emit green light from Alq, so the ETL of Alq is replaced with TPBI in order to eliminate the additive emitting properties occurred in Alq (since no multiple light happens in devices with ETL of TPBI). $BIIIOC_8$-OMe is the brightest (EL) compound among these three-conjugated ring oligomers, possessing (6050 cd/m^2, 4.1 V, 0.83%) for (the maximum electroluminescence, turn-on voltage, and Qext. efficiency) in the device of PVK:chromophore/TPBI (shown in Table 3.6). Because five-conjugated ring polymers have similar conjugation lengths as the five-conjugated ring oligomers, their PL and EL spectra are alike due to their comparable energy band gaps. In polymer systems, $PBVOC_8$-OEh is the brightest (EL) compound among these polymer derivatives, which possesses EL characteristics of (6972 cd/m^2, 5.0 V, 0.75%) shown in Table 3.7. $PBVOC_8$-OEh has the smallest FWHM value (74 nm) of EL spectra among $PBVOC_8$ polymer derivatives because it has the narrowest distribution of energy gaps in PVK. In general, three-conjugated ring BIII derivatives and polymer derivatives (PBV) have worse EL properties, e.g. the maximum electroluminescence, turn-on voltage, and Qext. efficiency, than five-conjugated ring BV derivatives.

Table 3.6 EL Characteristics of PVK: Chromophore (100:5)/TPBI Devices [a] with BIII Derivatives and ETL (40 nm) of TPBI

	BIII-OMe	BIIIOMe-Me	BIIIOMe-OMe	$BIIIOC_8$-OMe	$BIIIOC_{12}$-OMe	$BIIIOC_8$-OC_8
Turn-on voltage, V	3.7	5.7	4.1	4.1	4.5	5.0
Max. brightness, cd/m^2	5862	5320	2794	6050	5908	5774
Max. external quantum effic., %	1.10	0.97	0.72	0.83	0.67	0.61
Max. power effic., lm/W	0.59	0.43	0.19	0.34	0.22	0.19
λmax (FWHM), nm	468(88)	462(78)	462(80)	466(92)	470(100)	466(78)
CIE, x,y	0.16,0.20	0.15,0.17	0.15,0.19	0.16,0.21	0.16,0.20	0.16,0.19
Voltage at 100 mA/cm^2, V	10.9	11.5	15.2	13.7	13.2	13.0
Brightness at 100 mA/cm^2, cd/m^2	1410	1076	928	1012	898	805
External quantum effic. at 100 mA/cm^2, %	0.99	0.88	0.72	0.74	0.67	0.61
Power effic. At 100 mA/cm^2, lm/W	0.41	0.30	0.19	0.23	0.22	0.19

[a] The thickness of TPBI is 40 nm and PVK: chromophore =100: 5.

Table 3.7 EL Characteristics of PVK: Chromophore (100:5)/TPBI Devices [a] with $PBVOC_8$-R_5 Derivatives and ETL (40 nm) of TPBI

	$PBVOC_8$-OC_4	$PBVOC_8$-OC_8	$PBVOC_8$-OC_{12}	$PBVOC_8$-OEh
Turn-on voltage, V	4.9	3.8	3.7	5.0
Max. brightness, cd/m^2	3953	3778	2908	6972
Max. external quantum effic., %	0.67	0.58	0.71	0.75
Max. power effic., lm/W	0.29	0.35	0.29	0.44
λmax (FWHM), nm	500(138)	498(104)	492(168)	498(74)
CIE, x,y	0.19,0.34	0.21,0.36	0.19,0.28	0.20,0.33
Voltage at 100 mA/cm^2, V	17.6	14.6	15.6	12.9
Brightness at 100 mA/cm^2, cd/m^2	986	962	841	1020
External quantum effic. at 100 mA/cm^2, %	0.50	0.45	0.51	0.54
Power effic. At 100 mA/cm^2, lm/W	0.18	0.21	0.17	0.25

[a] The thickness of TPBI is 40 nm and PVK: chromophore =100: 5.

3.5 Conclusions

Highly efficient green EL emissions of PVK PLED devices doped with fluorescent oligo(p-phenylene-vinylene)s (BIII and BV) and polymer derivatives (PBV) were obtained by proper device configurations of multilayer design. $BVOC_8$-OC_8 is the brightest (EL) emitter among all chromophores used in this study. The brightest device PVK:$BVOC_8$-OC_8(100:20)/Alq (60 nm/60 nm) has a brightness of 56935 cd/m^2 with a power efficiency of 3.25 lm/W. It suggests that the emission mechanism (including the conjugated and excimer emissions of $BVOC_8$-OC_8 emitters as well as Alq emissions) originate from both of $BVOC_8$-OC_8 and ETL (Alq) by varying the concentration of chromophores and adjusting the thickness of ETL. The excimer emissions of $BVOC_8$-OC_8 emitters are affected by the concentration of the emitters (i.e. PVK: $BVOC_8$-OC_8 =100:20 is the best concentration among our study), the thickness and the type (different effect for Alq and TPBI) of ETL. Five-conjugated ring OPV (BV) derivatives with proper alkoxy groups possess excellent hole-transporting property and the highest brightness in PLED devices, and the main emitting source of these multilayer devices is confirmed to be the conjugated emissions and excimer emissions of the OPV emitters.

Chapter 4

Characterization of Light-emitting H-bonded Complexes and Polymers Containing Bis-pyridyl Emitting Acceptors

4.1 Abstract

A series of bis-pyridyl acceptor emitters are synthesized and the LC and photophysical (PL and EL) properties of their supramolecular structures, including H-bonded polymer networks and trimers, are explored. Unique mesomorphic properties may be introduced into these H-bonded complexes and polymers containing non-mesogenic acceptor emitters. In addition, the emission properties of bis-pyridyl acceptor emitters can be adjusted by their surrounding non-photoluminescent proton donors. Compared with pure bis-pyridyl acceptor emitters, red-shifts of PL emission wavelengths were observed in most of the H-bonded complexes and polymers. Due to the higher acidity value of *m*-$PC_{10}BA$ **(16)** and its stronger H-bonded effect in H-bonded polymer complexes, the largest red-shift of 93 nm in λmax value of PL has occurred in the fully H-bonded polymer network *p*-$PBBBP\text{-}OC_8$ **(8)**/*m*-$PC_{10}BA$ **(16)** in contrast to pure emitter *p*-$PBBBP\text{-}OC_8$ **(8)**. A very narrow full width at half maximum (FWHM) value (38 nm) of EL spectra can be obtained in the device of H-bonded complexes blended with PVK, and higher brightness of EL is produced at an appropriate annealing temperature.

4.2 Introduction

Recently, hydrogen bonds (H-bonds) are useful to be developed in the applications

of electronic and photonic devices.[106-109] The energy of H-bonds (25 to 40 kJ/mol) are stronger than van der Waals interactions (5 to 10 kJ/mol) but weaker than ionic bonds (200 to 400 kJ/mol).[110] Many kinds of H-bonds and building elements have been developed in the H-bonded structures to stabilize liquid crystalline phases. It has been demonstrated that liquid crystalline (LC) polymers,[111-114] copolymers,[115,116] and monomers[117-121] containing H-bonds are appropriate candidates for obtaining functionalized LC systems.

Since the report of Burroughes *et al.*,[1] rapid progress has been made in improving the efficiencies and lifetimes of light-emitting diodes (LED) based on conjugated polymers. A number of reports demonstrate polarized electroluminescence (EL) with the aim of incorporating such polymer LEDs as backlights into liquid crystal displays.[35] For instance, cyanobiphenyl liquid crystals can be aligned by rubbing polyimide and thus to have dichroic ratios in absorption spectra.[122] The frequently used materials are polyacrylate,[26,27] polyfluorene[35,31,32,36-40,123] and their oligomer derivatives.[42] Additionally, lyotropic liquid crystals, which possess a hexagonal mesophase to solubilize the monomer and direct its electropolymerization, are utilized to prepare poly(3,4-ethylenedioxythiophene) (PEDOT) films that replicate the texture and birefringence of the LC template.[43] In particular, liquid crystalline conducting polymers containing mesogenic parts in their side chains[44-46] or dyes doped in liquid crystalline structure[48] have attracted much interest in their molecular alignment, which is anticipated for use in polarized emissions. Moreover, polarized OLEDs were constructed using heptafluorene lightly doped with monodisperse conjugated oligomers for an efficient emission of blue light, and a high polarization ratio was obtained.[52] Besides, some other higher polarization ratios and dichroic ratios of emissions are reported as well.[32, 124]

Polymer light emitting diodes containing pyridine[125, 126] and thiophene[127] repeat units are of considerable interest in the areas of electron transporting. The photoluminescence (PL) of the polymers[113, 128] and copolymers[129,130] owning hydrogen bonds within and between the polymer chains are reported. For instance, hierarchical self-assembly are formed in comb-shaped supramolecules[131] consisting of poly(2,5-pyridinediyl), acid dopants, and H-bonded alkyl side chains. The observation of the thermoreversible gelation of fluorescent *p*-phenylenevinylene derivatives[132] control their gelation as a consequence of cooperative hydrogen bonds and self-assembly induced by π-π stacking. Among blue, green, and red emissions, one of the main problems of good polymer emitters is the demand for good color purity. Reducing the values of the full width at half maximum (FWHM) of polymer emissions, i.e. producing good color purity, in blend films were reported in the literature.[133-136]

To our knowledge, H-bonded effects on PL and electroluminescent (EL) properties of liquid crystalline supramolecules containing acceptor emitters have been scarcely reported.[119] Our preliminary results show that a red shift occurs in the bis-pyridyl emitters (as proton acceptors) when proton donor acids are H-bonded to the supramolecules (H-bonded trimers). Distinct liquid crystalline properties can be introduced by complexation of different acceptor emitters and complementary donors. However, the H-bonded trimers could not be utilized for LED applications due to the poor film-forming quality of the small molecules in our previous work.[119] In order to solve this problem, we have surveyed new H-bonded complexes containing photoluminescent bis-pyridyl acceptors, including H-bonded complexes blended with poly(9-vinylcarbozole) (PVK) matrixes, and it leads to high quality films of supramolecular LED polymer blends. Therefore, we also would like to illustrate the

H-bonded effects on the LC, PL, and EL properties of these light-emitting supramolecules.

4.3 Experimental

4.3.1 General Information

NMR spectra were carried out on a Bruker AC 300 M Hz spectrometer. The thermal transition temperatures and textures of all products were obtained from a Perkin–Elmer DSC-7 and Leitz Laborlux S polarizing optical microscope (POM) equipped with a THMS-600 heating stage. The heating and cooling rates were 10 °C min^{-1} for all measurements in N_2 unless mentioned. UV-Vis absorption spectra were recorded in dilute solutions (10^{-6} M) on a HP 8453 spectrophotometer. Fluorescence spectra were obtained on a Hitachi F-4500 spectrophotometer. The textures of mesophases were studied using a polarizing optical microscope (Leica DMLP) equipped with a hot stage. The highest occupied molecular orbital (HOMO) energy levels were estimated from the optical response on a Riken Photoelectron Spectrometer AC-2. The work function and ionization potential can be measured by the photoelectron spectrometer for the OLED materials in air. To align the liquid crystals into a monodomain, these materials were sealed in anti-parallel rubbing LC cells with a cell gap of 9 μm, and the polarized PL emission spectra were measured at corresponding mesomophic temperatures. Number-average and weight-average molecular weights, Mn and Mw, respectively, were determined by polystyrene-calibrated gel permeation chromatography (GPC; Jasco PU-1580 and Jasco RI-930) using THF as the eluent.

4.3.2 Device Fabrication

Pre-patterned ITO substrates with an effective individual device area of 3.14 mm^2 were cleaned by ultrasonic machine in various detergent solutions and D. I. water. After that the ITO substrates were treated with oxygen plasma for 2 minutes before spin-coating. The emission layer consists of synthesized emitters doped into poly(9-vinylcarbozole) (PVK) matrix with a concentration of 5 wt%, and polymer thin films were made by spin-coating from THF solution with a concentration of 1.65 wt%. The spin-coating rate of 3000 rpm was proceeded for 40 s, and the thickness of the emitting layer was about 60 nm (with a total thickness of 100 nm, including 40 nm of electron transporting layer). The electron transporting layer (40 nm) of 2,2',2"-(1,3,5-phenylene)-tris[1-phenyl-1H-benzimidazole] (TPBI) was deposited thermally at a rate around 0.1-0.3 Å/s under a pressure of ~$2x10^{-5}$ torr in an Ulvac Cryogenic deposition system. One layer of magnesium and silver alloy (ca. 10:1, 50 nm) was deposited as a cathode, which was capped with 100 nm of silver. The current-voltage-luminescence characteristics were measured on ambient conditions by Keithley 2400 Source meter and Newport 1835C Optical meter equipped with 818ST silicon photodiode.

4.3.3 Materials

Chemicals and solvents were reagent grades and purchased from Aldrich, ACROS, TCI, and Lancaster Chemical Co. THF was distilled to keep anhydrous before use. The other chemicals were used without further purification. The synthetic routes of oligo(p-phenylene-vinylene)s are shown in Chart 4.1 (for compounds **1-9**), and all proton donors (compounds **10-16**) are illustrated in Chart 4.2, and all products were identified as the required materials by ^{1}H, ^{13}C NMR spectroscopy and elementary analyses.

Chart 4.1

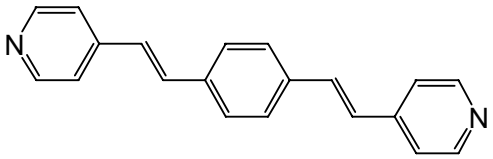

***p*-PBP (1)**

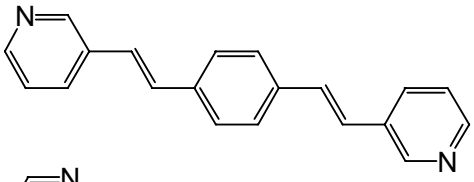

***m*-PBP (2)**

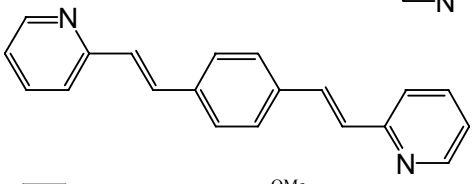

***o*-PBP (3)**

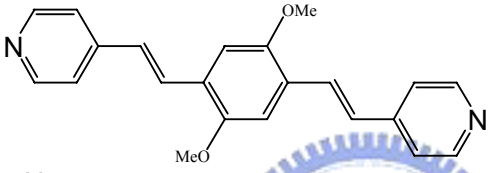

***p*-PBP-OMe (4)**

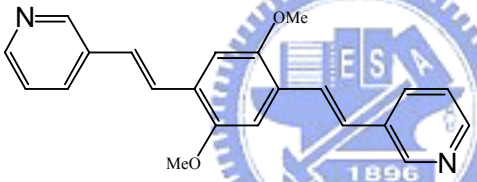

***m*-PBP-OMe (5)**

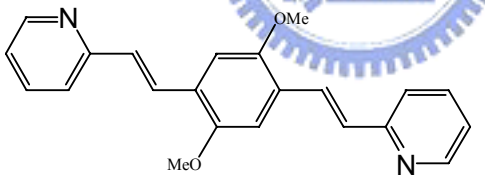

***o*-PBP-OMe (6)**

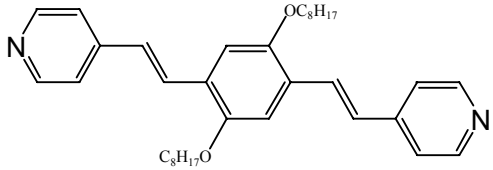

***p*-PBP-OC_8 (7)**

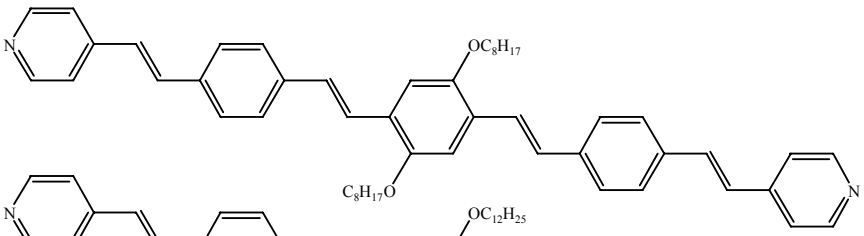

***p*-PBBBP-OC_8 (8)**

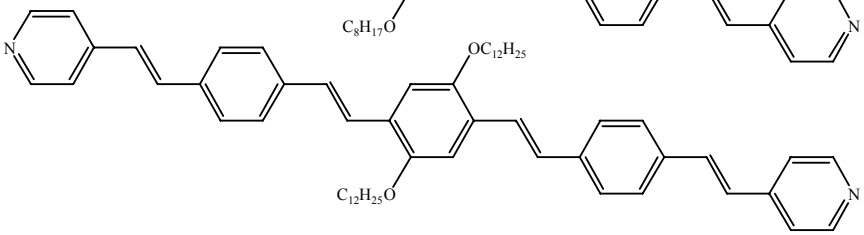

***p*-PBBBP-OC_{12} (9)**

Chart 4.2

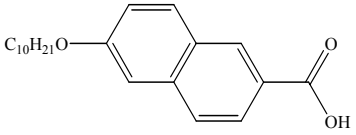

$C_{10}ONA$ **(10)**

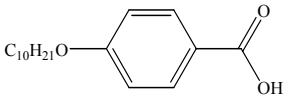

$C_{10}OBA$ **(11)**

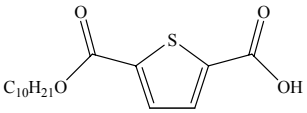

$C_{10}COOTHA$ **(12)**

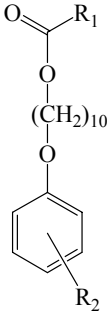

p-$MC_{10}BA$**(13)** for R_1 = vinyl (=) and R_2 = *p*-COOH

p-$PC_{10}BA$**(14)** for R_1 = poly-vinyl and R_2 = *p*-COOH

m-$MC_{10}BA$(**15**) for R_1 = vinyl (=) and R_2 = *m*-COOH

m-$PC_{10}BA$(**16**) for R_1 = poly-vinyl and R_2 = *m*-COOH

***p*-PBP (1).** Anal Calcd for $C_{20}H_{16}N_2$: C, 84.48; H, 5.67; N, 9.85. Found: C, 84.11; H, 5.89; N, 9.88.

***m*-PBP (2).** Anal Calcd for $C_{20}H_{16}N_2$: C, 84.48; H, 5.67; N, 9.85. Found: C, 84.08; H, 5.80; N, 9.88.

***o*-PBP (3).** Anal Calcd for $C_{20}H_{16}N_2$: C, 84.48; H, 5.67; N, 9.85. Found: C, 84.08; H, 5.89; N, 9.83.

***p*-PBP-OMe (4).** Anal Calcd for $C_{22}H_{20}N_2O_2$: C, 76.72; H, 5.85, N, 8.13. Found: C, 76.45; H, 5.98, N, 8.21.

***m*-PBP-OMe (5).** Anal Calcd for $C_{22}H_{20}N_2O_2$: C, 76.72; H, 5.85, N, 8.13. Found: C, 76.50; H, 6.02, N, 8.32.

***o*-PBP-OMe (6).** Anal Calcd for $C_{22}H_{20}N_2O_2$: C, 76.72; H, 5.85, N, 8.13. Found: C, 76.24; H, 6.00, N, 8.03.

***p*-PBP-OC_8 (7).** Anal Calcd for $C_{36}H_{48}N_2O_2$: C, 79.96; H, 8.95, N, 5.18. Found: C, 80.02; H, 9.08, N, 4.86.

***p*-PBBBP-OC$_8$ (8).** Anal Calcd for $C_{52}H_{60}N_2O_2$: C, 83.83; H, 8.12, N, 4.29. Found: C, 83.89; H, 8.12, N, 4.19.

***p*-PBBBP-OC$_{12}$ (9).** Anal Calcd for $C_{60}H_{76}N_2O_2$: C, 84.06; H, 8.94, N, 3.27. Found: C, 83.71; H, 9.11, N, 3.20.

Proton donors (**10-12**) were reported in our previous results.[14] Donor monomers *p*-MC$_{10}$BA **(13)** and *m*-MC$_{10}$BA **(15)** were prepared according to the procedure reported by Portugal et al.[137]

4-((6-(Acryloyloxy)decyl)oxy)benzoic acid monomer, *p*-MC$_{10}$BA **(13)** Anal Calcd for $C_{20}H_{28}O_5$: C, 68.91; H, 8.1. Found: C, 68.8; H, 7.96.

Poly{4-((6-(acryloyloxy)decyl)oxy)benzoic acid}, *p*-PC$_{10}$BA **(14)**

3-((6-(Acryloyloxy)decyl)oxy)benzoic acid monomer, *m*-MC$_{10}$BA **(15)** Anal Calcd for $C_{20}H_{28}O_5$: C, 68.94; H, 8.10. Found: C, 68.88; H, 8.18.

Poly{3-((6-(Acryloyloxy)decyl)oxy)benzoic acid}, *m*-PC$_{10}$BA **(16)**

The number average molecular weight (Mn) and polydispersity index (PDI) of polymers are as follows:

p-PC$_{10}$BA **(14)**: Mn = 5800 and PDI = 1.21.

m-PC$_{10}$BA **(16)**: Mn = 4400 and PDI = 1.06.

4.4 Results and discussion

4.4.1 Thermal properties

Phase transition temperatures and thermal behavior of H-bonded acceptor emitters (**1-9**), H-bonded donors (**10-16**), and their H-bonded complexes characterized by differential scanning calorimetry (DSC) and polarizing optical microscopy (POM) are summarized in Tables 4.1-4.4.

Table 4.1 Thermal Properties of Bis-pyridyl Acceptor Emitters (1-9)

Compd	Transition Temperature (°C) and Enthalpy (J/g)[a]
p-PBP**(1)**	**K** 280.0 (--)[b] / 267.0 (--)[b] **I**
m-PBP **(2)**	**K** 191.8 (82.0) / 174.3 (-53.9) **I**
o-PBP **(3)**	**K** 236.0 (--)[b] / 222.0 (--)[b] **I**
p-PBP-OMe **(4)**	**K** 265.1 (71.9) / 256.0 (--)[b] **I**
m-PBP-OMe **(5)**	K 201.6 (78.8) / 153.1 (-99.2) I
o-PBP-OMe **(6)**	K 207.0 (--)[b] / -- (--)[c] I
p-PBP-OC_8 **(7)**	K 136.1 (57.9) / 100.6 (-58.3) I
p-PBBBP-OC_8 **(8)**	K 128.5 (10.1) / 120.4 (-10.9) K' 230.2 (52.6) / 220.6 (-54.8) I
p-PBBBP-OC_{12}**(9)**	K 68.3 (8.1) / 194.9 (-64.9) K' 218.7 (63.7) / 63.7 (-8.8) I

[a] the enthalpy (J/g) is shown in the parentheses.
[b] the phase transition temperatures were obtained from POM.
[c] crystallization was not observed during the cooling process.

Table 4.2 Thermal Properties of Proton Donors **(10-16)**

Compd	Transition Temperature (°C) and Enthalpy (J/g)[a]
C_{10}ONA**(10)**	K $\underset{89.7\ (-1.7)}{\overset{104.8\ (0.7)}{\rightleftharpoons}}$ K' $\underset{120.3\ (-40.3)}{\overset{136.3\ (39.4)}{\rightleftharpoons}}$ Sc $\underset{138.4\ (-3.6)}{\overset{140.5\ (2.9)}{\rightleftharpoons}}$ N $\underset{173.3\ (-4.7)}{\overset{175.9\ (7.7)}{\rightleftharpoons}}$ I
C_{10}OBA**(11)**	K $\underset{89.7\ (-1.7)}{\overset{85.1\ (8.9)}{\rightleftharpoons}}$ Sx $\underset{120.3\ (-40.3)}{\overset{96.0\ (30.3)}{\rightleftharpoons}}$ Sc $\underset{138.4\ (-3.6)}{\overset{123.7\ (4.5)}{\rightleftharpoons}}$ N $\underset{173.3\ (-4.7)}{\overset{142.4\ (7.7)}{\rightleftharpoons}}$ I
C_{10}COOTHA**(12)**	K $\underset{94.8\ (-97.7)}{\overset{104.8\ (95.6)}{\rightleftharpoons}}$ I
p-MC_{10}BA**(13)**	K $\underset{53.4\ (-55.5)}{\overset{78.7\ (57.5)}{\rightleftharpoons}}$ Sc $\underset{95.0\ (--)^b}{\overset{97.0\ (--)^b}{\rightleftharpoons}}$ S_A $\underset{106.3\ (-9.3)}{\overset{109.8\ (9.3)}{\rightleftharpoons}}$ I
p-PC_{10}BA**(14)**	K $\underset{60.0\ (--)^b}{\overset{141.0\ (--)^b}{\rightleftharpoons}}$ I
m-MC_{10}BA**(15)**	K $\underset{47.4\ (-9.1)}{\overset{68.6\ (94.7)}{\rightleftharpoons}}$ S_A $\underset{53.7\ (-33.4)}{\overset{76.5\ (0.2)}{\rightleftharpoons}}$ I
m-PC_{10}BA**(16)**	K $\underset{31.0\ (--)^b}{\overset{81.0\ (--)^b}{\rightleftharpoons}}$ I

[a] the enthalpy (J/g) is shown in the parentheses.
[b] the phase transition temperatures were obtained from POM.

Table 4.3 Thermal Properties of H-bonded Complexes Containing Donors **(10-12)**

H-Bonded Complexes (molar ratio = 1:2)	Transition Temperature (°C) and Enthalpy (J/g)[a]
p-PBP-OC_8**(7)**/C_{10}ONA**(10)**	K $\underset{77.5\ (-51.2)}{\overset{103.5\ (103.5)}{\rightleftharpoons}}$ N $\underset{126.0\ (--)^b}{\overset{128.0\ (--)^b}{\rightleftharpoons}}$ I
p-PBP-OC_8**(7)**/C_{10}OBA**(11)**	K $\underset{53.1\ (-40.6)}{\overset{90.5\ (81.2)}{\rightleftharpoons}}$ N $\underset{98.0\ (--)^b}{\overset{104.0\ (--)^b}{\rightleftharpoons}}$ I
p-PBP-OC_8**(7)**/C_{10}COOTHA**(12)**	K $\underset{}{\overset{74.9\ (21.8)}{\rightleftharpoons}}$ K' $\underset{86.9\ (-70.7)}{\overset{101.9\ (61.2)}{\rightleftharpoons}}$ I
p-PBBBP-OC_8**(8)**/C_{10}ONA**(10)**	K $\underset{118.0\ (-3.2)}{\overset{128.9\ (-11.0)\ \text{K'}\ \ 141.9\ (48.7)}{\rightleftharpoons}}$ N $\underset{213.0\ (--)^b}{\overset{215.7\ (0.8)}{\rightleftharpoons}}$ I
p-PBBBP-OC_8**(8)**/C_{10}OBA**(11)**	K $\underset{136.7\ (-56.3)}{\overset{148.6\ (52.3)}{\rightleftharpoons}}$ N $\underset{187.4\ (-0.8)}{\overset{191.3\ (1.0)}{\rightleftharpoons}}$ I
p-PBBBP-OC_8**(8)**/C_{10}COOTHA**(12)**	K $\underset{116.8\ (-46.4)}{\overset{66.3\ (8.2)\ \text{K'}\ \ 138.4\ (45.2)}{\rightleftharpoons}}$ N $\underset{171.0\ (--)^b}{\overset{175.0\ (--)^b}{\rightleftharpoons}}$ I
p-PBBBP-OC_{12}**(9)**/C_{10}ONA**(10)**	K $\underset{76.7\ (-75.7)}{\overset{87.8\ (2.5)}{\rightleftharpoons}}$ K' $\underset{107.1(-107.1)}{\overset{128.8\ (37.1)}{\rightleftharpoons}}$ N $\underset{200.0\ (--)^b}{\overset{201.0\ (--)^b}{\rightleftharpoons}}$ I
p-PBBBP-OC_{12}**(9)**/C_{10}OBA**(11)**	K $\underset{116.3\ (-53.9)}{\overset{87.0\ (3.5)\ \text{K'}\ \ 135.3\ (43.8)}{\rightleftharpoons}}$ N $\underset{166.0\ (-1.6)}{\overset{175.6\ (1.4)}{\rightleftharpoons}}$ I
p-PBBBP-OC_{12}**(9)**/C_{10}COOTHA**(12)**	K $\underset{126.6\ (-50.0)}{\overset{147.3\ (50.7)}{\rightleftharpoons}}$ N $\underset{165.0\ (--)^b}{\overset{168.0\ (--)^b}{\rightleftharpoons}}$ I

[a] the enthalpy (J/g) is shown in the parentheses.
[b] the phase transition temperatures were obtained from POM.

Table 4.4 Thermal Properties of H-bonded Complexes Containing Donor Polymers **(14** and **16)**

H-Bonded Complexes (molar ratio = 1:2)	Transition Temperature (°C) and Enthalpy (J/g)[a]
p-PBBBP-OC_8**(8)**/*p*-PC_{10}BA**(14)**	K $\underset{125.7\ (-13.2)}{\overset{138.4\ (8.4)}{\rightleftharpoons}}$ Sx $\underset{158.7\ (-3.2)}{\overset{177.8\ (44.4)}{\rightleftharpoons}}$ I
p-PBBBP-OC_8**(8)**/*m*-PC_{10}BA**(16)**	K $\underset{121.5\ (-10.4)}{\overset{132.3\ (9.3)}{\rightleftharpoons}}$ Sx $\underset{171.9\ (-3.1)}{\overset{187.4\ (35.7)}{\rightleftharpoons}}$ I
p-PBBBP-OC_{12}**(9)**/*p*-PC_{10}BA**(14)**	K $\underset{58.9\ (-2.7)}{\overset{67.8\ (6.4)}{\rightleftharpoons}}$ Sx $\underset{162.0\ (-10.8)}{\overset{178.3\ (15.3)}{\rightleftharpoons}}$ I
p-PBBBP-OC_{12}**(9)**/*m*-PC_{10}BA**(16)**	K $\underset{58.3\ (-2.9)}{\overset{68.2\ (9.9)}{\rightleftharpoons}}$ Sx $\underset{165.8\ (-10.1)}{\overset{185.8\ (39.4)}{\rightleftharpoons}}$ I

[a] the enthalpy (J/g) is shown in the parentheses.

The phase transition temperatures of bis-pyridyl acceptor emitters (**1-9**), i.e. the melting and crystallization temperatures (Tm and Tcr), are demonstrated in the following order: *p*-PBP **(1)** > *p*-PBP-OMe **(4)** > *o*-PBP **(3)** > *o*-PBP-OMe **(6)** > *m*-PBP **(2)** > *m*-PBP-OMe **(5)** > *p*-PBP-OC_8 **(7)**, and *p*-PBBBP-OC_8 **(8)** > *p*-PBBBP-OC_{12} **(9)** > *p*-PBP-OC_8 **(7)** (shown in Table 4.1). In general, the phase transition temperatures (i.e. Tm and Tcr) of bis-pyridyl emitters (**1-9**) decrease with increasing the length of side chains. This phenomenon may be as a result of the long alkoxy side chains which hinder the molecular packing and result in the decrease of phase transition temperatures. For instance, the phase transition temperatures of *p*-PBBBP-OC_8 **(8)** > *p*-PBBBP-OC_{12} **(9)** and *p*-PBP **(1)** > *p*-PBP-OMe **(4)** > *p*-PBP-OC_8 **(7)** are observed with the same rigid cores. Besides, longer rigid cores with the same side chains have higher transition temperatures, for example, *p*-PBBBP-OC_8 **(8)** > *p*-PBP-OC_8 **(7)**. As for the phase transition temperatures of

p-PBP-OMe **(4)** > *o*-PBP-OMe **(6)** > *m*-PBP-OMe **(5)** in Tm and Tcr, it can be explained by that stronger dipole-dipole interaction occurred between para-pyridyl groups in the linear conjugated direction. Similar to methoxy substituted compounds (**4-6**), the phase transition temperatures of compounds (**1-3**) without methoxy side groups have the same tendency (i.e. *p*-PBP **(1)** > *o*-PBP **(3)** > *m*-PBP **(2)**).

For H-bonded donors C_{10}ONA **(10)**, C_{10}OBA **(11)**, and C_{10}COOTHA **(12)**, their phase transition temperatures (i.e. Tm and Tcr) are in the following order: C_{10}COOTHA **(12)** < C_{10}OBA **(11)** < C_{10}ONA **(10)** (shown in Table 4.2). In general, the phase transition temperatures will increase while the central cores are more linear and rigid. As for the phase transition temperatures of donor monomers *p*-MC_{10}BA **(13)** > *m*-MC_{10}BA **(15)** and donor polymers *p*-PC_{10}B**A (14)** > *m*-PC_{10}BA **(16)**, it can be explained by a more linear H-bonded dimeric architecture in para-acid structure and therefore results in higher transition temperatures. In addition, comparing donor monomers (*p*-MC_{10}BA **(13)** and *m*-MC_{10}BA **(15)**) with donor polymers (*p*-PC_{10}BA **(14)** and *m*-PC_{10}BA **(16)**), polymers have larger molecular weights to produce higher transition temperatures of Tm and Tcr.

By evaporation of the mixture of acceptor/donor (molar ratio = 1:2) in the THF solution, fully H-bonded complexes are formed. Since bis-pyridyl acceptor emitters (**1-9**) are bi-functional acceptors, double molar values of H-bonded donors are needed to complex with central bi-functional acceptors to generate fully H-bonded trimers. In order to elucidate the degree of H-boding in these H-bonded trimers containing isomeric acceptors with various positions of N-hetrocyclic atoms, i.e. *p*-PBP-OMe (**4**), *m*-PBP-OMe (**5**), and *o*-PBP-OMe (**6**). The evidence of different extents of H-bonding can be confirmed by IR spectra.[138] As shown in Figure 4.1, due to the H-bonding, the O-H bands at 2672 and 2556 cm^{-1} in pure donor acid *p*-MC_{10}BA (**13**)

are shifted to lower energy wavenumber around 2664-2514 cm^{-1} and 1920 cm^{-1} in H-bonded complex *p*-PBP-OMe (**4**)/*p*-$MC_{10}BA$ (**13**) with *para*-*N*-heterocycles and around 2698-2442 cm^{-1} and 1920 cm^{-1} in H-bonded complex *o*-PBP-OMe (**6**)/*p*-$MC_{10}BA$ (**13**) with *ortho*-*N*-heterocycles, which shows that the degree of H-bonding between acids and *ortho*-*N*-heterocyclic emitter *o*-PBP-OMe (**6**) is similar to that between acids and *para*-*N*-heterocyclic emitter *p*-PBP-OMe (**4**). However, the O-H bands at 2672 and 2558 cm^{-1} in H-bonded complex *m*-PBP-OMe (**5**)/*p*-$MC_{10}BA$ (**13**) with *meta*-*N*-heterocycles are almost the same as the pure donor acid *p*-$MC_{10}BA$ (**13**). Therefore, the degree of H-bonding between acids and *meta*-*N*-heterocyclic emitter *m*-PBP-OMe (**5**) is much less than the other isomeric emitters and may remain partially as non-H-bonded moieties in the mixture.

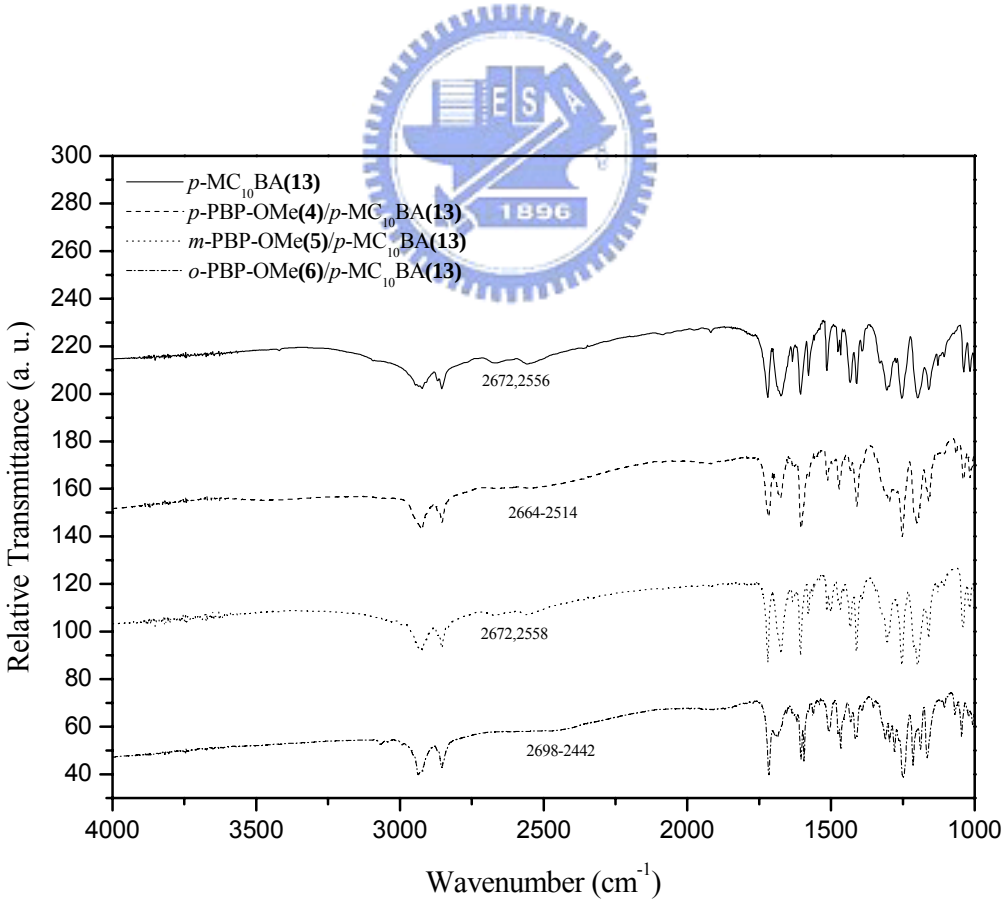

Figure 4.1 FTIR spectra of donor acid p-$MC_{10}BA$ (**13**) and its H-Bonded trimers containing isomeric acceptors with various positions of *N*-hetrocyclic atoms, i.e. *p*-PBP-OMe (**4**), *m*-PBP-OMe (**5**), and *o*-PBP-OMe (**6**).

Due to H-bonds, the physical properties of the bispyridyl emitters can be modified by donor monomers and polymers in the H-bonded complexes, including the formation of LC phases. Some of the thermal properties of H-bonded trimers are shown in Table 4.3. The nematic phase is introduced in all H-bonded trimers, except *p*-PBP-OC_8(**7**)/C_{10}COOTHA(**12**) due to the bending tail of thiophene structure in C_{10}COOTHA(**12**) and the shortest core of *p*-PBP-OC_8(**7**). In general, the bending structure of thiophene donor, i.e. C_{10}COOTHA(**12**), induces the lowest isotropization temperature in analogous H-bonded trimers, and the most rigid structure of naphthalene donor, i.e. C_{10}ONA(**10**), causes the highest isotropization temperatures in H-bonded trimer counterparts. Moreover, the longer conjugated cores induce the broader nematic phase in analogous H-bonded trimers. Once the proton donor polymers *p*-PC_{10}BA **(14)** and *m*-PC_{10}BA **(16)** are used, the bis-pyridyl acceptor emitters will act as H-bonded crosslinkers. Some of the thermal properties of fully H-bonded polymer networks (acceptor:donor = 1:2 by mole) containing H-bonded crosslinking emitters *p*-PBBBP-OC_8 **(8)** and *p*-PBBBP-OC_{12} **(9)** are shown in Table 4.4. Only H-bonded complexes containing donor polymers are reported, because donor monomers of H-bonded complexes seem easier to react in the H-bonded complexes than pure donor monomers during the heating process. The simplified schematic drawing of idealized H-bonded complexes formed among bis-pyridyl acceptor emitters and donor polymers are revealed in Figure 4.2, where the layered smectic structures are favored to form in the H-bonded polymeric networks. Table 4.4 reveals that lower melting temperatures are observed in analogous H-bonded polymeric networks bearing longer side chain of acceptor emitter *p*-PBBBP-OC_{12} **(9)**. However, regardless of the lower isotropization temperature in *m*-PC_{10}BA **(16)**, the H-bonded polymeric networks containing donor polymer *m*-PC_{10}BA **(16)** possess a

little higher isotropization temperatures. This might be possibly due to the stronger acidity of *m*-$PC_{10}BA$ **(16)** compared with that of *p*-$PC_{10}BA$ **(14)**,[139] and thus the stronger H-bonded effect is induced in the H-bonded polymeric networks containing donor polymer *m*-$PC_{10}BA$ **(16)**. Above all, mesomorphism is introduced in most H-bonded series (shown in Tables 4.3 and 4.4) by the complexation of non-mesogenic acceptor emitters with H-bonded donors.

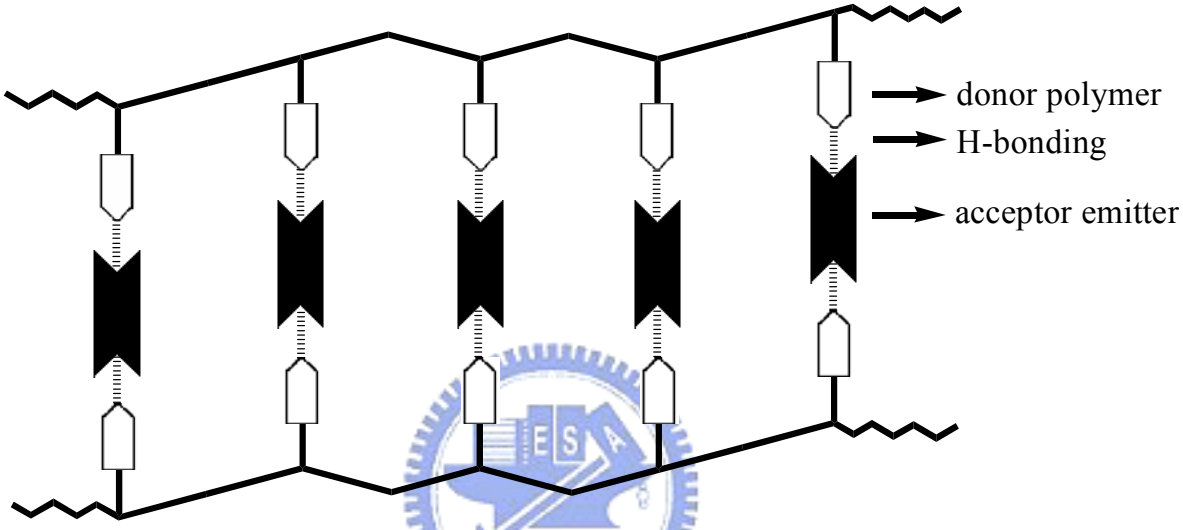

Figure 4.2 Simplified schematic drawing of idealized H-bonded polymer networks formed among bis-pyridyl acceptor emitters and donor polymers.

4.4.2 Optical properties

While materials possess mesomorphism, the polarized emission is anticipated for using the LC phase to be aligned in a rubbing cell. The PL emission has the highest intensity ($PL_{//}$) when the polarizer is parallel to the rubbing direction of the aligned cell, and has the lowest intensity ($PL_{\perp}$) perpendicular to the rubbing direction. The polarization ratio is defined by ($P_{//}/P_{\perp}$), where $P_{//}$ and $P_{\perp}$ are the maximum PL emission intensities as the polarizer is parallel and perpendicular to the rubbing direction, respectively. The maximum polarization ratios of H-bonded complexes (acceptor:donor = 1:2 by mole) containing bis-pyridyl acceptor emitters *p*-$PBBBP\text{-}OC_8$**(8)** and *p*-$PBBBP\text{-}OC_{12}$**(9)** are shown in Table 4.5. The

p-PBBBP-OC_{12}**(9)**/C_{10}ONA**(10)** complex shows the highest polarization ratio ($P_{//}/P_{\perp}$ = 9.5) among all of these H-bonded complexes. The polarized PL spectra ($PL_{//}$ and $PL_{\perp}$) of H-bonded complex *p*-PBBBP-OC_{12}**(9)**/C_{10}ONA**(10)** in the LC phase (the nematic phase at 198 °C) are also shown in Figure 4.3. In general, the polarization values of polymeric H-bonded complexes are lower than those of monomeric H-bonded complexes, because polymer chains are more difficultly aligned in the rubbing direction, which may be due to higher viscosity and entanglement of polymer chains in the H-bonded polymer networks.

Table 4.5 The Maximum Polarization Ratio of H-bonded Complexes

H-Bonded Complexes (molar ratio = 1:2)	Maximum Polarization Ratio
p-PBBBP-OC_8**(8)**/C_{10}ONA**(10)**	6.8
p-PBBBP-OC_{12}**(9)**/C_{10}ONA**(10)**	9.5
p-PBBBP-OC_8**(8)**/C_{10}OBA**(11)**	4.7
p-PBBBP-OC_{12}**(9)**/C_{10}OBA**(11)**	4.1
p-PBBBP-OC_8**(8)**/C_{10}COOTHA**(12)**	1.8
p-PBBBP-OC_{12}**(9)**/C_{10}COOTHA**(12)**	2.2
p-PBBBP-OC_8**(8)**/*p*-MC_{10}BA**(13)**	3.2
p-PBBBP-OC_8**(8)**/*p*-PC_{10}BA**(14)**	2.1
p-PBBBP-OC_8**(8)**/*m*-MC_{10}BA**(15)**	2.1
p-PBBBP-OC_8**(8)**/*m*-PC_{10}BA**(16)**	1.7
p-PBBBP-OC_{12}**(9)**/*p*-MC_{10}BA**(13)**	3.7
p-PBBBP-OC_{12}**(9)**/*p*-PC_{10}BA**(14)**	1.6
p-PBBBP-OC_{12}**(9)**/*m*-MC_{10}BA**(15)**	2.1
p-PBBBP-OC_{12}**(9)**/*m*-PC_{10}BA**(16)**	1.6

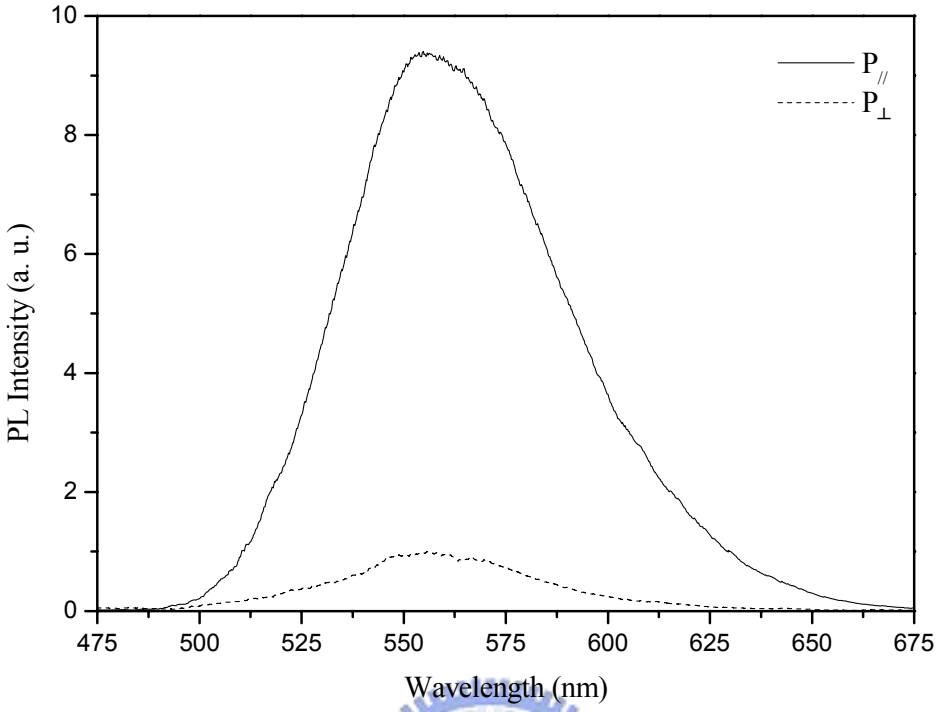

Figure 4.3 PL spectra ($PL_{//}$ and $PL_{\perp}$) of H-bonded complex *p*-PBBBP-OC_{12}**(9)**/C_{10}ONA**(10)** measured at 198 °C (in the nematic phase), where $PL_{//}$ and $PL_{\perp}$ are PL spectra measured as the polarizer parallel and perpendicular to the rubbing direction of LC cells, respectively.

The UV-Vis absorption and PL spectra of bis-pyridyl emitters in solutions (THF as solvent) are shown in Figure 4.4 and λmax values of UV-Vis, PL, and EL spectra are listed in Table 4.6. The peaks of UV-Vis spectra are about 357~359 nm for PBP derivatives, 397~403 nm for PBP-OMe derivatives, 408 nm for *p*-PBP-OC_8 **(7),** and 434~435 nm for *p*-PBBBP derivatives, respectively. Compared with *p*-PBP-OC_8 **(7)**, *p*-PBBBP-OR (-OR = -OC_8 and -OC_{12}) derivatives have larger λmax values of UV-Vis and PL spectra in solutions, i.e. red-shifted wavelengths, due to the smaller energy band gaps of longer conjugations in five-conjugated rings of *p*-PBBBP-OR derivatives. Owing to the aggregation in solid states, the λmax values of PL in pure films are red-shifted to different extent in contrast to those of solution states. The π-π

stacking effect appears in pure films to form excimers, so the red-shifted phenomena were observed. However, compared with pure films, the blend films (dopant emitter:PVK = 5:100 wt%) have less red-shifted λmax values of PL, where the polymer matrixes (PVK) act as solvents in the blend films. Similar results in PL spectra of bis-pyridyl acceptor emitter *p*-PBP-OC_8 **(7)** in pure film and blend film are observed in Figure 4.5. This indicates dopant emitters in pure films have stronger aggregation themselves than in PVK matrix. The blend films are similar to solid solutions which show concentration effects on the aggregation of dopant emitters as well as the λmax values of PL emissions. Hence, compared with pure films, the dilution effect of the solid solvent (PVK) induce blue-shift of PL in the blend films.

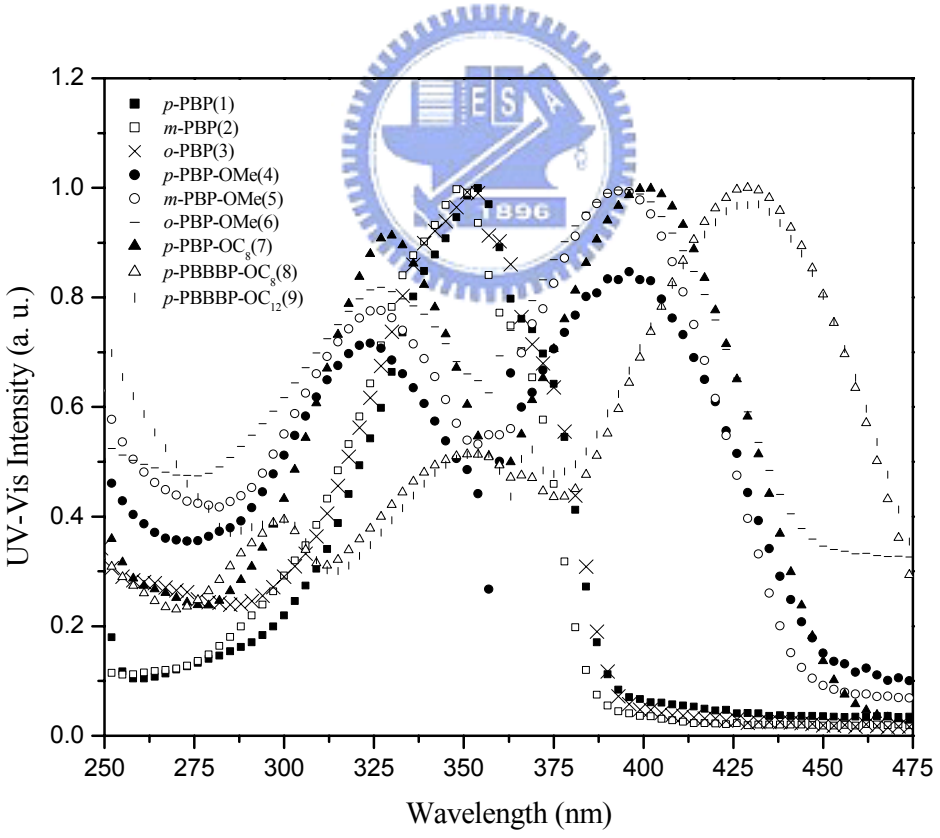

Figure 4.4 UV-vis spectra of bis-pyridyl acceptor emitters in solutions (THF as solvents).

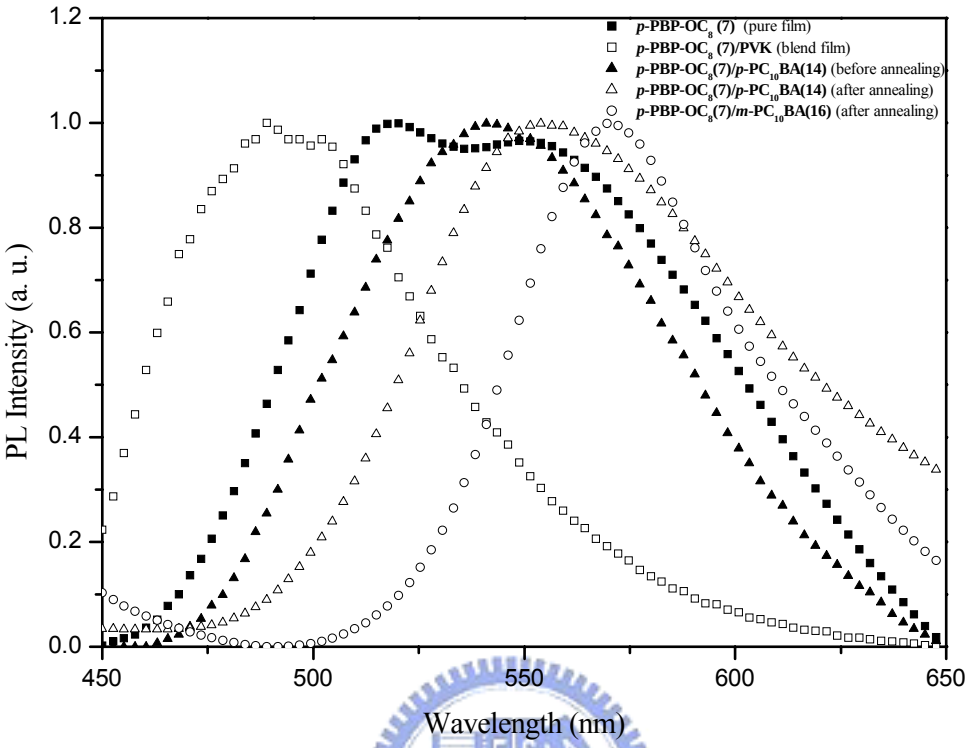

Figure 4.5 PL spectra of bis-pyridyl acceptor emitter *p*-PBP-OC_8 **(7)** and its H-bonded complexes.

Table 4.6 UV-Vis, PL, and EL Spectra of Bis-pyridyl Acceptor Emitters

Compd	λmax (nm)				
	UV-vis(abs)[a]	PL(solution)[a]	PL(pure film)	PL(blend film)[b]	EL(blend film)[b]
p-PBP **(1)**	357	414(392)[c]	444(463)	458	454
m-PBP **(2)**	357	412(392)	474(456)	441	450
o-PBP **(3)**	359	415	462	428	428
p-PBP-OMe **(4)**	403	463	558	464	468
m-PBP-OMe **(5)**	397	450	531	462	464
o-PBP-OMe **(6)**	403	452	548	456	456
p-PBP-OC_8 **(7)**	408	464	519(555)	490	494
p-PBBBP-OC_8 **(8)**	434	494	549	502	502
p-PBBBP-OC_{12} **(9)**	435	494	553	503	504

[a] the solvent is THF.
[b] the matrix is PVK (dopant emitter: PVK= 5:100 wt%).
[c] second peaks are shown in the parentheses.

In H-bonded complexes, the acids play both roles as solid solvents and H-bonded donors at the same time. Thus, the dilution effect of the acids (as solid solvents) to induce blue-shift of PL and the H-bonded effect of the acid donors to cause red-shift of PL are competitive. Table 4.7 shows both of the dilution effect and the H-bonded effect on λmax (PL) values of fully H-bonded polymer networks (acceptor:donor = 1:2 by mole) containing various bis-pyridyl acceptor emitters (**1-9**) and polymer donors, i.e. *p*-$PC_{10}BA$ **(14)** and *m*-$PC_{10}BA$ **(16)**. PL spectra of fully H-bonded complexes of bis-pyridyl acceptor emitters (**1-9**) with *m*-$PC_{10}BA$ **(16)** (molar ratio = 1:2) are even widely distributed from blue to red colors (from 390 nm to 642 nm). Compared with pure bis-pyridyl acceptor emitters, red-shifts of PL emission wavelengths have occurred, i.e. the H-bonded effect is dominant, in most of the H-bonded complexes. Some exceptions occur in polymeric H-bonded complexes containing bis-pyridyl acceptor emitters (**1-3**), where bis-pyridyl acceptor emitters (**1-3**) are highly aggregated in pure films owing to the lack of side chains (-OR = –OMe, $–OC_8$, and $–OC_{12}$) in PBP derivatives (**1-3**). In the meanwhile, the lack of side groups (–OR) in PBP derivatives (**1-3**) are also short of electron donor groups and thus to reduce the possible H-bonded effect. Thus, the dilution effect of the acid donors to induce blue-shift of PL is more dominant than the H-bonded effect (red-shift of PL) in polymeric H-bonded complexes containing bis-pyridyl acceptor emitters (**1-3**).

Among emitters **1-3** and **4-6** (see Table 4.6), λmax (PL) values in solution do not change substantially with regard to their heteroatom position of nitrogen, i.e. *para*-, *meta*-, and *ortho*-positions. Besides, the trend of heteroatom position effect is not consistent in pure and blend films. However, comparing analogous emitters PBP-OM**e** **(4-6)** with side alkoxy groups, *para*-heteroatom emitter, i.e. *p*-PBP-OMe **(4)**, has the

largest λmax (PL) values in various states of Table 4.6. As for H-bonded polymer networks (in Table 4.7), the heteroatom position effect is more obvious in H-bonded polymer networks containing emitters PBP-OMe **(4-6)** with side alkoxy groups, and polymer donors have induced the largest λmax (PL) values in *para*-heteroatom emitter, i.e. *p*-PBP-OMe**(4)**. Whereas H-bonded polymer networks contain emitters PBP **(1-3)** without side chains, λmax (PL) values of H-bonded complexes are almost equivalent and regardless of *para*-, *meta*-, and *ortho*-heteroatoms in emitters PBP **(1-3)**.

Table 4.7 PL Spectra of Bis-pyridyl Acceptor Emitters and Their H-bonded Polymer Networks in Solid Films

Compd	λmax (nm)		
	Pure Emitter (without Acid)	H-Bonded with *p*-$PC_{10}BA$ **(14)**[a]	H-Bonded with *m*-$PC_{10}BA$ **(16)**[a]
p-PBP**(1)**	444 (463)[b]	394	396
m-PBP**(2)**	474 (456)[b]	392	395
o-PBP**(3)**	462	389	390
p-PBP-OMe**(4)**	558	586	597
m-PBP-OMe**(5)**	531	539	551
o-PBP-OMe**(6)**	548	570	582
p-PBP-OC_8**(7)**	519 (555)[b]	542	577
p-PBBBP-OC_8**(8)**	549	579	642
p-PBBBP-OC_{12}**(9)**	573	589	612

[a] acceptor:donor = 1:2 by mole to form fully H-bonded polymer networks.
[b] second peaks are shown in the parentheses.

Comparing H-bonded complexes of various bis-pyridyl acceptor emitters (**1-9**) H-bonded with *p*-$PC_{10}BA$ **(14)** and *m*-$PC_{10}BA$ **(16)**, respectively, due to the higher acidity value of *m*-$PC_{10}BA$ **(16)**, stronger H-bonded effect occurs in H-bonded complexes containing *m*-$PC_{10}BA$ **(16)**, so larger λmax values of PL are observed in H-bonded complexes than those containing *p*-$PC_{10}BA$ **(14)** (shown in Table 4.7). This is possibly because of the dissimilar acidity values of donor polymers *p*-$PC_{10}BA$ **(14)**

and *m*-$PC_{10}BA$ **(16)**, i.e. pKa = 4.36 for *p*-$PC_{10}BA$ **(14)** and pKa = 4.19 for *m*-$PC_{10}BA$ **(16)**,[139] which may affect the red-shift of λmax value in PL as described in our previous work.[119] For instance, the pKa values of $C_{10}ONA$ **(10)**, $C_{10}OBA$ **(11)**, and $C_{10}COOTHA$ **(12)** are 4.17, 4.21, and 3.49, respectively, so H-bonded complexes of *p*-PBP-OC_8 **(7)** with $C_{10}ONA$ **(10)**, $C_{10}OBA$ **(11)**, and $C_{10}COOTHA$ **(12)** have different red-shifts in λmax values of PL, i.e. 4, 16, 94 nm, respectively, compared with bis-pyridyl acceptor emitter *p*-PBP-OC_8 **(7)** in pure films with λmax (PL) = 516 nm. In addition, H-bonded complexes of *p*-PBP **(1)** with $C_{10}ONA$ **(10)**, $C_{10}OBA$ **(11)**, and $C_{10}COOTHA$ **(12)** have 14, -5, and 24 nm of red-shifts in λmax values of PL, respectively, compared with bis-pyridyl acceptor emitter *p*-PBP **(1)** in pure films with λmax (PL) = 443 nm.[119] Similar results in PL spectra of *p*-PBP-OC_8**(7)**/*p*-$PC_{10}BA$**(14)** and *p*-PBP-OC_8**(7)**/*m*-$PC_{10}BA$**(16)** after annealing, i.e. λmax (PL) = 554 and 570 nm, correspondingly, are observed in Figure 4.5. Besides, a more complete H-bonded polymer network *p*-PBP-OC_8**(7)**/*p*-$PC_{10}BA$**(14)** can be further established after annealing at 150 °C (in the LC phase) compared with its pristine film by spin-coating (before annealing), so an additional red-shift of 15 nm (from 539 nm to 554 nm) in PL has been detected by annealing (see Figure 4.5).

On the other hand, the varition of λmax values (PL) fluctuates differently in each pair of H-bonded polymer networks as acceptor emitters (**1-9**) are H-bonded to donor polymers *p*-$PC_{10}BA$ **(14)** and *m*-$PC_{10}BA$ **(16)**, respectively. For instance, The largest difference of λmax values (PL), i.e. 63 nm, happens between H-bonded complexes *p*-PBBBP-OC_8**(8)**/*p*-$PC_{10}BA$**(14)** and *p*-PBBBP-OC_8**(8)**/*m*-$PC_{10}BA$**(16)** in Table 4.7. Moreover, the largest red-shift of 93 nm in λmax value of PL can be obtained from *p*-PBBBP-OC_8**(8)**/*m*-$PC_{10}BA$**(16)** in contrast to bis-pyridyl acceptor emitter *p*-PBBBP-OC_8**(8)** in pure films. Interestingly, very small variations of λmax values

(PL), i.e. 1~3 nm, occur in all H-bonded polymer networks contain emitters PBP **(1-3)** without side chains, e.g. the smallest variation of 1 nm take places between H-bonded complexes *p*-PBB**(1)**/*p*-PC_{10}BA**(14)** and *p*-PBB**(1)**/*m*-PC_{10}BA**(16)**. Thus, it depends on the types of acceptor emitters, i.e. PBP derivatives **(1-3)** without side chains or the other derivatives **(4-9)** with side chains, to distinguish the donor polymers *p*-PC_{10}BA **(14)** and *m*-PC_{10}BA **(16)**. Therefore, the acidity of *p*-PC_{10}BA **(14)** and *m*-PC_{10}BA **(16)** may not be the only controlling factor in the red-shift of λmax values (PL) for H-bonded polymer networks. Furthermore, the small difference of acidity between *para*- and *meta*-alkoxybenzoic acid may not be the only feature to introduce such a large red-shift of 93 nm in λmax value of PL in the fully H-bonded polymer network *p*-PBBBP-OC_8**(8)**/*m*-PC_{10}BA**(16)** in contrast to pure emitter *p*-PBBBP-OC_8**(8)**, so some other uncertain reason, such as various H-bonded conformation or conjugation depending on the bis-pyridyl acceptor emitters, may influence the red-shift of PL in H-bonded complexes by different ways.

4.4.3 Electro-optical properties

The λmax values of PL and EL luminescence in pure PVK are usually found around 400 nm and sometimes this emission wavelength is not detectable in the PL and EL spectra of PVK doped systems due to the energy transfer from PVK to dopants. Some of the energy-transfer effects of PVK in EL were found in Figure 4.6, such as *p*-PBP **(1)**, *p*-PBP-OMe **(4)**, and *p*-PBP-OC_8 **(7)** in devices of PVK:dopant(100:5)/TPBI(40 nm)/Mg:Ag, and EL spectra of analogous derivatives are compared. Therefore, the PVK matrix acts as an energy-transfer component as well as hole transporting component in some of the blend film systems. However, a strong emission of PVK or TPBI around 425 nm was observed in of PVK doped

devices containing emitting dopants *m*-PBP **(2)**, *o*-PBP **(3)**, and *p*-PBBBP-OC_8**(8)**. The lowest occupied molecular orbital (LUMO) values are calculated by the highest occupied molecular orbital (HOMO) values (from AC-2) minus the optical band gap values (from UV-Vis), which are also listed in Table 4.8. The band gaps of PBP and PBP-OMe derivatives are between 3.05 to 3.45 eV and 2.64 to 2.72 eV, respectively. Compared with PBP and PBP-OMe derivatives, *p*-PBBBP-OR derivatives possess smaller band gaps between 2.45 and 2.46 eV. The smaller band gaps are by reason of their longer conjugated lengths and their PL and EL spectra show greenish-blue light emissions.

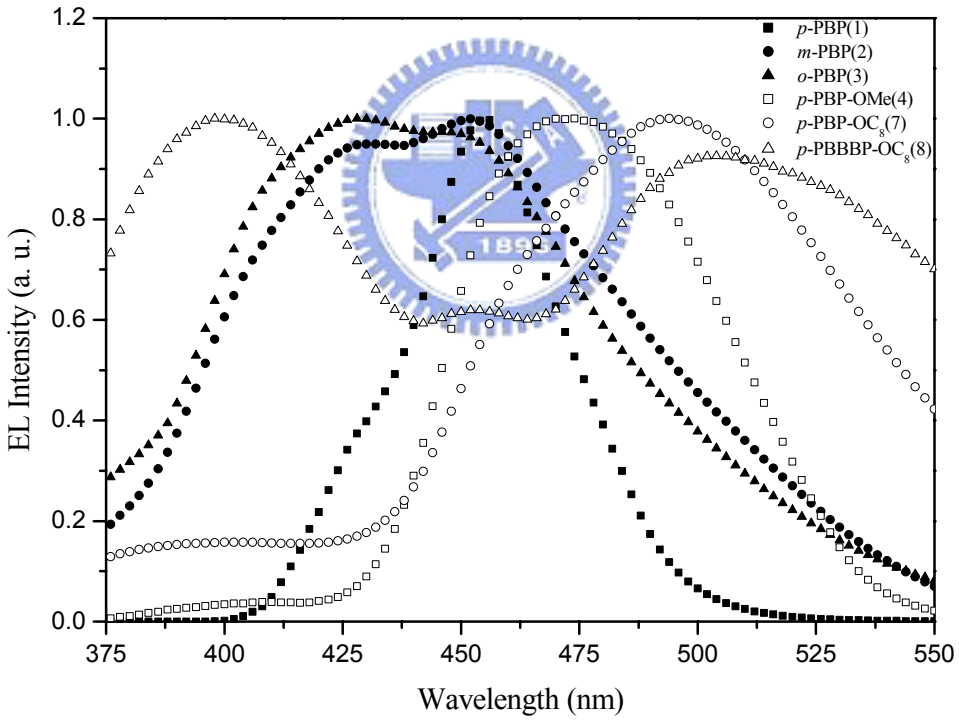

Figure 4.6 EL spectra of devices PVK:dopant(100:5 by weight)/TPBI(40 nm)/Mg:Ag containing bis-pyridyl emitters, i.e. *p*-PBP **(1)**, *m*-PBP **(2)**, *o*-PBP **(3)**, *p*-PBP-OMe **(4)**, *p*-PBP-OC_8 **(7)**, and *p*-PBBBP-OC_8 **(8)**.

Table 4.8 Electroluminescence Characteristics of PLED Devices Containing Various Bis-pyridyl Acceptor Emitters

	p-PBP**(1)**	*m*-PBP**(2)**	*o*-PBP**(3)**	*p*-PBP-OMe**(4)**	*m*-PBP-OMe**(5)**	*o*-PBP-OMe**(6)**	*p*-PBP-OC_8**(7)**	*p*-PBBBP-OC_8**(8)**	*p*-PBBBP-OC_{12}**(9)**
HOMO/LUMO(eV)	5.61/2.53	5.67/2.22	6.02/2.97	5.90/3.26	5.84/3.12	5.72/3.04	5.99/3.47	5.81/3.35	5.72/3.27
band gap (eV)	3.08	3.45	3.05	2.64	2.72	2.68	2.52	2.46	2.45
turn-on voltage, V	15.0	15.8	12.5	18.1	14.7	14.0	19.2	20.2	17.1
max. brightness, cd/m^2	932	1272	1643	1130	3167	2338	2435	684	2414
max. external quantum effic., %	0.67	0.81	0.73	0.62	1.00	0.60	0.70	0.33	0.94
max. power effic., lm/W	0.11	0.14	0.12	0.13	0.20	0.17	0.25	0.11	0.40
λ_{em} (FWHM), nm	454(38)	450(100)	428(96)	468(80)	464(76)	472(72)	494(92)	502(-)[b]	522(-)[b]
CIE, x,y	0.14,0.12	0.15,0.12	0.15,0.11	0.14,0.19	0.15,0.18	0.15,0.20	0.19,0.35	0.28,0.33	0.33,0.46
voltage at 100 mA/cm^2, V	20.0	20.1	14.5	23.4	21.2	16.1	23.5	25.7	22.6
brightness at 100 mA/cm^2, cd/m^2	390	591	550	641	1323	842	1276	498	1636
external quantum effic. at 100 mA/cm^2, %	0.49	0.69	0.73	0.55	1.00	0.60	0.59	0.24	0.31
power effic. At 100 mA/cm^2, lm/W	0.06	0.09	0.12	0.09	0.20	0.17	0.17	0.06	0.07

[a] the thickness of TPBI is 40 nm and PVK: chromophore =100: 5.
[b] FWHM can not be measured due to overlapping peak.

Due to the poor film quality of H-bonded complexes and polymers, including polymer donors *p*-$PC_{10}BA$ **(14)** and *m*-$PC_{10}BA$ **(16)**, so PVK is utilized as the polymer matrix in further study. To analyze the H-bonding effect on the LED device performance of H-bonded complexes, acceptor emitter *p*-PBP-OC_8 **(7)**, which possesses the best solubility among acceptor emitters, is doped into PVK either with or without proton donor $C_{10}OBA$ **(11)**. Hence, **Devices 1-3** containing PVK:*p*-PBP-OC_8 **(7)** (100:5 by weight, i.e. without H-bonding) and PVK:*p*-PBP-OC_8 **(7)**:$C_{10}OBA$ **(11)** (100:5:50 by weight, i.e. with H-bonding) blend films are investigated (with and without annealing). However, devices (with 40 nm of TPBI) of PVK:*p*-PBP-OC_8 **(7)** (100:5 by weight) annealed at 170 and 230 ºC (below and above T_g of PVK ~200 ºC, respectively) and PVK:*p*-PBP-OC_8 **(7)**:$C_{10}OBA$ **(11)** (100:5:50 by weight) without annealing have worse optical properties, so above device data are not demonstrated. With regard to **Devices 1-3** (see Figure 4.7 and Table 4.9), EL spectra obtained from **Devices 2** and **3** of PVK:*p*-PBP-OC_8**(7)**:$C_{10}OBA$**(11)**(100:5:50 by weight, i.e. with H-bonding)/TPBI(40 nm)/Mg:Ag, which were annealed at 170 and 230 ºC (above and below T_g of PVK), respectively, own more narrow full width at half maximum (FWHM) values (38 and 42 nm) of EL spectra than that from **Device 1** (92 nm) of PVK:*p*-PBP-OC_8**(7)** (100:5 by weight, i.e. without H-bonding)/TPBI(40 nm)/Mg:Ag. More Narrow FWHM values of EL spectra in the H-bonded LED devices maybe owe to the induction of fewer electron transition states in the supramolecular architecture. As shown in Table 4.9, **Device 3** annealed at 230 ºC possesses a better brightness of 5184 cd/m^2 than **Device 2** annealed at 170 ºC and also better than **Device 1** without donor $C_{10}OBA$ **(11)**. Finally, Devices with H-bonding between acceptor emitters and donors cannot only induce more narrow FWHM values of EL spectra but also redder shift in EL spectra in this supramolecular

architecture.

Table 4.9 The EL Characteristics of Devices 1-3 Containing Bis-pyridyl Acceptor Emitter *p*-PBP-OC_8**(7)**, i.e. Device 1 of PVK:*p*-PBP-OC_8**(7)** (100:5 by weight)/TPBI(40 nm)/Mg:Ag, Device 2 (with annealing at 170 °C for 2 minutes) and Device 3 (with annealing at 230 °C for 2 minutes) of PVK:*p*-PBP-OC_8**(7)**:C_{10}OBA**(11)** (100:5:50 by weight)/TPBI(40 nm)/Mg:Ag

	Device 1	**Device 2**	**Device 3**
turn-on voltage, V	19.2	26.5	22.3
max. brightness, cd/m^2	2599	1803	5184
max. external quantum effic., %	0.76	0.71	0.79
max. power effic., lm/W	0.27	0.23	0.31
λ_{em} (FWHM), nm	494(92)	510(38)	508(42)
CIE, x,y	0.19,0.35	0.08,0.65	0.09,0.64
voltage at 100 mA/cm^2, V	23.5	34.4	26.2
brightness at 100 mA/cm^2, cd/m^2	1362	1685	1777
external quantum effic. at 100 mA/cm^2, %	0.64	0.61	0.64
power effic. at 100 mA/cm^2, lm/W	0.18	0.15	0.21

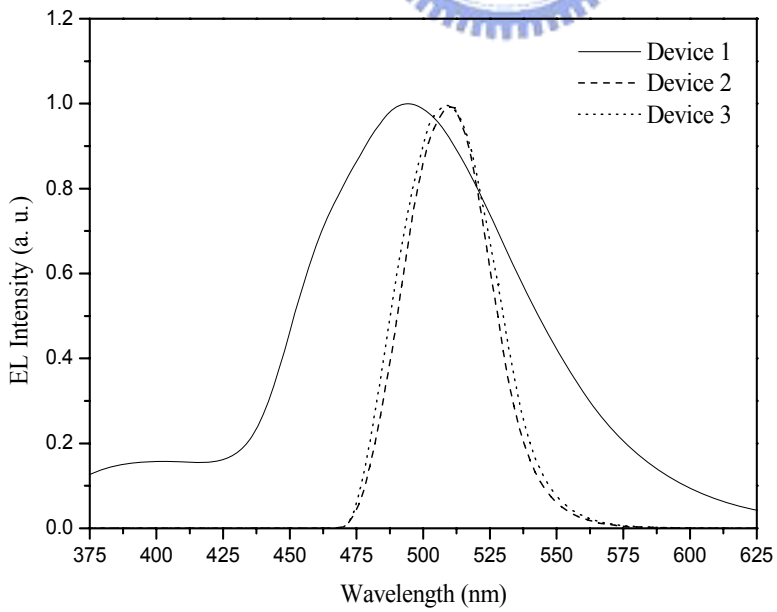

Figure 4.7 EL spectra of **Devices 1-3** containing *p*-PBP-OC_8**(7)**, i.e. **Device 1** of PVK:*p*-PBP-OC_8**(7)** (100:5)/TPBI(40 nm)/Mg:Ag, **Device 2** (with annealing at 170 °C for 2 minutes) and **Device 3** (with annealing at 230 °C for 2 minutes) of PVK:*p*-PBP-OC_8**(7)**:C_{10}OBA**(2)** (100:5:50)/TPBI(40 nm)/Mg:Ag.

4.5 Conclusions

In conclusion, the mesomorphic and photophysical properties of the H-bonded polymer networks and trimers can be easily adjusted by tuning the H-bonded donors (donor polymers) and acceptor emitters in the H-bonded complexes. Unique mesomorphic properties may be introduced into these supramolecular structures containing non-mesogenic acceptor emitters. In addition, the emission properties of bis-pyridyl acceptor emitters can be manipulated by their surrounding non-photoluminescent proton donors. Compared with pure bis-pyridyl acceptor emitters, red-shifts of PL emission wavelengths have occurred, i.e. the H-bonded effect is dominant, in most of the H-bonded complexes. Due to the higher acidity value of *m*-$PC_{10}BA$ **(16)** than that of *p*-$PC_{10}BA$ **(14)**, stronger H-bonded effect occurs in H-bonded complexes containing *m*-$PC_{10}BA$ **(16)**, so larger λmax values of PL are observed in H-bonded complexes. The largest red-shift of 93 nm in λmax value of PL has occurred in the fully H-bonded polymer network *p*-PBBBP-OC_8**(8)**/*m*-$PC_{10}BA$**(16)** in contrast to pure emitter *p*-PBBBP-OC_8**(8)**. However, the small difference of acidity between *para*- and *meta*-alkoxybenzoic acid, i.e. *p*-$PC_{10}BA$ **(14)** and *m*-$PC_{10}BA$ **(16)**, may not be the only feature to introduce such large red-shifts in λmax values of PL in the fully H-bonded polymer networks. PL and EL spectra of all blend films in PVK (dopant emitter: PVK= 5:100 wt%) show blue to green light emissions. PL spectra of fully H-bonded complexes of bis-pyridyl acceptor emitters (**1**-**9**) with *m*-$PC_{10}BA$ **(16)** (molar ratio = 1:2) are even widely distributed from blue to red colors (from 396 nm to 642 nm). A very narrow FWHM value (38 nm) of EL spectra can be obtained in the H-bonded complexes blended with PVK, and higher brightness of EL is produced at an appropriate annealing temperature.

Chapter 5

Novel Red and White PLED Devices Consisting of PVK Blended with Blue-emitting Fluorene Derivatives and Carbazole Dopants

5.1 Abstract

Highly fluorescent polymeric LEDs (PLEDs) utilizing blue-emitting FB fluorene derivatives (FBFl4 and FBPh4) blended with PVK are demonstrated. Significant red shift of the emission from blue to red can be achieved by increasing the concentration of FB in the blend. The origin of emission was attributed to electromer (or electroplex) formation. Addition of Carb9 in the blend enhanced the electromer (or electroplex) formation, and red- or white-emission device with high brightness (3440 cd/m^2 for red; and 17368 cd/m^2 for white) was obtained.

5.2 Introduction

Recently, organic light-emitting diodes (OLEDs) and polymeric light-emitting diodes (PLEDs) have been applied to display technologies. They can also be combined with color filters to provide red, green, and blue light-emitting pixels. Small-molecule organic LEDs have shown quite high efficiency and brightness in white light LEDs.[140] In order to achieve this goal, numerous approaches have been explored, such as dye-dispersed matrixes of poly(*N*-vinylcarbazole) (PVK),[8,141,142] polyfluorene,[103,143-145] and other polymers.[146,147] Metal-containing complexes also received considerable attention since the seminal work by Thompson.[148] These

crystalline materials normally have to be doped into some small molecule[149] or polymer[52] hosts. There have been some reports using Ir[98, 104,150-154] and Ru[99, 155-158] derivatives doped into polymer matrixes for red-emitting devices. It is interesting to note that a single blue-emitting phosphor[159] dopant in combination with its excimer emission generated white light efficiently. This may avoid complex device structure using multiple dopants. Heeger[160] and List[161] et al reported some other polymer devices applied in white light also.

In this work, we found that 9-ethyl-*N,N'*-diphenyl-*N,N'*-dipyren-1-yl-9*H*-carbazole-3,6-diamine (Carb9)[162] doped into fluorescent FB fluorene derivatives (FBFl4 or FBPh4)[163] and blended with PVK to induce the shift of the emission color which eventually leads to red and white light. By increasing the concentration of the FB molecule in the presence of Carb9 dopant, the red electroplex (or electromer) emission was enhanced at the expense of the blue emission from the FB molecule. Furthermore, white light emission can also be achieved in these devices.

5.3 Experimental

The molecular structures of materials used are shown in Figure 5.1. The synthesis and characterization of Carb9 has been published before[162] and FB derivatives (FBPh4 and FBFl4)[163] will be reported elsewhere. The synthetic procedures of BCP (hole-blocking layer) and Alq (electron-transporting layer) were reported in the literature.[164]

Glass slides precoated with indium tin oxide (ITO) with sheet resistances of ~20 Ω/square and with an effective individual device area of 3.14 mm^2 were used for fabrication of devices. The ITO glasses were routinely cleaned by ultrasonic treatment

in detergent solution, followed by through rinsing in acetone and then ethanol, and dried in oxygen plasma for 3 min before being loaded into the vacuum chamber. The Carb9 dopant and FB derivatives blended in PVK are dissolve in 1,2-dichloroethane with a concentration of 30 mg/ml and the spin coating rate was 3000 rpm for 40 s. The hole-blocking and electron-transporting layers were deposited thermally at a rate of 0.1-0.3/s under a pressure of ~$2x10^{-5}$ torr in an Ulvac Cryogenic deposition system. An alloy of magnesium and silver (ca. 10:1, 50 nm) was deposited as a cathode, which was then capped with 100 nm of silver. The device configuration is shown in Figure 5. 2.

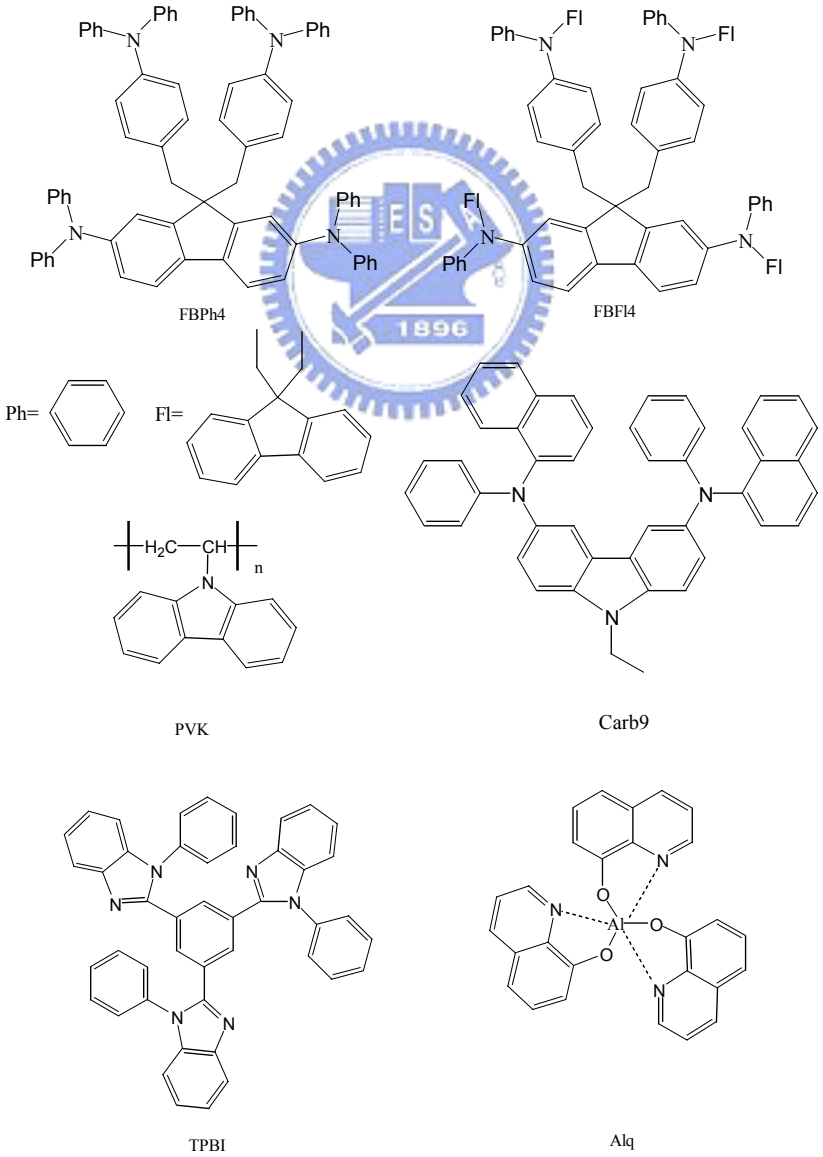

Figure 5.1 Molecular structures of materials used in this study.

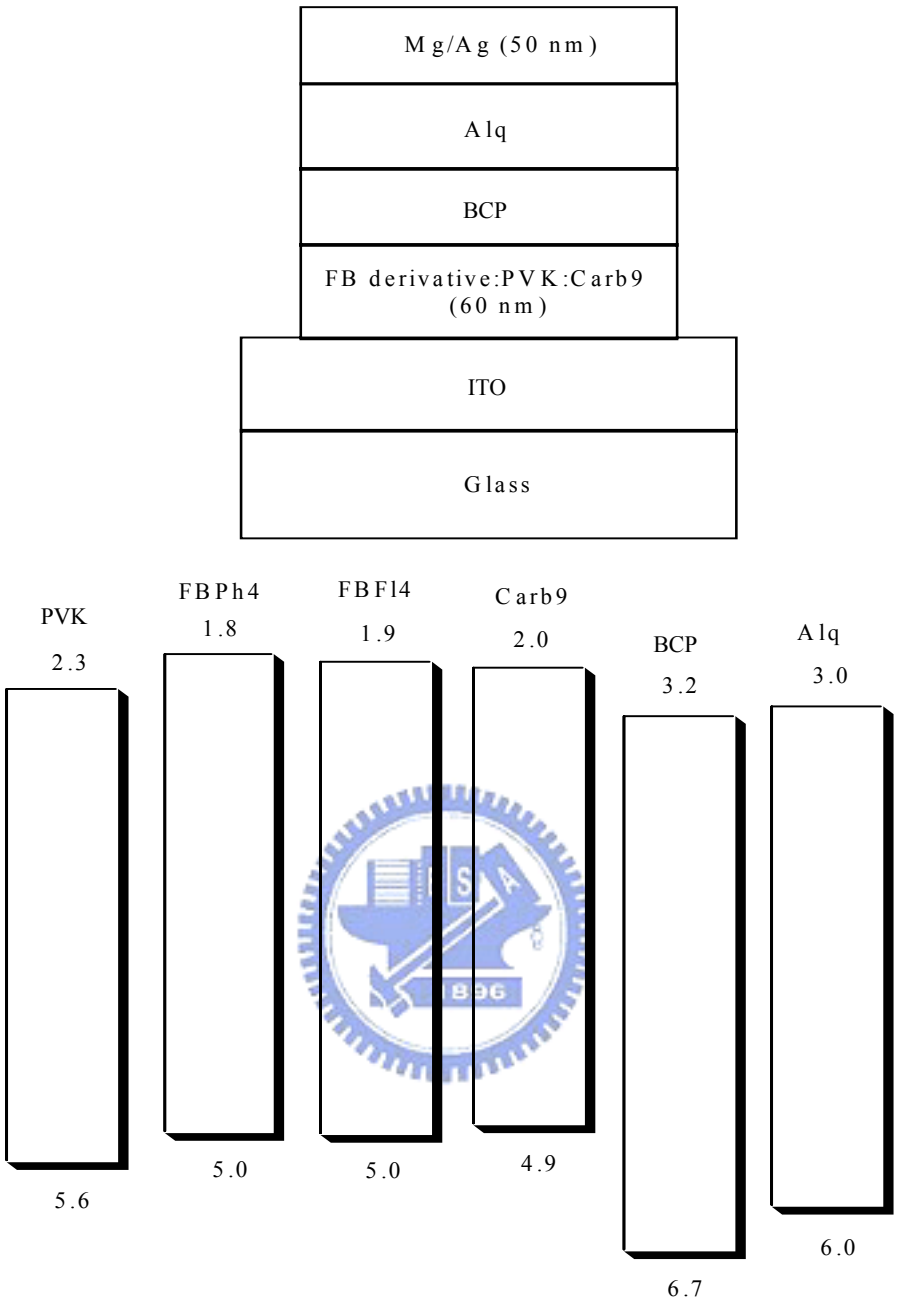

Figure 5.2 The device configuration and the HOMO, LUMO values of PVK, FB derivatives, Carb9, hole-blocking BCP, and electron-transporting Alq.

The HOMO and LUMO values shown in Figure 5. 2 were calculated from cyclic voltammetry (vide supra) using ferrocene (4.8 eV) as the reference. The current-voltage-luminescence (I-V-L) spectra were measured in ambient conditions with Keithley 2400 Source meter and a Newport 1835C Optical meter equipped with 818ST silicon photodiode and emission spectra of photoluminescence (PL) and electroluminescence (EL) were recorded on a Hitachi spectrofluorometer.

5.4 Results and Discussion

The PL spectra of FBPh4 in dichloroethane solution (10^{-6} M), and blend films (with various concentrations in PVK) are shown in Figure 5.3. The energy transfer from PVK to FBPh4 is evident from the PL spectra of PVK:FBPh4 blend. The emission of FBPh4 is red shifted as the relative concentration of FBPh4 increases in the blend up to x = 150, where PVK:FBPh4 = 100:x by weight. This could be attributed to the aggregation of FBPh4. The EL spectra of FBPh4 in blend films (with various concentrations in PVK) are also demonstrated in Figure 5.3. Surprisingly, in addition to the characteristic band of FBPh4 at ~410 nm, the EL spectra of PVK:FBPh4 (100:150) and PVK:FBPh4 (100:300) blend films have a prominent band at ~583 nm (Figure 5.3), which was not observed in the PL spectra of the previous PVK:FBPh4 blends. This strongly implies that the EL emission peak at ~583 nm is owing to the formation of electromers[22] from FB or electroplexes[21, 165-169] from PVK/FB. The ratio of electromer (or electroplex) emission (ca. 583 nm) to intrinsic emission (ca. 410 nm) increases as the relative concentration of FBPh4 in the PVK:FBPh4 blend increases. However, the intrinsic emission of FBPh4 still remains up to a weight ratio of 100:300 (PVK:FBPh4).

When Carb9 was added to the PVK:FBPh4 blend, emission of FBPh4 (ca. 410 nm) was completely suppressed (Figure 5.4), possibly due to the efficient energy transfer from FBPh4 and PVK to Carb9 which emits at ~460 nm. It is interesting to note that the higher concentration of FBPh4 vs. Carb9 or PVK will lead to a decrease of the emission from Carb9 (ca. 460 nm). The emission of Carb9 was completely suppressed, and only the electromer (or electroplex) emission was detected at a blend concentration of 100:300:15 (PVK:FBPh4:Carb9) (as shown in Figure 5.4). The enhancement of the electromer (or electroplex) emission with increasing ratio of

FBPh4 vs. PVK in the PVK:FBPh4:Carb9 blend is consistent with that observed for the PVK:FBPh4 blend. However, the complete suppression of FBPh4 and Carb9 emission (ca. 410 nm and 460 nm, respectively) occurs only in the PVK:FBPh4:Carb9 blend at a ratio of 100:300:15. Possibly FBPh4 can transfer the electron to the excited Carb9, and the process is deemed favorable based on the relative HOMO and LUMO energy levels between the two (Figure 5.2). Alternately, the higher concentration of FBPh4 not only competes favorably with Carb9 for carriers, but may also facilitate the aggregation of Carb9. It appears to be interesting that the orange-emitting devices (with blend concentrations of PVK:FBPh4:Carb9 = 100:150:15 and 100:300:15) can be obtatined from three purple/blue-emitting components. The performance parameters of the orange-emitting device with PVK:FBPh4:Carb9 ratio of 100:150:15 are listed in Table 5.1. It is interesting that appropriate combination of Carb9 emission and the electromer (or electroplex) emission can lead to white-light in the PVK:FBPh4:Carb9 blend. Since all three components in this blend are hole carriers, hole blocker (BCP) and electron transporter (Alq) were inserted between the blend film and the cathode. The multi-layered devices, ITO/PVK:FBPh4:Carb9(100:200:15)/BCP(5 nm)/Alq(20 nm)/Mg:Ag, was fabricated. The EL spectra (at different voltages) and pertinent data of the device are demonstrated in Figure 5.5(a) and Table 1, respectively. The device emits white light which has relatively constant chroma at applied voltages ranging from 10 – 14 V: CIE coordinate (0.33, 0.35) at 10 V, (0.30, 0.330 at 12 V, and (0.27, 0.30) at 14 V (Figure 5.6). The performance of the device appears to be good with brightness reaching 17368 cd/m^2 at 13 V. The CIE diagram is shown in Figure 5.6, and the I-V-L plot of the device is illustrated in Figure 5.7. Table 5.1 compiles the important performance parameters of the devices from the PVK:FBPh4:Carb9 blend.

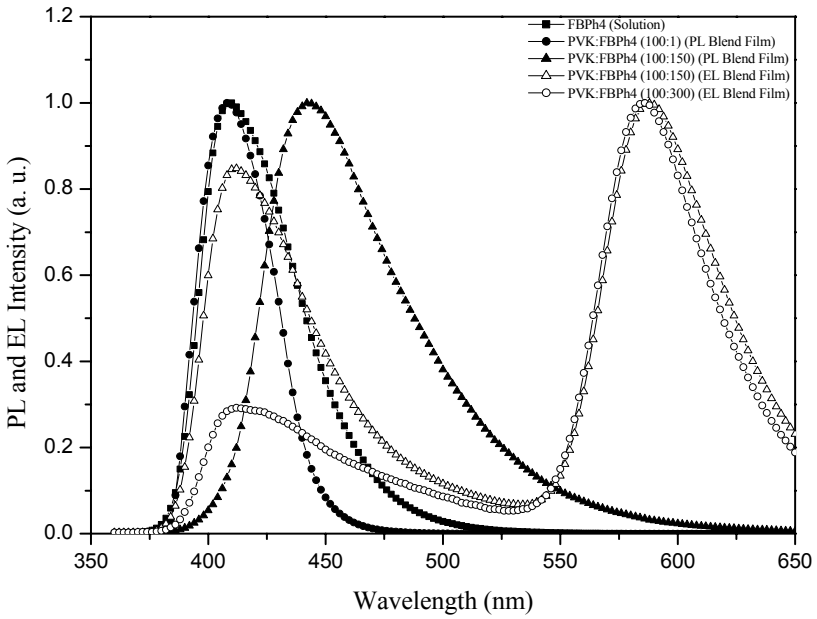

Figure 5.3 PL and EL spectra of FBPh4 in solution (10^{-6} M in dichloroethane) and blend films (with various concentrations in PVK).

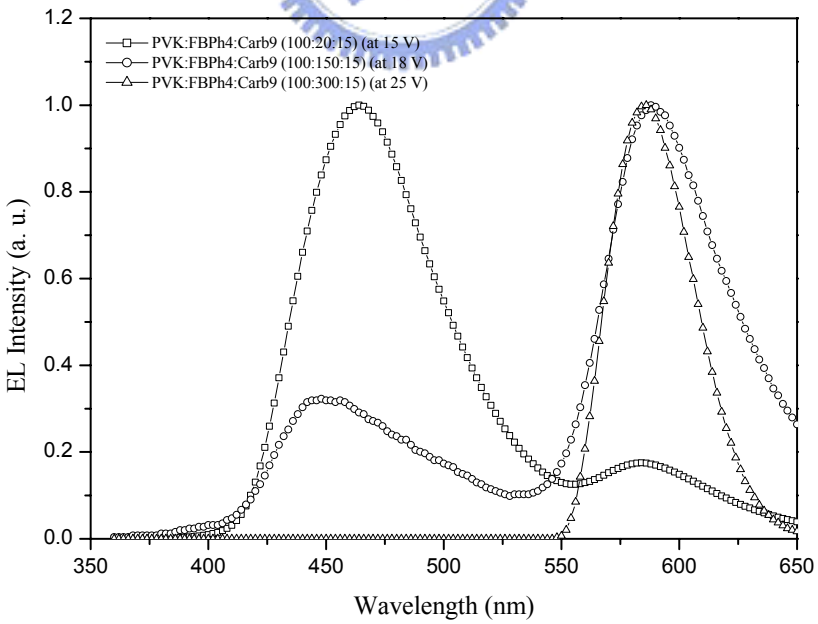

Figure 5.4 EL spectra of blend films with various concentrations of FBPh4.

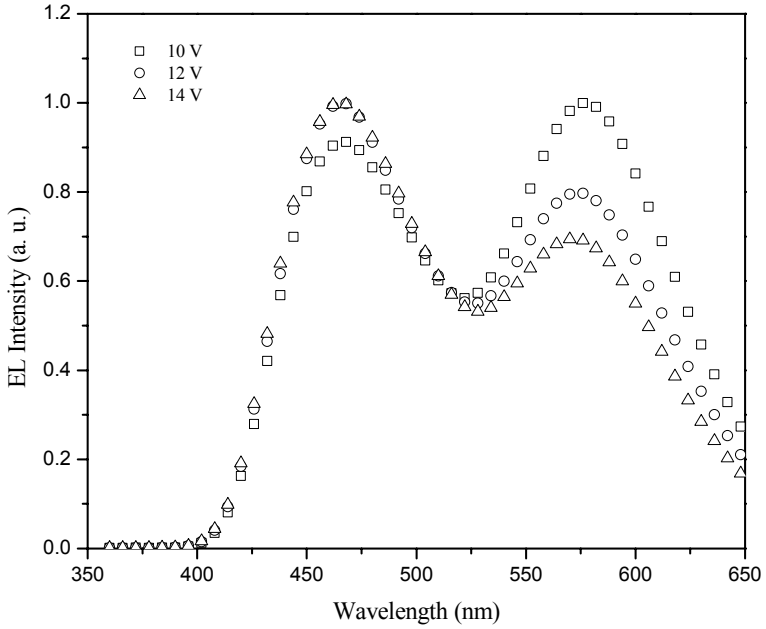

(a)

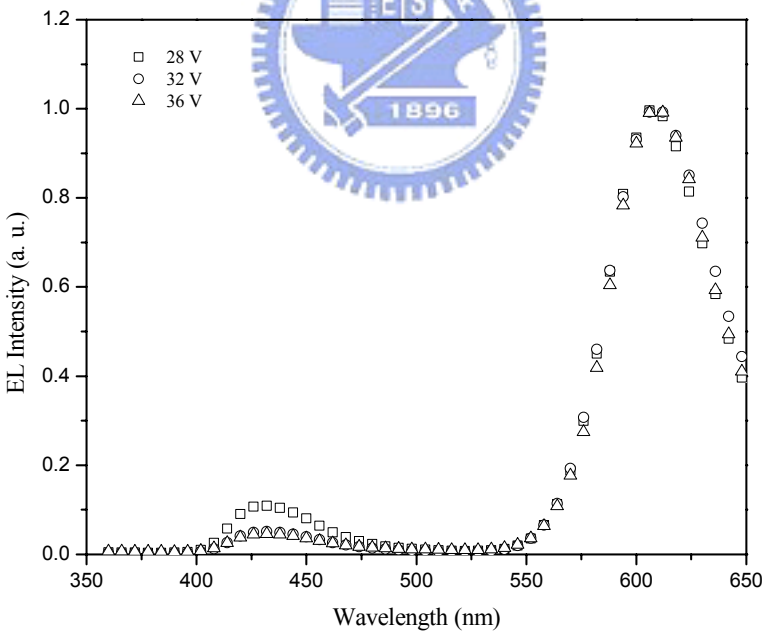

(b)

Figure 5.5 EL spectra of the devices: (a) PVK:FBPh4:Carb9(100:200:15)/BCP(5nm)/Alq(20nm) and (b) PVK:FBFl4:Carb9(100:200:15)/BCP(10nm)/Alq(10nm) with different driving voltages.

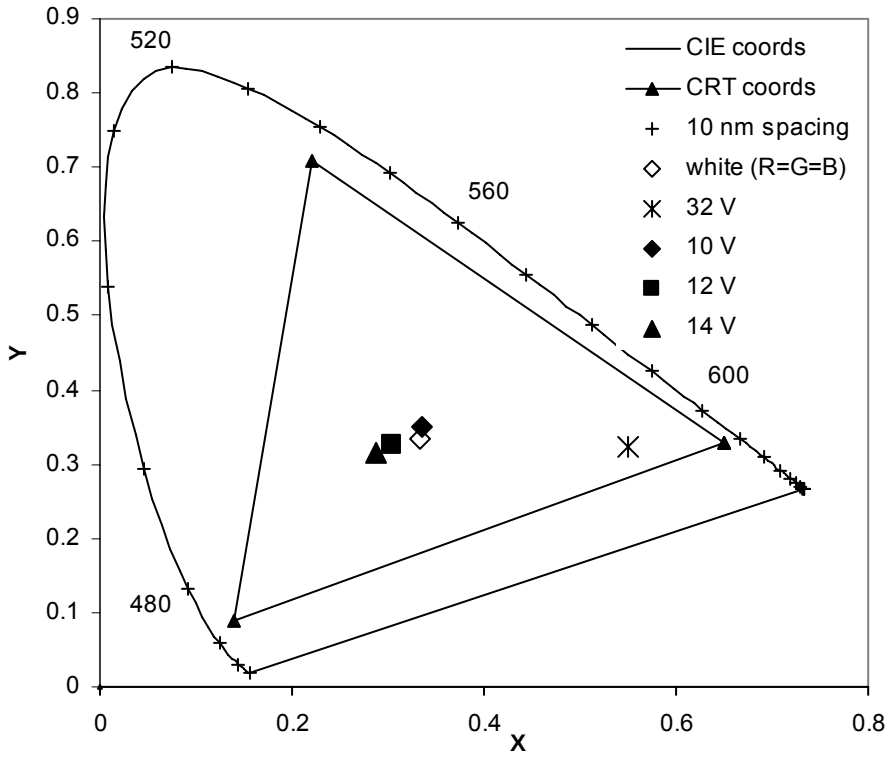

Figure 5.6 CIE coordinate of PVK:FBFl4:Carb9(100:200:15)/BCP(10nm) /Alq(10nm) at 32 V and PVK:FBPh4:Carb9(100:200:15)/BCP(5nm)/Alq(20nm) at 10 V, 12 V, and 14 V.

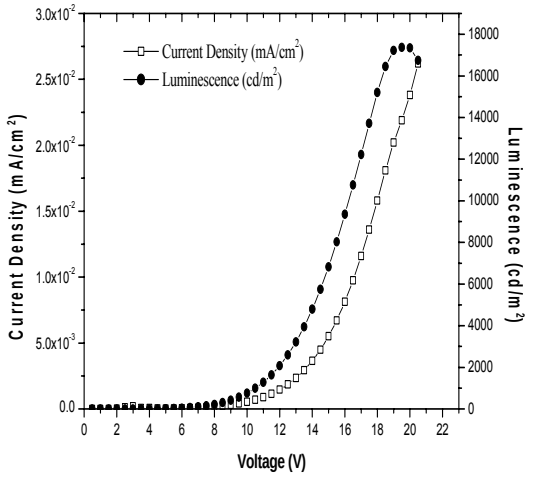

Figure 5.7 I-V-L spectra of device PVK:FBPh4:Carb9 (100:200:15)/BCP(5nm)/Alq (20nm).

Though energy transfer from PVK to FBFl4 is also evident, the formation of the electromers (or electroplexes) in the EL devices of PVK:FBFl4 blend does not appear to be as significant as the PVK:FBPh4 congener (Figure 5.8). In contrast to the device of PVK:FBPh4:Carb9 blend, we found no complete suppression of the Carb9 emission in the EL devices of PVK:FBFl4:Carb9 blend. Nevertheless, device of the structure ITO/PVK:FBFl4:Carb9(100:200:15)/BCP(10 nm)/Alq(10 nm)/Mg:Ag has orange-red emission (EL spectra with different voltages shown in Figure 5.5(b)) and the maximum brightness reaches 3440 cd/m^2 (CIE coordinate = 0.56, 0.32 in Figure 5.6) at 32 V. The I-V-L plots of this device are shown in Figure 5.9, and device of structure ITO/PVK:FBFl4:Carb9(100:200:15)/BCP(10 nm)/Alq(10 nm)/Mg:Ag has red emission when the applied voltage is higher than 40 V. No white light-emitting devices can be obtained from PVK:FBFl4:Carb9 blend; however, their EL characteristics of FB derivatives are also listed in Table 5.1.

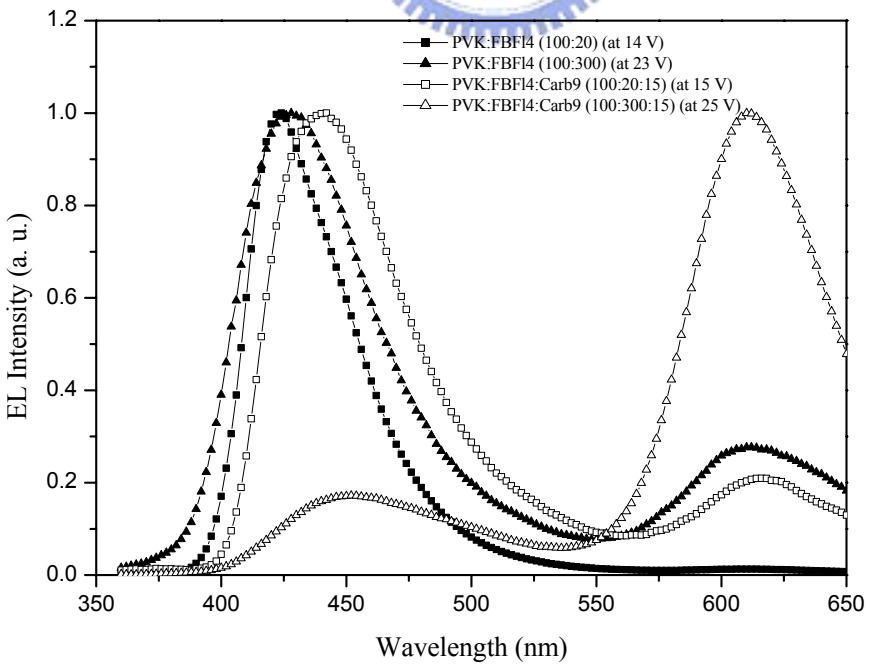

Figure 5.8 EL spectra of blend films with various concentrations of FBFl4 and Carb9.

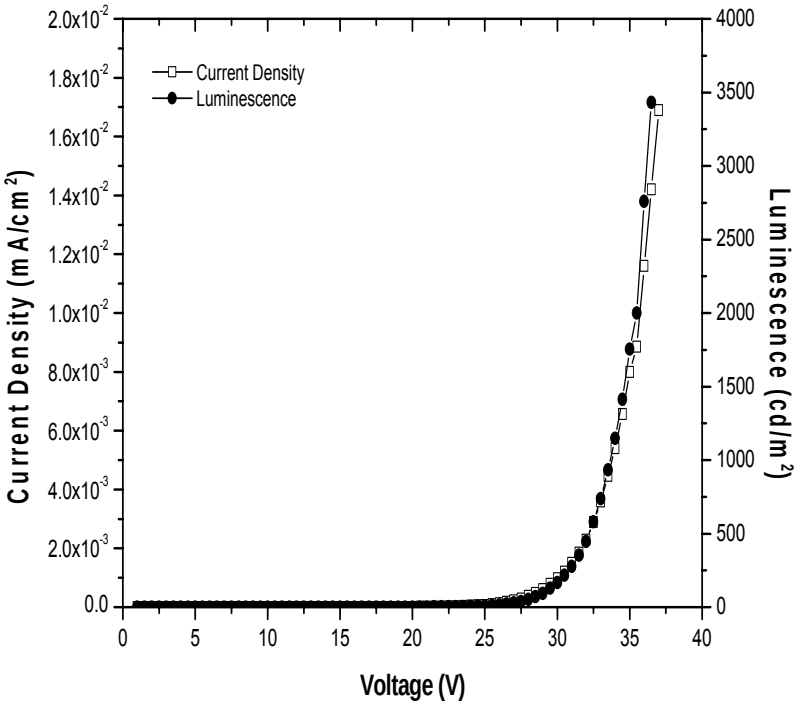

Figure 5.9 I-V-L spectra of device PVK:FBFl4:Carb9(100:200:15)/BCP(10nm)/Alq (10nm).

Table 5.1 EL Characteristics of PLED Devices

	PVK:FBPh4:Carb9	PVK: FBPh4: Carb9/BCP/Alq	PVK: FBFl4: Carb9/BCP/Alq
	(100:150:15)	(100:200:15)/(5 nm)/(20 nm)	(100:200:15)/(10 nm)/10 nm)
turn-on voltage, V	8.8	10.1	28.7
max. brightness, cd/m^2	747	17368	3440
max. external quantum effic., %	0.18	1.84	0.42
max. power effic., lm/W	0.06	1.36	0.06
λ_{em} (FWHM), nm	446, 586 (186)	470, 586 (190)	614, 448 (70)
CIE, x,y	0.40, 0.31	0.33, 0.35	0.56,0.32

5.5 Conclusions

Under applied voltages, blends of PVK and blue-emitting FB derivatives emit orange or red colors due to the formation of electromers from FB or electroplexes from PVK/FB. Orange- or red-emitting electroluminescent devices can be achieved if a carbazole derivative, Carb9, is added to the blends at an appropriate ratio. White-light emission is also possible from the device of PVK/FB/Carb9 blend.

Chapter 6

Conclusions

BV series by the replacement of 3-conjugated rings with 5-conjugated phenyl cores are modified to possess mesomorphism, which can have the most appropriate chain length on both terminals (on both end rings) and sides (on the central ring) of the conjugated core to own the widest mesophasic range in BV series. Highly efficient and bright blue-green EL emissions of PVK PLED devices doped with fluorescent oligo(p-phenylene-vinylene)s (BIII and BV) and polymer derivatives (PBV) were obtained by proper device configurations of multilayer design. Five-conjugated ring OPV (BV) derivatives with proper alkoxy groups possess excellent hole-transporting property and the highest brightness in PLED devices, and the main emitting source of these multilayer devices is confirmed to be the conjugated emissions and excimer emissions of the OPV emitters.

The mesomorphic and photophysical properties of the H-bonded polymer networks and trimers can be easily adjusted by tuning the H-bonded donors (donor polymers) and acceptor emitters in the H-bonded complexes. In addition, the emission properties of bis-pyridyl acceptor emitters can be manipulated by their surrounding non-photoluminescent proton donors. Compared with pure bis-pyridyl acceptor emitters, red-shifts of PL emission wavelengths have occurred, i.e. the H-bonded effect is dominant, in most of the H-bonded complexes. A very narrow FWHM value (38 nm) of EL spectra was obtained in the H-bonded complexes blended with PVK, and higher brightness of EL was produced at an appropriate annealing temperature.

Under applied voltages, blends of PVK and blue-emitting FB derivatives emit orange or red colors due to the formation of electromers from FB or electroplexes

from PVK/FB. Orange- or red-emitting electroluminescent devices were achieved if a carbazole derivative (Carb9) was added to the blends at an appropriate ratio. White-light emission is also possible from the device of PVK/FB/Carb9 blends.

References

(1) Burroughes, J. H.; Bradley, D. D. C.; Brown, A. R.; Marks, N.; Mackay, K. R.; Friend, H.; Burn, P. L.; Holmes, A. B. *Nature* **1990**, *347*, 539.

(2) Kraft, A.; Grimsdale, A. C.; Holmes, A.B. *Angew. Chem. Int. Ed.* **1998**, *37*, 402.

(3) Kido, J.; Hongawa, K.; Okuyama, K.; Nagai, K. *Appl. Phys. Lett.* **1994**, *64*, 815.

(4) Johnson, G. E.; McGrane, K. M.; Stolka, M. *Pure Appl. Chem.* **1995**, *67*, 175.

(5) Brütting, W.; Berleb, S.; Egerer, G.; Schwoerer, M.; Wehrmann, R.; Elschner, A. *Synth. Met.* **1997**, *91*, 325.

(6) Gautier-Thianche, E.; Sentein, C.; Lorin, C.; Denis, A.; Raimond, P.; Nunzi, J. -M. *J. Appl. Phys.* **1998**, *83*, 4236.

(7) Zhang, C.; von Seggern, H.; Kraabel, B.; Schmidt, H. -W.; Heeger, A. J. *Synth. Met.* **1995**, *72*, 185.

(8) Kido, J.; Shionoya, H.; Nagai, K. *Appl. Phys. Lett.* **1995**, *67*, 2281.

(9) Gautier-Thianche, E.; Sentein, C.; Nunzi, J. -M.; Lorin, A.; Denis, C.; Raimond, P. *Synth. Met.* **1997**, *91*, 323.

(10) Kido, J.; Kohda, M.; Okuyama, K.; Nagai, K. *Appl. Phys. Lett.* **1992**, *61*, 761.

(11) Yang, Y.; Jiang, H.; Liu, S. *Synth. Met.* **1997**, *91*, 335.

(12) Lin, H. C.; Tsai, C. M.; Huang, G. H.; Lin, J. M. *J. Poly. Sci: Part A: Poly. Chem.* **2006**, *44*, 783.

(13) Lin, H. C.; Tsai, C. M.; Tao, Y. T. *J. Poly. Sci: Part A: Poly. Chem.* Accepted.

(14) Lin, H. C.; Tsai, C. M.; Huang, G. H.; Tao, Y. T. *Macromolecules*, **2006**, *39*, 557.

(15) Justin Thomas, K. R.; Lin, J. T.; Tsai, C. M.; Lin, H. C. *Tetrahedron*, Accepted.

(16) Lin, H. C.; Tsai, C. M.; Justin Thomas, K. R.; Lin J. T. *Synth. Met.* Revised.

(17) Förster, T. *Discuss Faraday Soc.* **1959**, *7*, 27.

(18) Dexter, D. L. *J. Chem. Phys.* **1953**, *21*, 836.

(19) Nguyen, T. Q.; Martini, I. B.; Liu, J.; Schwartz B. J. *J. Phys. Chem. B* **2000,** *104,* 237.

(20) Blatchford, J. W.; Jessen, S. W.; Lin, L.-B.; Gustafson T. L.; Fu, D.-K.; Wang, H.-L.; Swager, T. M.; MacDiarmid, A. G.; Epstein, A. J. *Phys. Rev. B* **1996**, *54*, 9180.

(21) Granlund, T.; Pettersson, L. A. A.; Anderson, M. R.; Inganas, O. *J. Appl. Phys.* **1997**, *81*, 8097.

(22) Lee, Y. Z.; Chen, X.; Chen, M. C.; Chen, S. A.; Hsu, J. H.; Fann, W. *Appl. Phys. Lett.* **2001**, *79*, 308.

(23) Sirringhaus, H.; Wilson, R. J.; Friend, R. H.; Inbasekaran, M.; Wu, W.; Woo, E. P.; Grell, M.; Bradley, D. D. C. *Appl. Phys. Lett.* **2000**, *77*, 406.

(24) West, J. L.; Magyar, G. R.; Kelly, J. R. *Appl. Phys. Lett.* **1995**, *67*, 155.

(25) Lam, J. W. Y.; Tang, B. Z. *J. Poly. Sci. A Poly. Chem.* **2003**, *41*, 2607.

(26) Lam, J. W. Y.; Kong, X.; Dong, Y.; Cheuk, K. K. L.; Xu, K.; Tang, B. Z. *Macromolecules* **2000**, *33*, 5027.

(27) Chen, J.; Xie, Z.; Lam, J. W. Y.; Law, C. C. W.; Tang, B. Z. *Macromolecules* **2003**, *36*, 1108.

(28) Huang, Y. M.; Lam, J. W. Y.; Cheuk, K. K. L.; Ge, W.; Tang, B. Z. *Mater. Sci. Eng.* **2001**, *B85*, 122.

(29) Lin, H. C.; Sung, H. H.; Tsai, C. M.; Li, K. C. *Polymer* **2005**, *46*, 9810.

(30) Meisel, A.; Miteva, T.; Glaser, G.; Scheumann, V.; Neher, D. *Polymer* **2002**, *43*, 5235.

(31) Neher, D. *Macromol. Rapid Commun.* **2001**, *22*, 1365.

(32) Banach, M. J.; Friend, R. H.; Sirringhaus, H. *Macromolecules* **2003**, *36*, 2838.

(33) Millaruelo, M.; Oriol, L.; Pinol, M.; Saez, P. L.; Serrano, J. L. *J. Photochem. Photobio. A Chem.* **2003**, *55*, 29.

(34) Yang, X. H.; Neher, D.; Spitz, C.; Zojer, E.; Brédas, J. L.; Guntner, R.; Scherf, U. *J. Chem. Phys.* **2003**, *119*, 6832.

(35) Godbert, N.; Burn, P. L.; Gilmour, S.; Markham J. P. J.; Samuel, I. D. W. *Appl. Phys. Lett.* **2003**, **83**, 5347.

(36) Zen, A.; Neher, D.; Bauer, C.; Asawapirom, U.; Scherf, U.; Hagen, R.; Kosttomine, S.; Mahrt, R. F. *Appl. Phys. Lett.* **2002**, *80*, 4699.

(37) Whitehead, K. S.; Grell, M.; Bradley, D. D. C.; Jandke, M.; Strohriegel, P. *Appl. Phys. Lett.* **2000**, *76*, 2946.

(38) Miteva, T.; Meisel, A.; Knoll, W.; Nothofer, H. G.; Scherf, U.; Müller, D. C.; Meerholz, K.; Yasuda, A.; Neher, D. *Adv. Mater.* **2001**, *13*, 565.

(39) Grozema, F. C.; Savenije, T. J.; Vermeulen, M. J. W.; Siebbeles, L. D. A.; Warman, J. M.; Meisel, A.; Neher, D.; Nothofer, H. G.; Scherf, U. *Adv. Mater.* **2001**, *13*, 1627.

(40) Sainova, D.; Zen, A.; Nothofer, H. G.; Asawapirom, U.; Scherf, U.; Hagen, R.; Bieringer, T.; Kostromine, S.; Neher, D. *Adv. Funct. Mater.* **2002**, *12*, 49.

(41) Geng, Y.; Culligan, S. W.; Trajkovska, A.; Wallace, J. U.; Chen, S. H. *Chem. Mater.* **2003**, *15*, 542.

(42) Geng, Y.; Chen, A. C. A.; Ou, J. J.; Chen, S. H.; Klubek, K.; Vaeth, K. M.; Tang, C. W. *Chem. Mater.* **2003**, *15*, 4352.

(43) Hulvat, J. F.; Stupp, S. I. *Adv. Mater.* **2004**, *16*, 589.

(44) Chen, J.; Peng, H.; Law, C. C. W.; Dong, Y.; Lam, J. W. Y.; Williams, I. D.; Tang, B. Z. *Macromolecules* **2003**, *36*, 4319.

(45) Mochizuki, H.; Hasui, T.; Kawamoto, M.; Ikeda, T.; Adachi, C.; Tanighchi, Y.;

Shirota, Y. *Macromolecules* **2003**, *36*, 3457.

(46) Kawamoto, M.; Mochizuki, H.; Shishido, A.; Tsutsumi, O.; Ikeda, T.; Lee, B.; Shirota, Y. *Macromolecules* **2003**, *107*, 4887.

(47) Chang, S. W.; Li, A. K.; Liao, C. W.; Hsu, C. S. *Jpn. J. Appl. Phys.* **2001**, *41*, 1374.

(48) Grahchev, I.; Moneva, I.; Bojinov, V.; Guittonneau, S. *J. Mater. Chem.* **2000**, *10*, 1291.

(49) Contoret, A. E. A.; Farrar, S. R.; Jackson, P. O.; O'Neill, M.; Nicholls, J. E.; Kelly, S. M.; Rochards, G. J. *Synth. Met.* **2001**, *121*, 1645.

(50) Sung, H. H.; Lin, H. C. *Liq. Cryst.* **2004**, *31*, 831.

(51) Pei, Q.; Yang, Y. *Adv. Mater.* **1995**, *7*, 559.

(52) Andrew, A. C.; Chen, S. W.; Culligan, Y. G.; Chen, S. H.; Klubek, K. P.; Vaeth, K. M.; Tang, C. W. *Adv. Mater.* **2004**, *16*, 783.

(53) Hoag, B. P.; Gin, D. L. *Liq. Cryst.* **2004**, *31*, 185.

(54) Precup-Blaga, F. S.; Schenning, A. P. H. J.; Meijer, E. W. *Macromolecules* **2003**, *36*, 565.

(55) Eckert, J. F.; Nicoud, J. F.; Nierengarten, J. F.; Liu, S. G.; Echegoyen, L.; Barigelletti, F.; Armaroli, N.; Ouali, L.; Krasnikov, V.; Hadziioannou, G. *J. Am. Chem. Soc.* **2000**, *122*, 7467.

(56) Beckers, E. H. A.; Hal, P. A.; Schenning, A. P. H. J.; El-ghayoury, A.; Peeters, E.; Rispens, M. T.; Hummelen, J. C.; Meijer, E. W.; Janssen, R. A. J. *J. Mater. Chem.* **2002**, *12*, 2054.

(57) Peeters, E.; van Hal, P. A.; Knol, J.; Brabec, C. J.; Sariciftci, N. S.; Hummelen, J. C.; Janssen, R. A. J. *J. Phys. Chem. B* **2000**, *104*, 10174.

(58) Wang, H.; Wang, H. H.; Urban, V. S.; Littrell, K. C.; Thiyagarajan, P.; Yu, L. *J.*

Am. Chem. Soc. **2000**, *122*, 6855.

(59) Dudek, S. P.; Sikes, H. D.; Chidsey, C. E. D. *J. Am. Chem. Soc.* **2001**, *123*, 8033.

(60) Seferos, D. S.; Banach, D. A.; Alcantar, N. A.; Israelachvili, J. N.; Bazan, G. C. *J. Org. Chem.* **2004**, *69*, 1110.

(61) Wong, M. S.; Li, Z. H.; Shek, M. F.; Samoc, M.; Samoc, A.; Barry, L. D. *Chem. Mater.* **2002**, *14*, 2999.

(62) Jonkheijm, P.; Hoeben, F. J. M.; Kleppinger, R.; Herrikhuyzen, J.; Schenning, A. P. H. J.; Meijer, E. W. *J. Am. Chem. Soc.* **2003**, *125*, 15941.

(63) Jonkheijm, P.; Fransen, M.; Schenning, A. P. H. J.; Meijer, E. W. J. *Chem. Soc., Perkin Trans. 2*, **2001**, 1280.

(64) Gesquiere, A.; Jonkheijm, P.; Schenning, A. P. H. J.; Mena-Osteritz, E.; Bauerle, P.; De Feyter, S.; De Schryver, F. C.; Meijer, E. W. *J. Mater. Chem.* **2003**, *13*, 2164.

(65) Jorgensen, M.; Krebs, F. C. *J. Org. Chem.* **2004**, *69*, 6688.

(66) Goodson, T; Li, W.; Gharavi, A.; Yu, L. *Adv. Mater.* **1997**, *9*, 639.

(67) Bittner, R.; Daubler, T. K.; Neher, D.; Meerholz, K. *Adv. Mater.* **1999**, *11*, 119.

(68) Wong, M. S.; Li, Z. H.; Tao, Y.; D'Iorio, M. *Chem. Mater.* **2003**, *15*, 1198.

(69) Precup-Blaga, F. S.; Garcia-Martinez, J. C.; Schenning, A. P. H. J.; Meijer, E. W. *J. Am. Chem. Soc.* **2003**, *125*, 12953.

(70) Wong, M. S.; Li, Z. H.; Shek, M. F.; Chow, K. H.; Tao, Y.; D'Iorio, M. *J. Mater. Chem.* **2000**, *10*, 1805.

(71) Lee, G. Y.; Park, B.; Woo, H. S.; Kim, Y.; Ha, C. S.; Lee, C. M.; Jeong, K.; Ha, J. H.; Kim, Y. R. *Solid State Commun.* **1997**, *102*, 895.

(72) Detert, H.; Schollmeyer, D.; Sugiono, E. *Eur. J. Org. Chem.* **2001**, 2927.

(73) Gebherdt, V.; Bacher, A.; Thelakkat, M.; Stalmach, U.; Meier, H.; Schmidt, H. W.;

Haarer, D. *Synth. Met.* **1997**, *90*, 123.

(74) Choong, Y.; Park, Y.; Gao Y.; Wehrmeister, T.; Mullen, K.; Hsieh, B. R.; Tang, C. W. *Appl. Phys. Lett.* **1996**, *69*, 1492.

(75) Hulvat, J. F.; Sofos, M.; Tajima, K.; Stupp, S. I. *J. Am. Chem. Soc.* **2005**, *127*, 366.

(76) Gill, R. E.; Hadziioannou, G. *Adv. Mater.* **1996**, *8*, 212.

(77) Babudri, F.; Farinola, G. M.; Lopez, L. C.; Martinelli, M. G.; Naso, F. *J. Org. Chem.* **2001**, *66*, 3878.

(78) Brouwer, H. J.; Krasnikov, V. V.; Hilberer, A.; Hadziioannou, G. *Adv. Mater.* **1996**, *8*, 935.

(79) Tang, C. W.; VanSlyke, S. A. *Appl. Phys. Lett.* **1987**, *51*, 913.

(80) Ling, Q.; Yang, M.; Wu, Z.; Zhang, X.; Wang, L.; Zhang, W. *Polymer* **2001**, *42*, 4605.

(81) Janssen, F. J. J.; van Ijzendoorn, L. J.; Denier van der Gon, A. W.; de Voigt, M. J. A.; Brongersma, H. H.. *Phys. Rev. B* **2004**, *70*, 165425.

(82) Yang, Z.; Sokolik, I.; Karasz, F. E. *Macromolecules* **1993**, *26*, 1188.

(83) Hu, B.; Yang, Z.; Karasz, F. E. *J. Appl. Phys.* **1994**, *76*, 2419.

(84) Hu, B.; Yang, Z.; Karasz, F. E. *J. Appl. Phys.* **2003**, *93*, 1995.

(85) Brown, A. R.; Katsuki, A.; Greenham, N. C.; Bradley, D. D. C.; Friend, R. H.; Holmes, A. B. *Chem. Phys. Lett.* **1993**, *210*, 61.

(86) Shozo, T. K.; Katsuki, A.; Kobori, Y. *J. Photochem. Potobiol. C* **2001**, *2*, 17.

(87) Wohlgenannt, M.; Tandon, K.; Mazumdar, S.; Ramasesha, S.; Vardeny, Z. V. Nature **2001**, *409*, 494.

(88) Heeger, A. J. *Angew. Chem. Int. Ed. Engl.* **2001**, *40*, 2591.

(89) Friend, R. H.; Gymer, R. W.; Holmes, A. B.; Burroughes, J. H.; Marks, R.N.;

Bradley, D. D. C.; Dos Santos, D. A.; Bredas, J. L.; Logdlund, M.; Salaneck, W. R. *Nature* **1999**, *397*, 121.

(90) Cao, Y.; Parker, I. D.; Yu, G.; Zhang, C.; Heeger, A. J. *Nature* **1999**, *397*, 414.

(91) Yu, L. S.; Tseng, H. E.; Lu, H. H.; Chen, S. A. *Appl. Phys. Lett.* **2002**, *81*, 2014.

(92) An, B. K.; Kim, Y. H.; Shin, D. C.; Park, S. Y.; Yu, H. S.; Kwon, S. K. *Macromolecules* **2001**, *34*, 993.

(93) Kim, Y. H.; Ahn, B. K.; Shin, C.; Yu, H. S.; Kim, H.; Kwon, S. K. *Macromol. Symp.* **2000**, *154*, 171.

(94) Chen, F. C.; Chang, S. C.; He, G.; Pyo, S.; Yang, Y.; Kurotaki, M.; Kido, J. *J. Poly. Sci: Part B: Poly. Phys.* **2003**, *41*, 2681.

(95) Lkai, M.; Tokito, S.; Sakamoto, Y.; Auzuki, T.; Taga, Y. *Appl. Phys. Lett.* **2001**, *79*, 156.

(96) Yang, M. J.; Tshutsui, T. *Jpn. J. Appl. Phys.* **2000**, *39*, 828.

(97) Xia, H.; Zhang, C.; Qiu, S.; Lu, P.; Zhang, J.; Ma, Y. *Appl. Phys. Lett.* **2004**, *84*, 290.

(98) Shen, F.; Liu, X.; Lin, D.; Xia, H.; Zhang, C. *Appl. Phys. Lett.* **2004**, *84*, 55.

(99) Yang, J.; Gordon, K. C. Chem Phys Lett 2004, 385, 481.

(100) Tao, Y. T.; Balasubramaniam, E.; Danel, A.; Jarosz, B.; Tomasik, P. *Appl. Phys. Lett.* **2000**, *77*, 1575.

(101) Kwong, R. C.; Nugent, M. R.; Michalski, L.; Ngo, T.; Rajan, K.; Tung, Y. J.; Weaver, M. S.; Zhou, T. X.; Hack, M.; Thompson, M. E.; Forrest, S. R.; Brown, J. J. *Appl. Phys. Lett.* **2002**, *81*, 162.

(102) Adachi, C.; Baldo, M. A.; Forrest, S. R.; Lamansky, S.; Thompson, M. E.; Kwong, R. C. *Appl. Phys. Lett.* **2001**, *78*, 1622.

(103) Xu, Q.; Duong, H. M.; Wudl, F.; Yang, Y. *Appl. Phys. Lett.* **2004**, *85*, 3357.

(104) Gonga, X.; Ostrowski, J. C.; Moses, D.; Bardeen, C. J.; Bazan, G. C. *J. Appl. Phys.* **2004**, *95*, 948.

(105) Kobayashi, N.; Uemura, S.; Kusabuka, K.; Nakahira, T.; Takahashi, H. *J. Mater. Chem.* **2001**, *11*, 1766.

(106) Ikkala, O.; Brinke, G. ten *Science* **2002**, *295*, 2407.

(107) Brunsveld, L.; Folmer, B. J. B.; Meijer, E. W.; Sijbesma, R. P. *Chem. Rev*. **2001**, *101*, 4071.

(108) Paleos, C. M.; Tsiourvas, D. *Liq. Crys.* **2001**, *28*, 1127.

(109) Kreuzer, M.; Benkler, E.; Paparo, D.; Casillo, G.; Marrucci, L. *Phys. Rev. E* **2003**, *68*, 011701.

(110) Huyskens, P. L.; Luck, W. A. P. *Intermolecular Forces*, *Third Edition*; Springer-Verlag: Berlin, **1991**.

(111) Kato, T.; Kihara, H.; Ujiie, S.; Uryu, T.; Fréchet, J. M. J. *Macromolecules* **1996**, *29*, 8734.

(112) Shandryuk, G. A.; Kuptsov, S. A.; Shatalova, A. M.; Plate', N. A.; Talroze, R. V. *Macromolecules* **2003**, *36*, 3417.

(113) Cheuk, K. K. L.; Lam, J. W. Y.; Lai, L. M.; Dong, Y.; Tang, B. Z. *Macromolecules* **2003**, *36*, 9752.

(114) Lu, L.; Jenekhe, S. A. *Macromolecules* **2001**, *34*, 6249.

(115) Osuji, C.; Chao, C. Y.; Bita, I.; Ober, C. K.; Thomas, E. L. *Adv. Funct. Mater.* **2002**, *12*, 753.

(116) Barmatov, E.; Filippov, A.; Andreeva, L.; Barmatova, M.; Kremer, F.; Shibaev, V. *Macromol. Rapid Commun.* **1999**, *20***,** 521.

(117) Kihara, H.; Kato, T.; Uryu, T.; Fréchet, J. M. J. *Chem. Mater.* **1996**, *8*, 961.

(118) Thote, A. J.; Gupta, R. B. *Ind. Eng. Chem. Res.* **2003**, *42,* 1129.

(119) Lin, H. C.; Sheu, H. Y.; Chang, C. L.; Tsai, C. *J. Mater. Chem*. **2001**, *11*, 2958.

(120) Lin, H. C.; Ko, C. W.; Guo, K.; Cheng, T. W. *Liq. Crys.* **1999**, *26*, 613.

(121) Lin, H. C.; Shiaw, J. M.; Wu, C. Y.; Tsai, C. *Liq. Crys.* **2000**, 27, 1103.

(122) West, J. L.; Magyar, G. R.; Kelly, J. R. *Appl. Phys. Lett.* **1995**, *67*, 155.

(123) Sung, H. H.; Lin, H. C. *Macromolecules* **2004**, *37*, 7945.

(124) Culligan, S. W.; Geng, Y.; Chen, S. H.; Klubek, K.; Vaeth, K. M.; Tang, C. W. *Adv. Mater.* **2003**, *15*, 1176.

(125) Wang, C.; Kilitziraki, M.; Hugh MacBride, J. A.; Bryce, M. R.; Horsburgh, L. E.; Sheridan, A. K.; Monkman, A. P.; Samuel, D. W. *Adv. Mater.* **2000**, *12*, 217.

(126) Monkman, A. P.; Pålsson, L. O. Higgins, R. W. T.; Wang, C.; Bryce, M. R.; Batsanov, A. S.; Howard, J. A. K. *J. Am. Chem. Soc.* **2002**, *124*, 6049.

(127) Porzio, W.; Destri, S.; Giovanella, U.; Meille, S. V.; Raos, G.; Consonni, R.; Zotti, G. *Chem. Mater.* **2005,** *17,* 242.

(128) Pei, J.; Liu, X. L.; Chen, Z. K.; Zhang, X. H.; Lai, Y. H.; Huang, H. *Macromolecules* **2003**, *36*, 323.

(129) Zhang, H.; Zhou, Z.; Liu, K.; Wang, R.; Yang, B. *J. Mater. Chem*. **2003**, *13*, 1356.

(130) Sierra, C. A.; Lahti, P. M. *Chem. Mater.* **2004,** *16,* 55.

(131) Knaapila, M.; Lkkala, O.; Torkkeli, M.; Jokela, K.; Serimaa, R.; Dolbnya, I. P.; Bras, W.; Brinke, G.; Horsburgh, L. E.; Pålsson, L. O.; Monkman, A. P. *Appl. Phys. Lett.* **2002**, *81*, 1489.

(132) Ajayaghosh, A.; George, S. J. *J. Am. Chem. Soc.* **2001**, *123*, 5148.

(133) Yuan, C. H.; Hoshino, S.; Toyoda, S.; Suzuki, H.; Fujiki, M.; Matsumoto, N. *Appl. Phys. Lett.* **1997**, *71*, 3326.

(134) Liu, J.; Shi, Y.; Yang, Y. *Appl. Phys. Lett.* **2001**, *79*, 578.

(135) Niu, Y. H.; Yang, W.; Cao, Y. *Appl. Phys. Lett.* **2002**, *81*, 2884.

(136) Zhang, Y.; Peng, J.; Mo, Y.; Cao, Y. *Appl. Phys. Lett.* **2004**, *85*, 5170.

(137) Portugall, M.; Ringsdorf, H.; Zentel, R. *Makromol. Chem.* **1982**, 183, 2311.

(138) Kato, T.; Fréchet, J. M. J.; Wilson, P. G.; Saito, T.; Uryu, T.; Fujishima, A.; Jin, C.; Kaneuchi, F. *Chem. Mater.* **1993**, *5*, 1094.

(139) Tehan, B. G.; Lloyd, E. J.; Wong, M. G.; Pitt, W. R.; Montana, J. G.; Manallack, D. T.; Gancia, E. *Quant. Struct.-Act. Relat.* **2002**, *21*, 457.

(140) Cheon, K. O.; Shinar, J. *Appl. Phys. Lett.* **2002**, *81*, 1738.

(141) Huang, J. S.; Yang, K. X.; Xie, Z. Y.; Liu, S. Y.; Jiang, H. J. *Opti. Quan. Electro.* **2001**, *33*, 165.

(142) Chao, C. L.; Chen, S. A. *Appl. Phys. Lett.* **1998**, *73*, 426.

(143) Kim, J. H.; Herguth, P.; Kang, M. S.; Jen, A. K. Y.; Tseng, Y. H.; Shu, C. F. *Appl. Phys. Lett.* **2004**, *85*, 1116.

(144) Ho, G. K.; Meng, H. F.; Lin, S. C.; Horng, S. F.; Hsu, C. S.; Chen, L. C.; Chang, S. M. *Appl. Phys. Lett.* **2004**, *85*, 4576.

(145) Tu, G.; Zhou, Q.; Cheng, Y.; Wang, L.; Ma, D.; Jing, X.; Wang, F. *Appl. Phys. Lett.* **2004**, *85*, 2172.

(146) Bai, S. J.; Wu, C. C.; Dang, T. D.; Arnold, F. E.; Sakaran, B. *Appl. Phys. Lett.* **2004**, *84*, 1656.

(147) Lee, Y. Z.; Chen, X.; Chen, M. C.; Chen, S. A.; Hsu, J. H.; Fann, W. *Appl. Phys. Lett.* **2001**, *79*, 308.

(148) Furuta, P.; Brooks, J.; Thompson, M. E.; Fréchet, J. M. J. *J. Am. Chem. Soc.* **2003**, *125*, 13165.

(149) Chiang, C. L.; Wu, M. T.; Dai, D. C.; Wen, Y. S.; Wang, J. K.; Chen, C. T. *Adv. Funct. Mater.* **2005**, *15*, 231.

(150) Noh, Y. Y.; Lee, C. L.; Kim, J. J.; Yase, K.; *J. Chem. Phys.* **2003**, *118*, 2853.

(151) Kawamura, Y.; Yanagida, S.; Forrest, S. R. *J. Appl. Phys.* **2002**, *92*, 87.

(152) Tekin, E.; Holder, E,; Marin, V.; Gans, B. J.; Schubert, U. S. *Macromol. Rapid Commun.* **2004**, *25*, 1491.

(153) Chen, X.; Liao, J. L.; Liang, Y.; Ahmed, M. O.; Tseng, H. E.; Chen, S. A. *J. Am. Chem. Soc.* **2003**, *125*, 636.

(154) Gong, X.; Ostrowski, J. C.; Bazan, G. C.; Moses, D.; Heeger, A. J. *J. Poly. Sci. B Poly. Phys.* **2003**, *41*, 2691.

(155) Tekin, E.; Holder, E,; Marin, V.; Gans, B. J.; Schubert, U. S. *Macromol. Rapid Commun.* **2005**, *26*, 293.

(156) Xia, H.; Zhang, C.; Qiu, S.; Lu, P.; Zhang, J.; Ma, Y. *Appl. Phys. Lett.* **2004**, *84*, 290.

(157) Xia, H.; Zhang, C.; Liu, X.; Qiu, S.; Lu, P.; Shen, F.; Zhang, J.; Ma, Y. *J. Phys. Chem. B* **2004**, *108*, 3185.

(158) Shen, F.; Xia, H.; Zhang, C.; Lin, D.; He, L.; Ma, Y. *J. Phys. Chem. B* **2004**, *108*, 1014.

(159) D'Andrade, B. W.; Brooks, J.; Adamovich, V.; Thompson, M. E.; Forrest, S. R. *Adv. Mater.* **2002**, *14*, 1032.

(160) Gong, X.; Ma, W. L.; Ostrowski, J. C.; Bazan, G. C.; Moses, D.; Heeger, A. J. *Adv. Mater.* **2004**, *16*, 615.

(161) Tasch, S.; List, E. J. W.; Ekstrom, O.; Graupner, W.; Leising, G.; Schlichting, P.; Rohr, U.; Geerts, Y.; Scherf, U.; Mullen, K. *Appl. Phys. Lett.* **1997**, *71*, 2883.

(162) Thomas, K. R. J.; Lin, J. T.; Tao, Y. T.; Ko, C. W. *J. Am. Chem. Soc.* **2001**, *123*, 9404.

(163) K. R. J. Thomas, J. T. Lin, C. M. Tsai, H. C. Lin, *Tetrahedron* (**2006**) in Press.

(164) Balasubramaniam, E.; Tao, Y. T.; Danel, A.; Tomasik, P. *Chem. Mater.* **2000**, *12*, 2788.

(165) Jiang, X. Z.; Register, R. A.; Killeen, K. A.; Thompson, M. E.; Pschenitzka, F.; Hebner, T. R. *J. Appl. Phys.* **2002**, *91*, 6717.

(166) Zhang, Z. M.; Li, G. W.; Shen, Y. M. J. *Mater. Chem. Phys.* **2003**, *82*, 613.

(167) Cho, N. S.; Hwang, D. H.; Jung, B. J.; Oh, J.; Chu, H. Y.; Shim, H. K. *Synth. Met.* **2004**, *143*, 277.

(168) Wang, Y. M.; Teng, F.; Xu, Z.; Hou, Y. B.; Wang, Y. S.; Xu, X. R. Appl. Surf. Sci. **2005**, *243*, 355.

(169) Wang, Y. M.; Teng, F.; Xu, Z.; Hou, Y. B.; Wang, Y. S.; Xu, X. R. *Eur. Polym. J.* **2005**, *41*, 1020.